NASA TECHNICAL NOTE

NASA TN D-7633

NASA TN D-7633

EXPERIMENTAL LOW-SPEED AND CALCULATED HIGH-SPEED AERODYNAMIC CHARACTERISTICS OF A HYPERSONIC RESEARCH AIRPLANE CONCEPT HAVING A 65° SWEPT DELTA WING

by Jim A. Penland, Theodore R. Creel, Jr., and Floyd G. Howard

Langley Research Center
Hampton, Va. 23665

NATIONAL AERONAUTICS AND SPACE ADMINISTRATION • WASHINGTON, D. C. • AUGUST 1974

1. Report No.	2. Government Accession No.	3. Recipient's Catalog No.
NASA TN D-7633		

4. Title and Subtitle	5. Report Date
EXPERIMENTAL LOW-SPEED AND CALCULATED HIGH-SPEED AERODYNAMIC CHARACTERISTICS OF A HYPERSONIC RESEARCH AIRPLANE CONCEPT HAVING A 65° SWEPT DELTA WING	August 1974
	6. Performing Organization Code

7. Author(s)	8. Performing Organization Report No.
Jim A. Penland, Theodore R. Creel, Jr., and Floyd G. Howard	L-9453
	10. Work Unit No. 760-66-01-02
9. Performing Organization Name and Address	11. Contract or Grant No.
NASA Langley Research Center Hampton, Va. 23665	
	13. Type of Report and Period Covered
12. Sponsoring Agency Name and Address	Technical Note
National Aeronautics and Space Administration Washington, D.C. 20546	14. Sponsoring Agency Code

15. Supplementary Notes

16. Abstract

An experimental wind-tunnel investigation has been carried out to determine the static longitudinal, lateral, and directional stability and control characteristics of a model of a large-body, delta-wing hypersonic research airplane concept at low speed. This investigation was conducted at a dynamic pressure of 239.4 Pa (5 psf) and a Reynolds number, based on fuselage length, of 2×10^6. The configuration variables included vertical fins, engine modules, canards, and a canopy.

The aerodynamic results of a computer study at Mach numbers of 3 to 12 are presented.

17. Key Words (Suggested by Author(s))	18. Distribution Statement
Hypersonic aircraft Low-speed stability Lift Theory	Unclassified – Unlimited STAR Category 02

19. Security Classif. (of this report)	20. Security Classif. (of this page)	21. No. of Pages	22. Price*
Unclassified	Unclassified	71	$3.75

*For sale by the National Technical Information Service, Springfield, Virginia 22151

EXPERIMENTAL LOW-SPEED AND CALCULATED HIGH-SPEED AERODYNAMIC CHARACTERISTICS OF A HYPERSONIC RESEARCH AIRPLANE CONCEPT HAVING A 65° SWEPT DELTA WING

By Jim A. Penland, Theodore R. Creel, Jr., and Floyd G. Howard
Langley Research Center

SUMMARY

An experimental wind-tunnel investigation has been carried out to determine the static longitudinal, lateral, and directional stability and control characteristics of a model of a large-body, delta-wing hypersonic research airplane concept at low speed. This investigation was conducted at a dynamic pressure of 239.4 Pa (5 psf) and a Reynolds number, based on fuselage length, of 2×10^6. The configuration variables included vertical fins, engine modules, canards, and a canopy.

The configuration exhibited positive static longitudinal, lateral, and directional stability up to an angle of attack of about 30° and was trimmable throughout this angle-of-attack range with elevon deflections of 30° or less. Differential elevons were effective in producing roll as were tip rudders in producing yaw, with only small cross derivatives showing for either case.

A computer study was made of the aerodynamic characteristics at Mach numbers from 3 to 12, and the results presented show a marked loss in longitudinal and directional stability with increasing Mach number.

INTRODUCTION

The increasing demand for petroleum and the knowledge that there is only a finite supply point to the need of an alternate source of fuel for engines of all types. It has been shown (ref. 1) that hydrogen, with its enormous energy content, low pollution effects, and high heat-sink capacity in liquid form, is a prime candidate for the fuel of the future. The use of hydrogen as an aircraft fuel is dependent on the development of propulsion systems that utilize hydrogen throughout the flight speed range, structures that not only withstand the aerodynamic loads and heating but efficiently contain the cryogenic liquid fuel, and aerodynamic configurations that not only have the volume to carry the necessary fuel but retain sufficient aerodynamic cleanness to be efficiently worthwhile. These and many

other practical problems associated with aircraft fueled by liquid hydrogen will be identified and solved only through experience in the actual design and operation of such an aircraft.

Experience and recent studies indicate that the use of a hypersonic research airplane specifically designed for the purpose could meet the requirements of extensive data gathering and still remain within reasonable cost bounds. The present test configuration is one of several concepts under study that meet some of the size and aerodynamic specifications required of a hypersonic research airplane. Its design is an outgrowth of the studies presented in reference 2, in which an all-body concept was found to meet the particular mission requirements then envisioned. The present model design utilized most of the body and scramjet engine design of the all-body concept but incorporated wings and redesigned vertical tails. The primary purpose of the present study was to determine the experimental lift and stability characteristics of this large-fuselage, small-wing design during the low-speed landing phase of flight. The aerodynamic results of a computer study of the configuration at Mach numbers from 3 to 12 at a constant dynamic pressure of 71.8 kPa (1500 psf) are presented for reference.

SYMBOLS

Values are given both in the SI Units and the U.S. Customary Units. Experimental measurements were made in the U.S. Customary Units.

A_r	reference area, area of wing including fuselage intercept
b	wing span
c	wing chord
C_A	axial-force coefficient, $F_A/q_\infty A_r$
C_D	drag coefficient, $F_D/q_\infty A_r$
C_F	skin-friction coefficient
C_L	lift coefficient, $F_L/q_\infty A_r$
C_{L_α}	rate of change of lift coefficient with angle of attack, per deg
C_l	rolling-moment coefficient, $M_X/q_\infty A_r b$

C_{l_β} rate of change of C_l with angle of sideslip, per deg

C_{l_δ} incremental rolling-moment coefficient due to control deflection, per deg

C_m pitching-moment coefficient, $M_Y/q_\infty A_r l$

C_{m_α} rate of change of C_m with angle of attack, per deg

$\frac{\partial C_m}{\partial C_L}$ rate of change of C_m with lift coefficient, longitudinal stability parameter

C_N normal-force coefficient, $F_N/q_\infty A_r$

C_n yawing-moment coefficient, $M_Z/q_\infty A_r b$

C_{n_β} rate of change of C_n with angle of sideslip, per deg

C_{n_δ} incremental yawing-moment coefficient due to control deflection, per deg

C_Y side-force coefficient, $F_Y/q_\infty A_r$

C_{Y_β} rate of change of C_Y with angle of sideslip, per deg

C_{Y_δ} incremental side-force coefficient due to control deflection, per deg

F_A axial force along X-axis; positive direction, -X

$F_D = F_N \sin \alpha + F_A \cos \alpha$

$F_L = F_N \cos \alpha - F_A \sin \alpha$

F_N normal force along Z-axis; positive direction, -Z

F_Y side force along Y-axis; positive direction, Y

l length of body

L/D lift-drag ratio, C_L/C_D

M Mach number

M_X, M_Y, M_Z moment about X-, Y-, and Z-axis, respectively

q_∞ free-stream dynamic pressure

R_∞ free-stream Reynolds number based on body length

x distance along X-axis from nose to body station

X,Y,Z reference axes

α angle of attack, deg

β angle of sideslip, deg

δ angle of control deflection, positive to produce positive force or moment, deg

Subscripts:

e both elevon controls

h differential horizontal-control (elevon) deflection

s stability-axis system

t trim condition, $C_m = 0$

v both vertical rudder controls

Model nomenclature:

B body or fuselage

W wing

V_T tip fins

V_C center vertical tail

E_O open flow-through engine

E_R retracted engine

C_1 trapezoidal-planform canards

C_2 delta-planform canards

C_P deployed canopy

MODEL

A photograph of the 0.062-scale test model installed in the tunnel is shown in figure 1. Details of the geometric characteristics of the model and the various components are shown in figures 2 and 3 and are listed in table I. The basic model consisted of a 1.505-m-long (59.25-in.) fuselage and wing built in one piece and elevons capable of deflections from 10^o to -30^o located at the trailing edge of the wing. Two types of detachable vertical tails were utilized: twin wing-tip fins with rudders capable of $\pm 10^o$ deflection (fig. 2) and a center vertical tail with no rudder, positioned on the top aft section of the fuselage (fig. 3). The scramjet engine was represented in the retracted and open positions, the latter configuration having a constant-area duct. As shown in figure 2, the canopy was designed to retract into the fuselage nose with the canopy top faired in with the fuselage contour. In the present tests the canopy was either in place or removed to simulate the deployed and retracted condition, respectively.

Trapezoidal- and delta-planform canards were mounted with the leading-edge–fuselage juncture in the wing-chord plane at body station $x/l = 0.149$ for the trapezoidal canards and $x/l = 0.104$ for the delta canards. These controls were tested only at zero deflection.

The model was constructed of wood and fiberglass, and the various removable components were screwed in place and located by dowels.

APPARATUS AND TESTS

The tests were conducted in the low-speed tunnel with a 12-foot (3.66-meter) octagonal test section at the Langley Research Center at a Reynolds number, based on body length, of 2×10^6 and a dynamic pressure of 239.4 Pa (5 psf). A six-component strain-gage balance was installed inside the model fuselage and attached to the tunnel sting-support system. Force and moment data were measured through an angle-of-attack range from 0^o to 30^o and at angles of sideslip of 0^o, 5^o, and 10^o. All joints and hinge-line cracks were sealed with plastic tape prior to each test run. The tests were made with fixed transition by the method of reference 3, although brief tests without fixed transition indicated

no parameter variations other than a fractional percent decrease in drag. No corrections were made for base pressures. Moments were calculated about a center of gravity located on the vehicle center line at body station $x/l = 0.646$. The longitudinal characteristics are presented in the stability-axis system and the lateral-directional characteristics, in the body-axis system (fig. 4).

Because of the very low test Reynolds number of this investigation and the relatively high turbulence factor of the tunnel flow, it is not recommended that the drag data be extrapolated to flight Reynolds numbers. Lift-curve slopes, moments, and drag increments due to component variations, however, are considered valid.

RESULTS AND DISCUSSION

Static Longitudinal Characteristics

Configuration buildup.- The static longitudinal aerodynamic characteristics of the basic body-wing configuration with zero elevon deflection and the variations due to the addition of the various vertical tails are presented in figure 5 for angles of attack of 0° to 30°. All test configurations exhibit the slightly nonlinear lift curves with angle of attack (fig. 5(a)) that are typical for delta-wing shapes with low aspect ratio, that is, an increasing lift-curve slope at low angles of attack followed by a nearly linear slope to about $\alpha = 25^{\circ}$. Slightly higher lift coefficients were measured at $\alpha = 0^{\circ}$ to 20° on the configurations having the tip fins installed. These fins would be expected to act as end plates and thereby alter the conventional wing-tip flow, or in effect, increase the wing aspect ratio. Also, because of their 5° toe-in (which is needed for directional stability in hypersonic flight (ref. 4)), a low-pressure region may form on the inside of the fins and thus contribute to the overall configuration lift. This increased lift with tip fins installed is further shown in figure 5(b) to improve the untrimmed lift-drag ratio, although the addition of the tip fins increased the drag at the lower angles of attack. The increase in lift also helped offset the increase in drag due to the addition of the center vertical tail (V_C) to the BWV_T configuration. The rearward location of the wing-tip region where this increased lift increment occurs contributes to a nose-down, or stabilizing, pitching moment (figs. 5(c) and 5(d)), particularly in the low angle-of-attack region, where the addition of the tip fins altered the angle of attack for $C_m = 0$ by almost 5°. It may therefore be concluded that the addition of tip fins to the untrimmed body-wing configuration increased the lift and, because of the aft location of this increased lift, increased the nose-down pitching moment and thus the longitudinal stability.

Elevon effectiveness.- The basic longitudinal aerodynamic characteristics of the body-wing configuration with tip fins and the body-wing configuration with the center vertical tail are presented in figures 6 and 7, respectively, for a range of elevon deflections

and angles of attack up to 30°. The longitudinal characteristics of the body-wing configuration with tip fins (BWV_T) for a range of elevon deflections and angles of attack up to 30° are given in figure 8 for the open scramjet installation and in figure 9 for the retracted scramjet. The longitudinal characteristics of the BWV_T configuration at trim are compared with those of the BWV_C configuration in figure 10. These data show that both configurations may be trimmed to an angle of attack of 28° and lift coefficients of about 0.75 with elevon deflections of -25° (fig. 10(a)) and both are statically stable throughout this trim range (fig. 10(b)). The BWV_C configuration has a higher lift-drag ratio throughout the trim angle-of-attack range and a 13-percent higher maximum lift-drag ratio than the BWV_T configuration.

This reversal in configuration efficiency, as measured by the lift-drag ratio, between the tip-fin and the center-tail configurations in the untrimmed (fig. 5) and trimmed conditions (fig. 10) may be explained as follows: The addition of tip fins to the body-wing configuration has been shown to increase the lift in the lower angle-of-attack range as well as the static longitudinal stability over the values obtained by addition of the center vertical tail. This increased static stability requires more negative elevon deflection for trim, which may be seen in figure 10 to be as much as 5°, than the BWV_C configuration. Also, because of the negatively deflected elevons, the trim lift is decreased. The combination of decreased lift and additional drag from the larger elevon deflection results in the overall lower lift-drag ratio for the configuration equipped with tip fins. It may be concluded that the use of tip fins, however desirable at hypersonic speeds for directional stability, is detrimental in the development of trim lift-drag ratios at low speeds because of the large elevon deflections required for trim.

The longitudinal aerodynamic characteristics at trim of the BWV_T configuration with the open and retracted scramjet engines installed are presented in figure 11. The addition of engines to the BWV_T configuration (fig. 10) may be seen to lower the trim lift-drag ratio, to have little effect on the trim angle-of-attack or lift range (fig. 11(a)), and to increase slightly the static longitudinal stability at trim (fig. 11(b)). The lower trim lift-drag ratio is due primarily to the increased drag of the engine modules, the open engine having the lower installed drag. A study of the untrimmed data in figures 8 and 9, however, shows that there were other contributing factors that could result in even lower trim lift-drag ratios. A comparison of figures 8(c) and 9(c) with the BWV_T configuration data in figure 6(c) indicates that the addition of the engine modules increased the nose-up or positive pitching moments, particularly in the lower angle-of-attack range, and by so doing reduced the elevon deflection required to trim at a given angle of attack. The nose-up pitching moment is probably due to a separated flow region, which was observed during tuft studies, downstream of the engine modules on the bottom aft portion of the model. The net effect was that the trim drag due to elevon deflection was reduced from that for the BWV_T configuration (fig. 10), and the drag increase due to the addition of engines was

therefore partly nullified. It should be kept in mind that flow separation of this nature is highly dependent on Reynolds number and would vary with model size and test conditions. It may be concluded that the addition of engine modules, as expected, reduced the trim lift-drag ratio but had a negligible effect on the trim angle-of-attack range.

Trapezoidal- and delta-planform canards.- The longitudinal aerodynamic characteristics of the BWV_T configuration equipped with canards are presented in figure 12. The purpose of these tests was to determine the effect of the undeflected canards on the configuration aerodynamics. The results show that the overall lift (fig. 12(a)) was reduced with the installation of either canard, the delta canard causing the greatest loss. This loss in lift is due in part to interference by the wake and downwash of the canards with the airflow around the downstream main lifting surface and was accompanied by a slight decrease in drag (fig. 12(b)). The less-than-expected increase in positive pitching moment is shown in figure 12(c), where the delta canards provide the greater effectiveness in the higher angle-of-attack range and the trapezoidal canards give only a 5^o change in trim angle of attack. Figure 12(d) shows that stability was decreased slightly with the addition of the canard surfaces. Since the local Reynolds number on both sets of canards was quite low and early separation was observed to occur during tuft tests, the results were considered inconclusive and no further tests with canards were made.

Canopy deployment.- This research aircraft concept was designed to fly nearly a complete mission with the canopy retracted and to have the canopy deployed just prior to landing, hence the less-than-ideal aerodynamic shape of the canopy. The results of tests with the canopy installed on the BWV_T configuration are presented in figure 13, where the plots show that all parameters were altered slightly, but none to such an extent as to require alteration of a normal landing maneuver. It may be concluded, therefore, that the deployment of the canopy will not adversely affect the longitudinal characteristics of the aircraft for landing.

Static Lateral and Directional Stability

The static lateral and directional stability of the test model with the various fin, engine, and canopy combinations is presented in figure 14. The body-wing configuration is shown in figure 14(a) to be directionally unstable throughout the angle-of-attack range but to have positive dihedral effect $\left(-C_{l_\beta}\right)$ to an angle of attack of about 23^o. The addition of the tip fins (BWV_T) increased the directional stability so that the configuration was statically stable up to an angle of attack of about 26^o, while the substitution of the more effective center tail (BWV_C) extended the stable angle-of-attack range to about 30^o. The data for the fins and the center tail installed (BWV_TV_C) indicate that the influence of each fin on the static lateral and directional stability was additive and that there was no serious aerodynamic interaction between the two controls.

The addition of either the retracted or the open engine module to either the configuration with tip fins or with the center tail (figs. 14(c) to 14(f)) resulted in only minor variations of the lateral-directional characteristics. The engine was purposely located at design center of gravity of the configuration, and these data indicate that such a location can be expected not to affect the lateral-directional characteristics of the vehicle adversely.

The model was tested with the canopy added to the BWV_T and BWV_C configurations and the lateral-directional results are shown in figures 14(b) and 14(g). These data show that, as with the longitudinal characteristics, there were only small changes in the stability derivatives with the addition of the canopy; therefore, its deployment will not require special lateral or directional considerations during the landing phase of flight.

Yaw and Roll Control

The results of tests to determine the degree of yaw control of the BWV_T configuration are presented in figure 15. These data show that the tip-fin rudders were effective for yaw control throughout the angle-of-attack range and that the roll due to yaw control was relatively small.

The results of tests to determine the degree of roll control of the BWV_T configuration are presented in figure 16. These data show that the differential elevon controls are highly effective in producing roll control, sufficient not only to provide normal control but also to correct the small amount of roll due to yaw control mentioned previously. The yaw due to roll control is negligible. It may be concluded that the test configuration has adequate yaw and roll control and that the cross derivatives are small.

COMPUTER STUDY OF THE HYPERSONIC AERODYNAMICS OF A RESEARCH AIRPLANE CONCEPT

To complement the experimental test program at low speeds, a computer study of a 24.6-m-long (80.6-ft) flight-size version of the present configuration was carried out through a Mach number range from 3 to 12 by using the methods of reference 5. Tangent-wedge inviscid theory was used for compression-surface areas on the wings and tip fins; tangent-cone theory, on the fuselage. Expansion-surface areas were calculated by application of Prandtl-Meyer coefficients determined by expanding the flow from free stream. Turbulent skin friction was calculated within the program by the Spalding-Chi theory of reference 6. The altitude, velocity, and Reynolds number at a constant dynamic pressure of 71.8 kPa (1500 psf) used in the study are given in the following table:

M	Altitude		Velocity		R_∞
	m	ft	m/sec	ft/sec	
3	15 027	49 300	885	2 904	296.5×10^6
4	19 054	62 514	1180	3 872	210.2
6	24 272	79 633	1787	5 864	136.6
8	28 054	92 040	2403	7 885	100.2
10	31 034	101 818	3024	9 921	78.8
12	33 528	110 000	3668	12 033	63.6

The configuration was divided into approximately 700 elements, as shown in figure 17, for the calculation of both the inviscid and viscid aerodynamics.

The calculated results, presented in figures 18 to 27, are intended primarily as a reference and to show the wide variations that occur in configuration aerodynamics with Mach number at hypersonic velocities. The basic normal-force and axial-force coefficients are presented in figures 18 and 19. The axial-force coefficients shown include both the inviscid pressure forces and the calculated turbulent skin friction. The base pressure was assumed to be equal to stream static pressure. The skin-friction coefficients are presented separately in figure 20, and a comparison with figure 19 shows that at maximum lift-drag ratio (fig. 23), the skin friction amounts to about 27 percent of the axial force at $M = 3$ and 34 percent at $M = 12$.

The lift, lift-curve slope, drag, and lift-drag ratio (figs. 21 to 23) steadily decrease with increasing Mach number and the curves of lift against angle of attack become progressively nonlinear. The curves of drag due to lift (fig. 24) also show marked nonlinearities with increasing Mach number.

The curves of pitching moment against angle of attack (fig. 25) and of pitch against lift (fig. 26) show the serious loss in longitudinal stability with Mach number as well as double trim points, that is, two angles of attack or lift coefficients for which $C_m = 0$, at the highest Mach numbers. The validity of these subtle variations in predicted pitching moments can only be verified by wind-tunnel tests on the particular configuration at the desired Mach number. The same is true for the lateral and directional stability characteristics presented in figure 27, which show not only the expected drastic loss in directional stability with Mach number but also a loss with angle of attack for a given Mach number. The positive effective dihedral is shown to decrease with Mach number but to increase with angle of attack. A high level of positive effective dihedral $\left(-C_{l_\beta}\right)$ is desirable, as this term is a major contributor to positive dynamic directional stability.

CONCLUSIONS

An analysis of experimental wind-tunnel data on a model of a large-body, delta-wing hypersonic research airplane concept at low subsonic speed and a Reynolds number, based on the model fuselage length, of 2×10^6 leads to the following conclusions:

1. All configurations were statically stable longitudinally and controllable up to angles of attack of about 30° with elevon deflections of no more than -30°.

2. The addition of wing-tip fins to this untrimmed low-aspect-ratio delta-wing configuration increased the lift because of a reduction in tip losses and, because of the aft location of this increased lift, increased the nose-down pitching moment.

3. The addition of wing-tip fins to the present trimmed configuration decreased the trim lift-drag ratio because of the large elevon deflections required for trim.

4. As expected, the addition of dummy engine modules reduced the trim lift-drag ratio but had a negligible effect on the trim angle-of-attack range.

5. The deployment of the canopy had no serious effect on the longitudinal, lateral, or directional characteristics of the configuration.

6. The deflection of the wing-tip rudders provided effective yaw control throughout the angle-of-attack range, and the roll due to yaw control was relatively small.

7. Differential elevon controls were highly effective in producing roll control, and the yaw due to roll control was negligible.

8. The configuration was statically stable both laterally and directionally with either tip fins or the center vertical tail up to high angles of attack, and the addition of engine modules or the canopy had little or no effect.

Langley Research Center,
National Aeronautics and Space Administration,
Hampton, Va., April 30, 1974.

REFERENCES

1. Nagel, A. L.; and Becker, J. V.: Key Technology for Airbreathing Hypersonic Aircraft. AIAA Paper No. 73-58, Jan. 1973.

2. McDonnell Aircraft Co.: Research Requirements and Ground Facility Synthesis. Vol. II Pt. I of Hypersonic Research Facilities Study. NASA CR-114323, 1970.

3. Braslow, Albert L.; and Knox, Eugene C.: Simplified Method for Determination of Critical Height of Disturbed Roughness Particles for Boundary-Layer Transition at Mach Numbers From 0 to 5. NACA TN 4363, 1958.

4. McLellan, Charles H.: A Method for Increasing the Effectiveness of Stabilizing Surfaces at High Supersonic Mach Numbers. NACA RM L54F21, 1954.

5. Gentry, Arvel E.: Hypersonic Arbitrary-Body Aerodynamic Computer Program (Mark III Version). Vol. I – User's Manual. Rep. DAC 61552, McDonnell Douglas Corp, Apr. 1968. (Available from DDC as AD 851 811.)

6. Spalding, D. B.; and Chi, S. W.: The Drag of a Compressible Turbulent Boundary Layer on a Smooth Flat Plate With and Without Heat Transfer. J. Fluid Mech., vol. 18, pt. I, Jan. 1964, pp. 117-143.

TABLE I.- GEOMETRIC CHARACTERISTICS OF MODEL

Wing:	
Area, total, m^2 (in^2)	0.3419 (530)
Area, exposed, m^2 (in^2)	0.1458 (226)
Area, wetted, m^2 (in^2)	0.2916 (452)
Span, m (in.)	0.6462 (25.44)
Aspect ratio	1.22
Root chord, at fuselage center line, m (in.)	0.9218 (36.29)
Root chord, exposed, m (in.)	0.6339 (24.96)
Tip chord, m (in.)	0.1712 (6.74)
Mean aerodynamic chord, m (in.)	0.62865 (24.75)
Sweepback angles:	
Leading edge, deg	65.0
25-percent-chord line, deg	56.8
Trailing edge, deg	-15.0
Taper ratio	0.186
Dihedral angle, deg	0
Incidence angle, deg	0
Airfoil section (see fig. 2)	Wedge-slab-wedge
Airfoil thickness ratio	0.05
Leading-edge radius at –	
Fuselage-line chord, m (in.)	0.0016 (0.063)
Tip, m (in.)	0.0016 (0.063)
Area of both elevons, m^2 (in^2)	0.0379 (58.76)
Tip fin:	
Area, each, m^2 (in^2)	0.0319 (49.6)
Span, m (in.)	0.1588 (6.25)
Aspect ratio	0.79
Taper ratio	0.24
Root chord, m (in.)	0.3302 (13)
Tip chord, m (in.)	0.0800 (3.15)
Mean aerodynamic chord, m (in.)	0.2311 (9.1)
Sweepback angles:	
Leading edge (top), deg	68.8
Leading edge (bottom), deg	77.8
Trailing edge, deg	18.5
Toe-in angle, deg	5

TABLE I.- GEOMETRIC CHARACTERISTICS OF MODEL – Continued

Airfoil section:	
Constant thickness, m (in.)	0.0064 (0.25)
Trailing-edge thickness	0
Leading-edge radius, m (in.)	0.0032 (0.125)
Rudder:	
Area, m^2 (in^2)	0.0119 (18.4)
Chord (constant), m (in.)	0.0800 (3.15)
Center vertical tail:	
Area, exposed, m^2 (in^2)	0.0645 (100)
Span, exposed, m (in.)	0.2413 (9.5)
Aspect ratio of exposed area	0.9
Taper ratio	0.5
Root chord, at fuselage surface line, m (in.)	0.3622 (14.3)
Tip chord, m (in.)	0.1775 (6.99)
Mean aerodynamic chord of exposed area, m (in.)	0.2784 (10.96)
Sweepback angles:	
Leading edge, deg	58
Trailing edge, deg	50
Airfoil section	NACA 0004
Leading-edge radius, m (in.)	0.0016 (0.063)
Trapezoidal-planform canards:	
Area, total, m^2 (in^2)	0.0093 (14.43)
Area, exposed, m^2 (in^2)	0.0065 (10.1)
Span, m (in.)	0.2357 (9.28)
Aspect ratio	6
Root chord, at fuselage center line, m (in.)	0.0526 (2.07)
Root chord, exposed, m (in.)	0.0459 (1.81)
Tip chord, m (in.)	0.0264 (1.04)
Mean aerodynamic chord, m (in.)	0.0409 (1.61)
Sweepback angles:	
Leading edge, deg	3.4
25-percent-chord line, deg	0
Trailing edge, deg	-9.5
Taper ratio	0.5
Dihedral	0
Airfoil section	NACA 0012
Hinge-line location	25 percent chord

TABLE I.- GEOMETRIC CHARACTERISTICS OF MODEL – Concluded

Delta-planform canards:		
Area, total, m^2 (in^2)	0.0145	(22.4)
Area, exposed, m^2 (in^2)	0.0065	(10.1)
Span, m (in.)	0.1600	(6.3)
Aspect ratio	1.76	
Root chord, at fuselage center line, m (in.)	0.1803	(7.1)
Root chord, exposed, m (in.)	0.1389	(5.47)
Mean aerodynamic chord, m (in.)	0.1201	(4.73)
Sweepback angles:		
Leading edge, deg	65	
Trailing edge, deg	-6.5	
Dihedral, deg	0	
Airfoil section	Circular arc	
Airfoil thickness ratio	0.05	
Leading-edge radius, m (in.)	0.0008	(0.032)
Fuselage:		
Length:		
Theoretical, sharp nose, m (in.)	1.528	(60.15)
Actual, blunt nose, m (in.)	1.505	(59.25)
Maximum height, m (in.)	0.1933	(7.61)
Maximum width, m (in.)	0.2769	(10.9)
Fineness ratio of equivalent round body	6.76	
Base area, m^2 (in^2)	0.0189	(29.43)
Wetted area, m^2 (in^2)	0.6855	(1062.6)
Nose radius, m (in.)	0.0032	(0.125)
Complete model:		
Area, planform, m^2 (in^2)	0.400	(620.2)
Aspect ratio of planform	1.04	

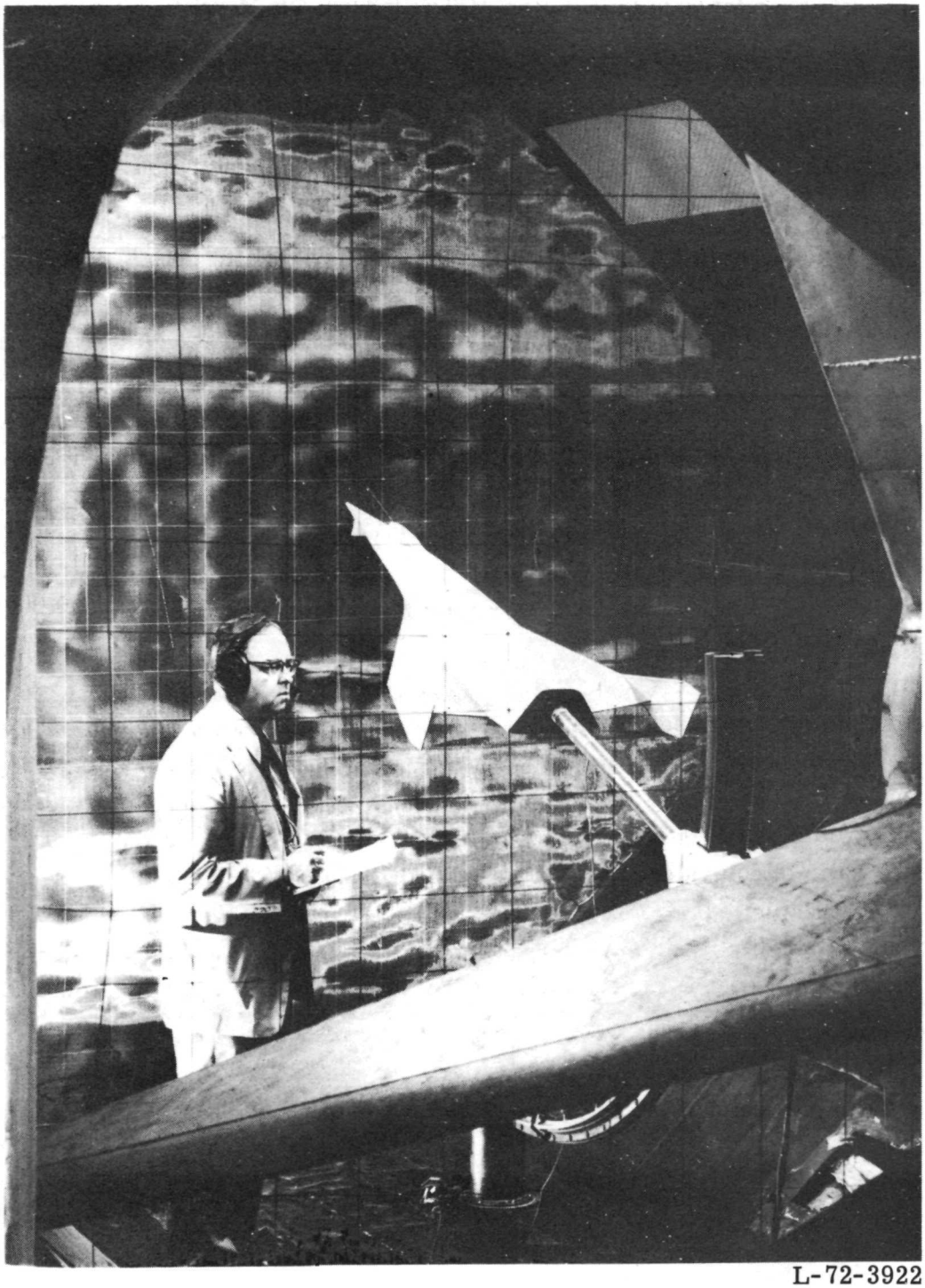

L-72-3922

Figure 1.- Model installed in the tunnel.

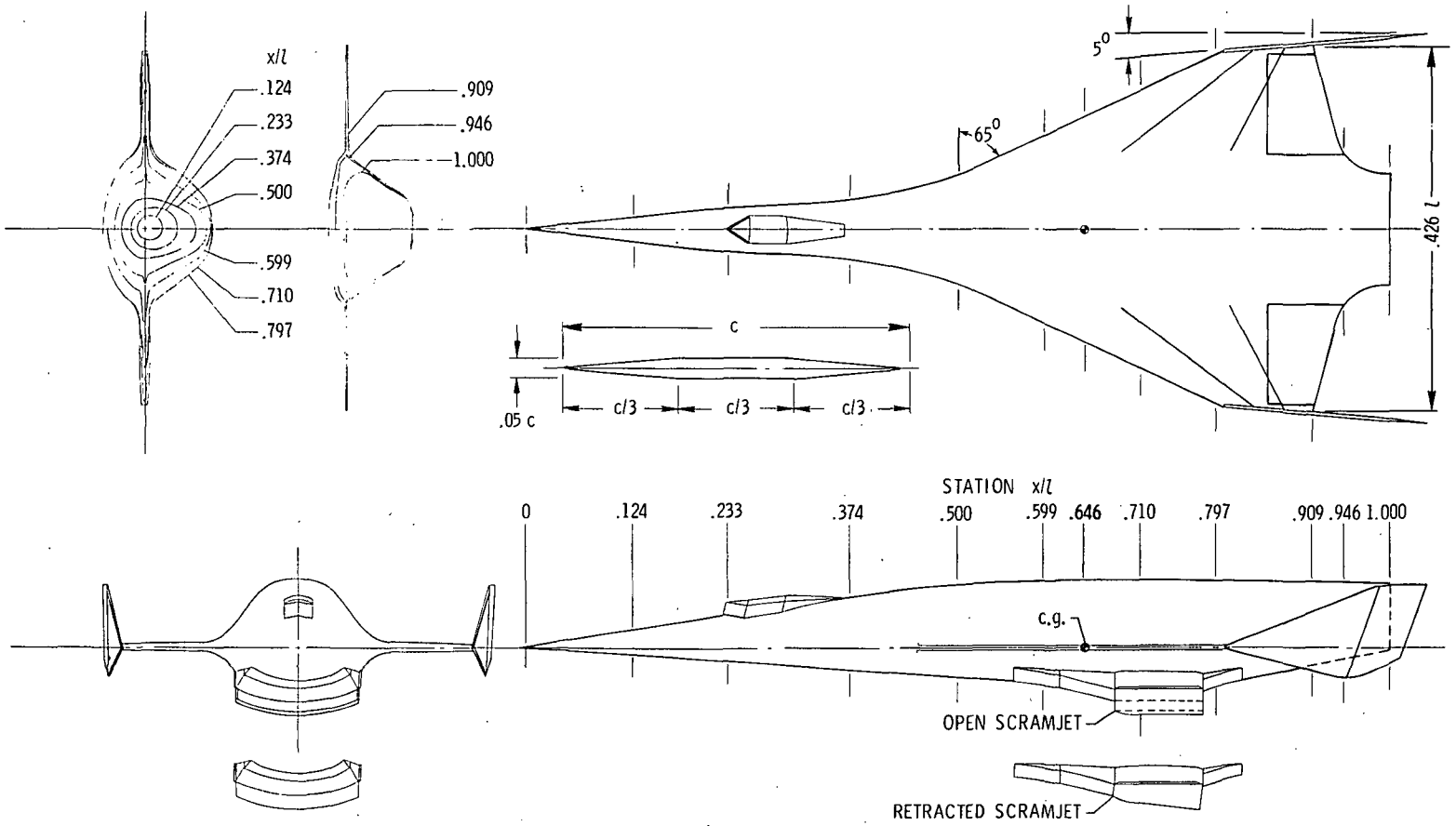

Figure 2.- Details of wind-tunnel model. Dimensions shown have been normalized by the body length l.

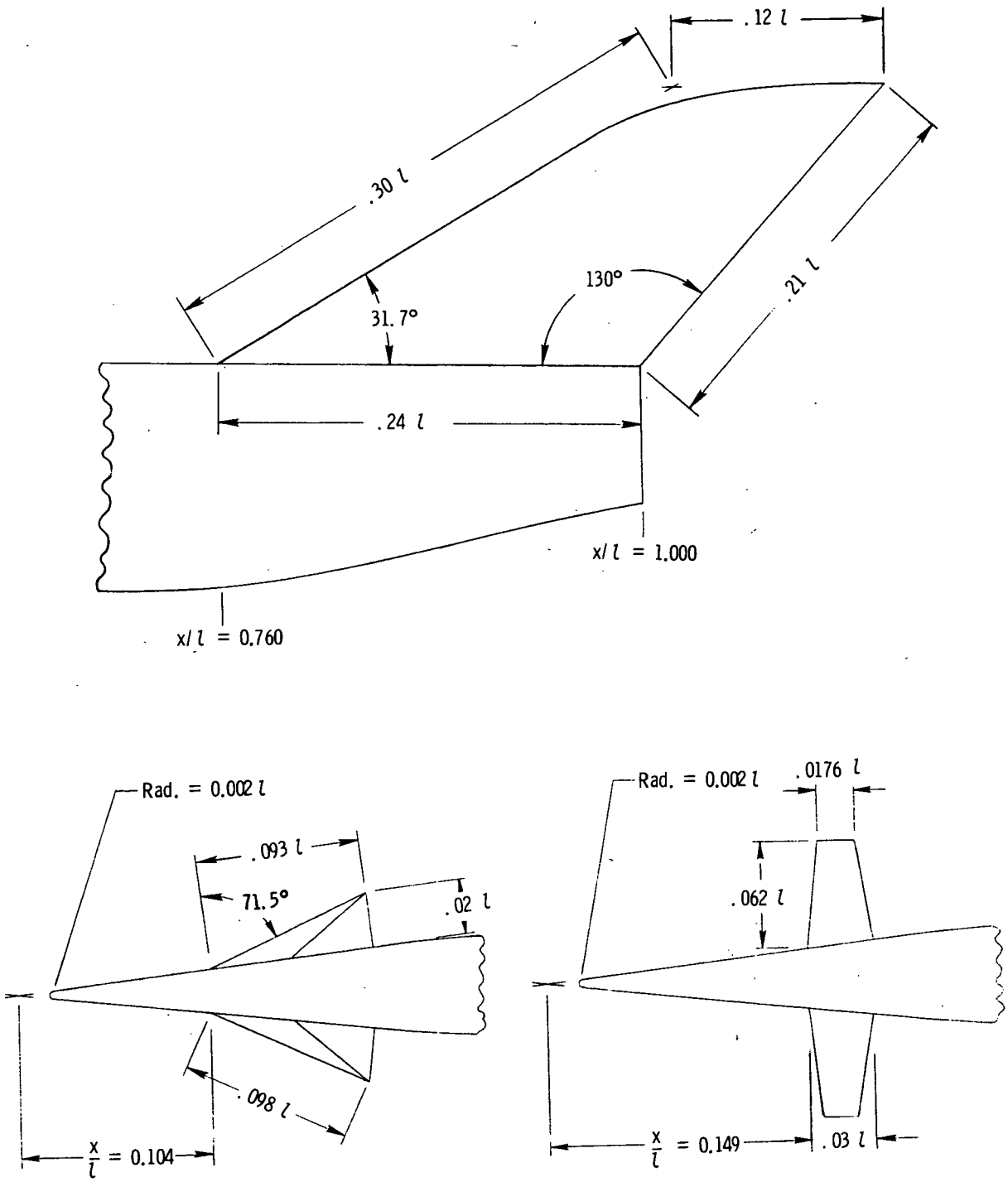

Figure 3.- Details of center vertical tail and canards used in investigation.

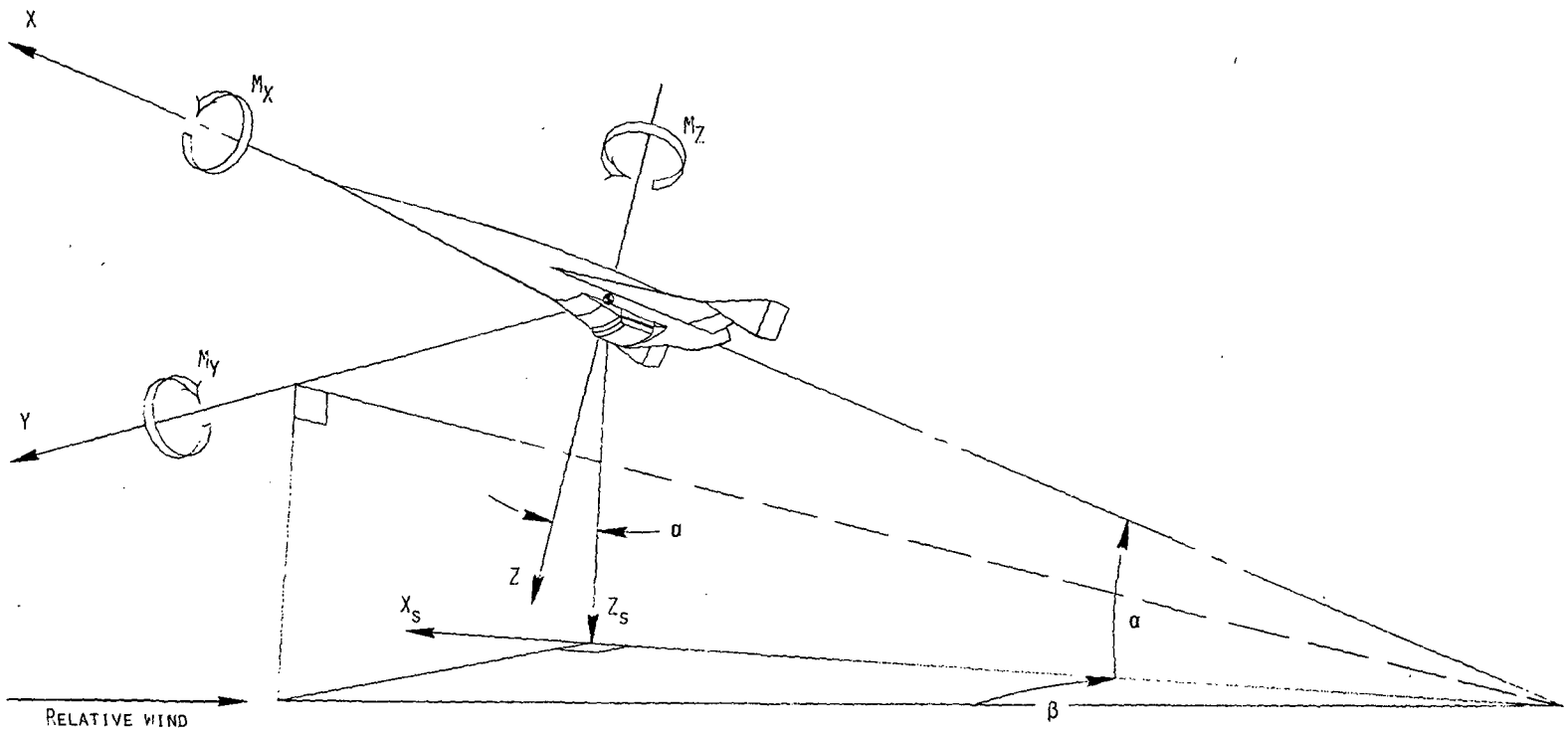

Figure 4.- Systems of reference axes. Arrows indicate positive directions.

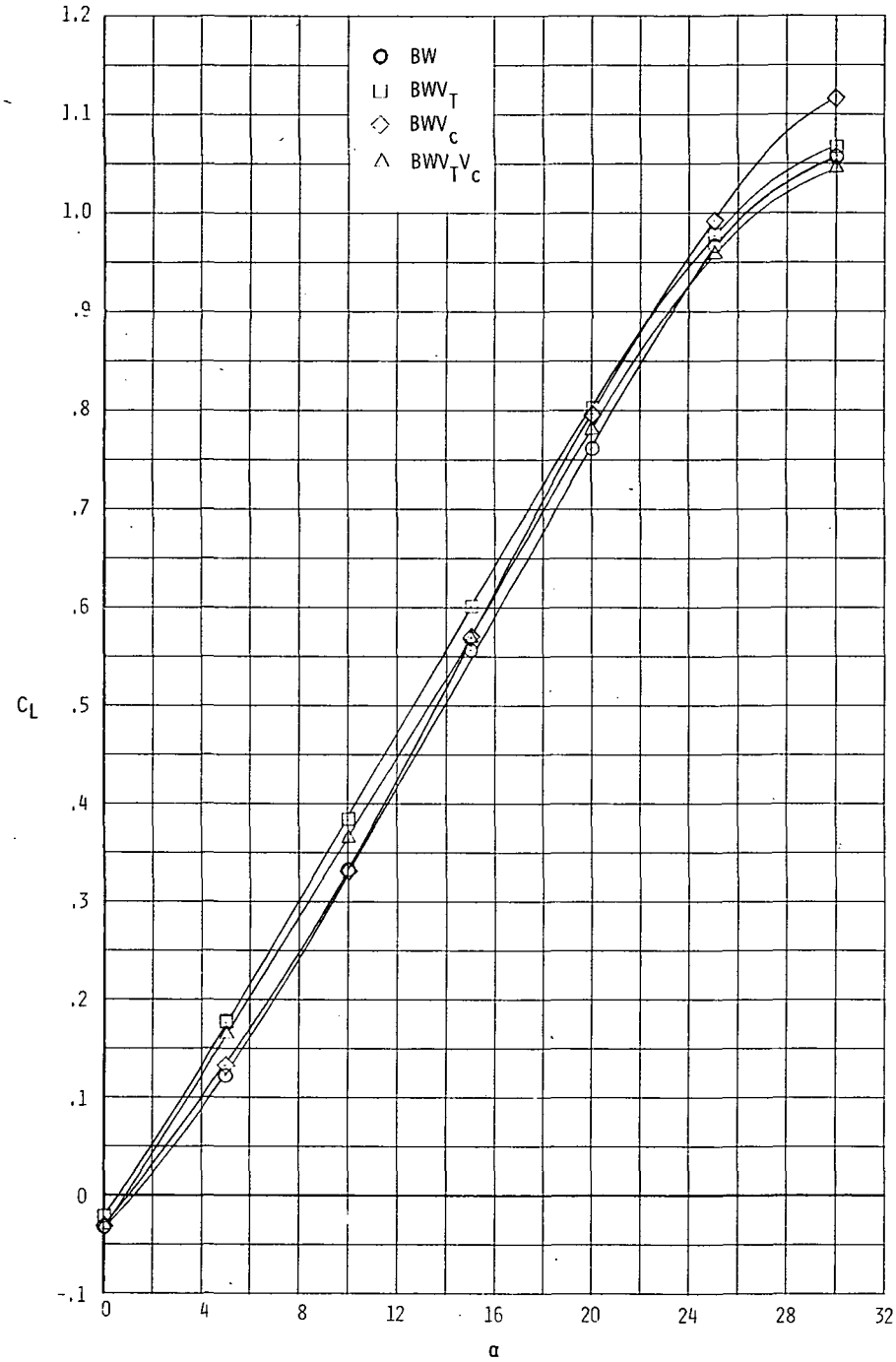

(a) Lift.

Figure 5.- Longitudinal characteristics of BW configuration and of BW configuration with various vertical tails. $\delta_e = 0^o$.

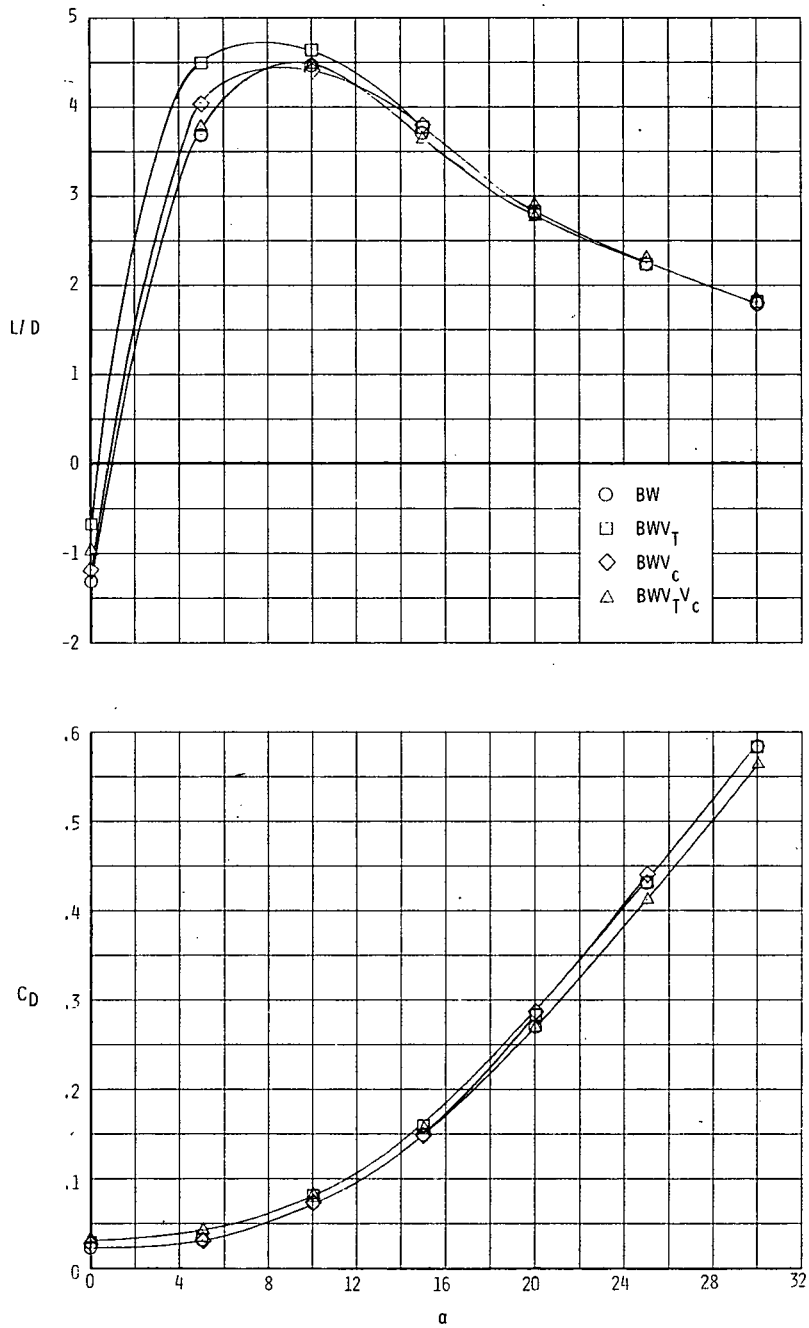

(b) Drag and lift-drag ratio.

Figure 5.- Continued.

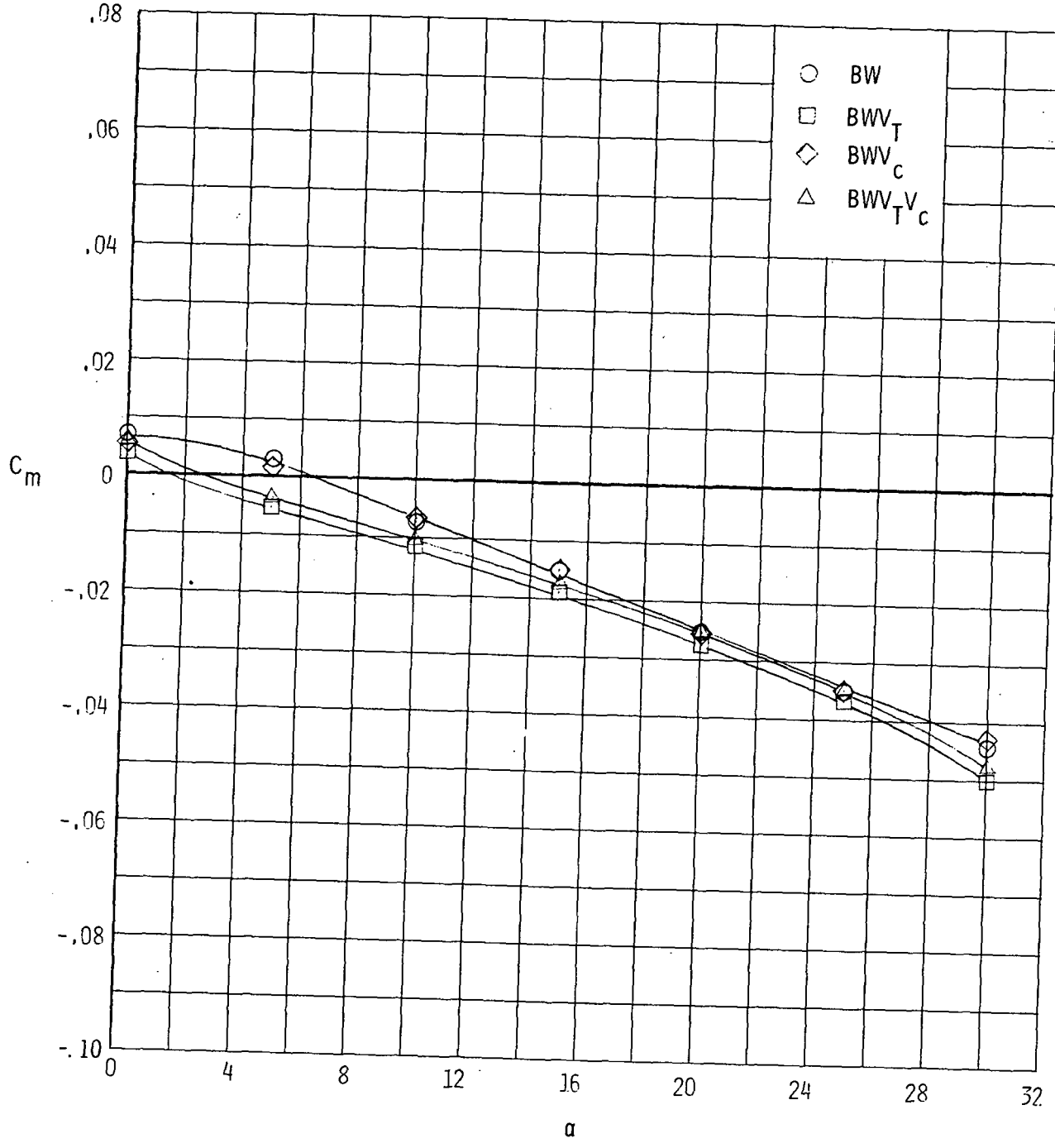

(c) Pitch.

Figure 5.- Continued.

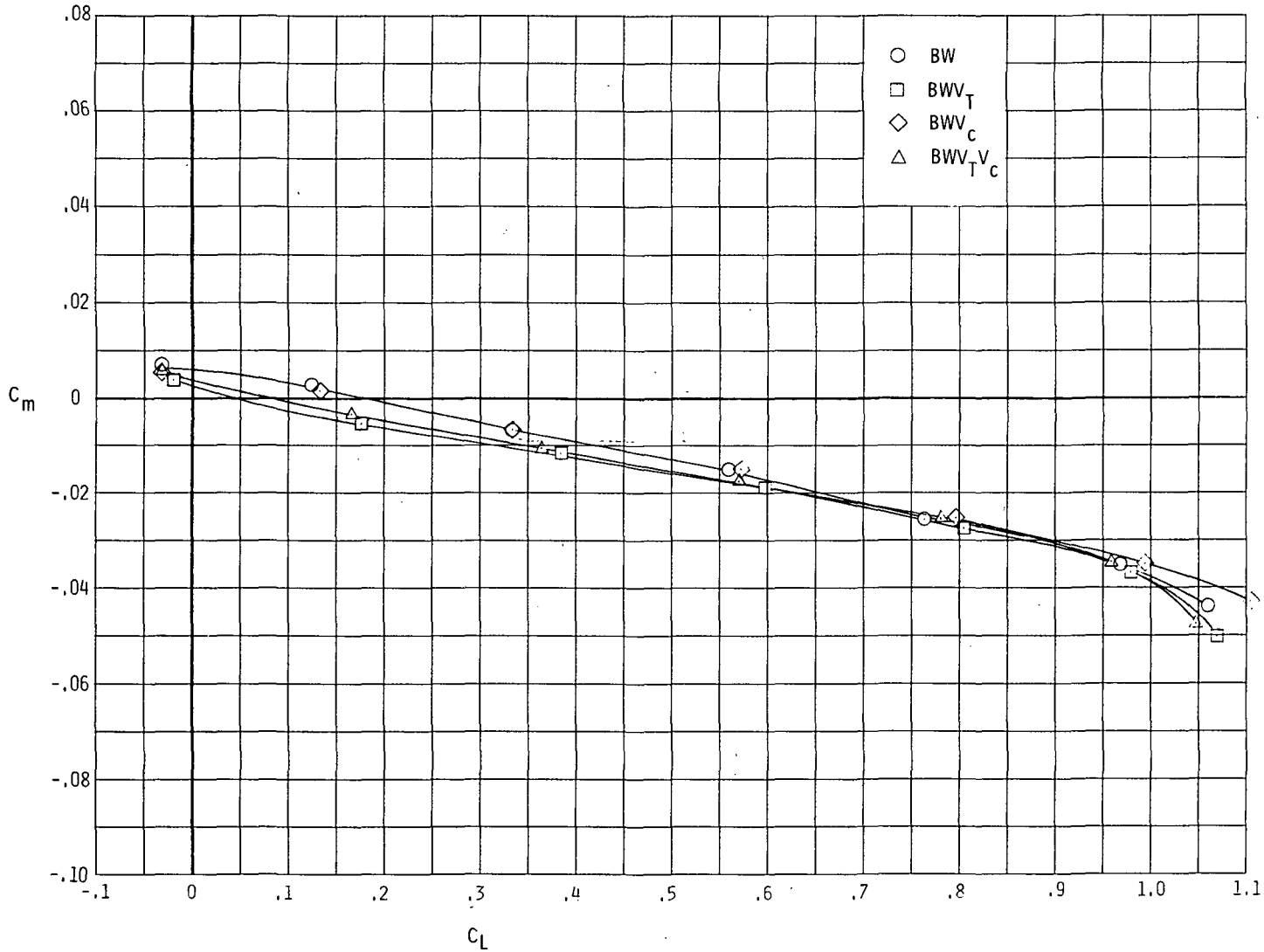

(d) Stability.

Figure 5.- Concluded.

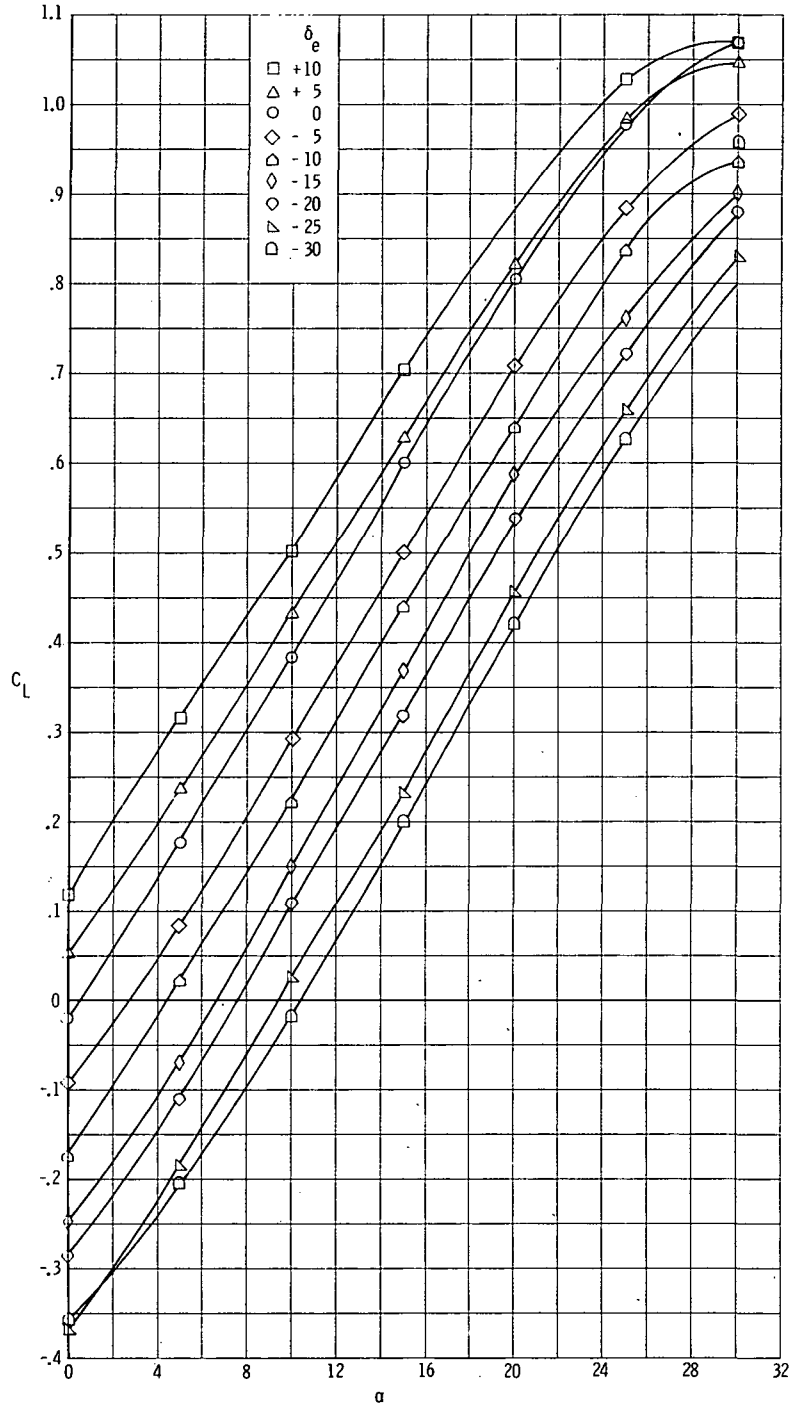

(a) Lift.

Figure 6.- Longitudinal characteristics of BWV_T configuration.

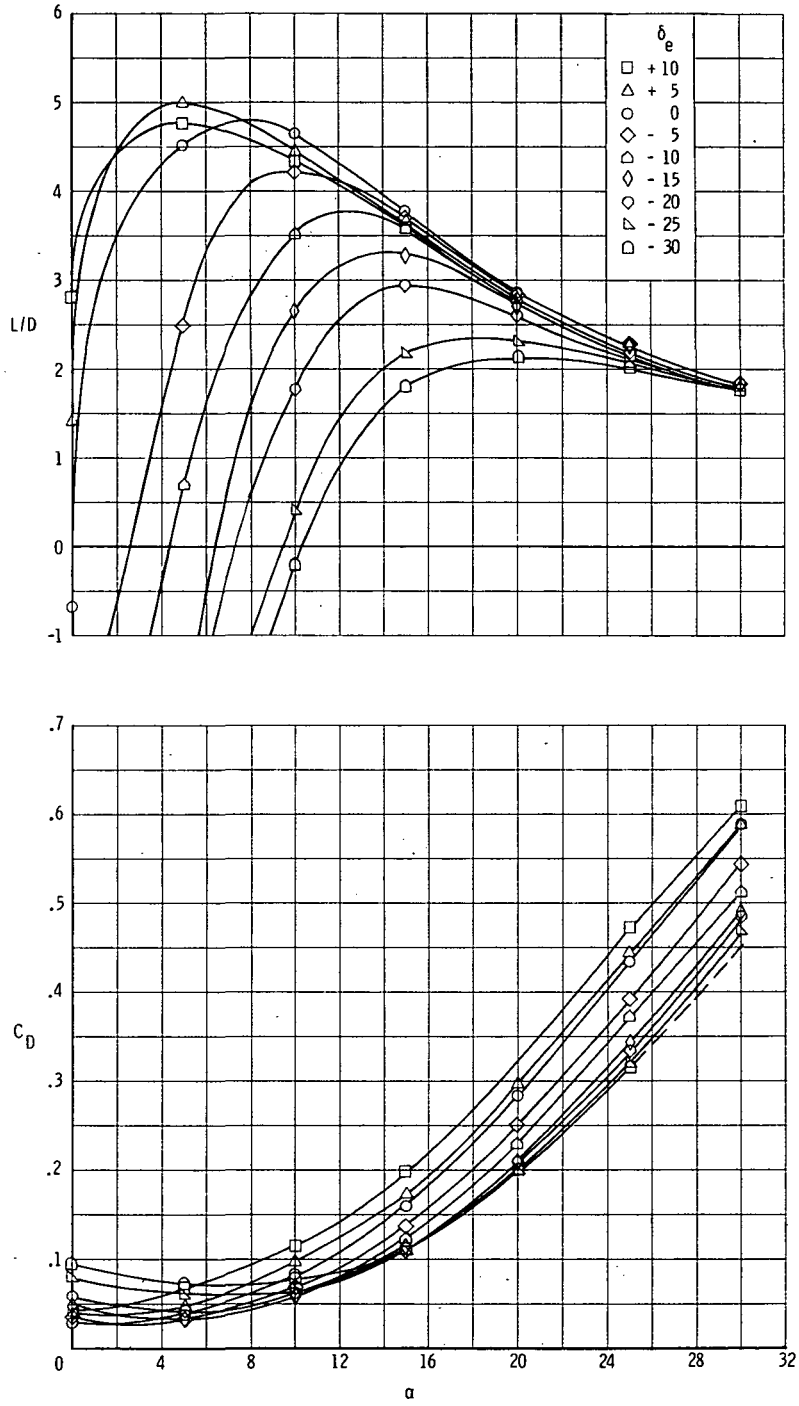

(b) Drag and lift-drag ratio.

Figure 6.- Continued.

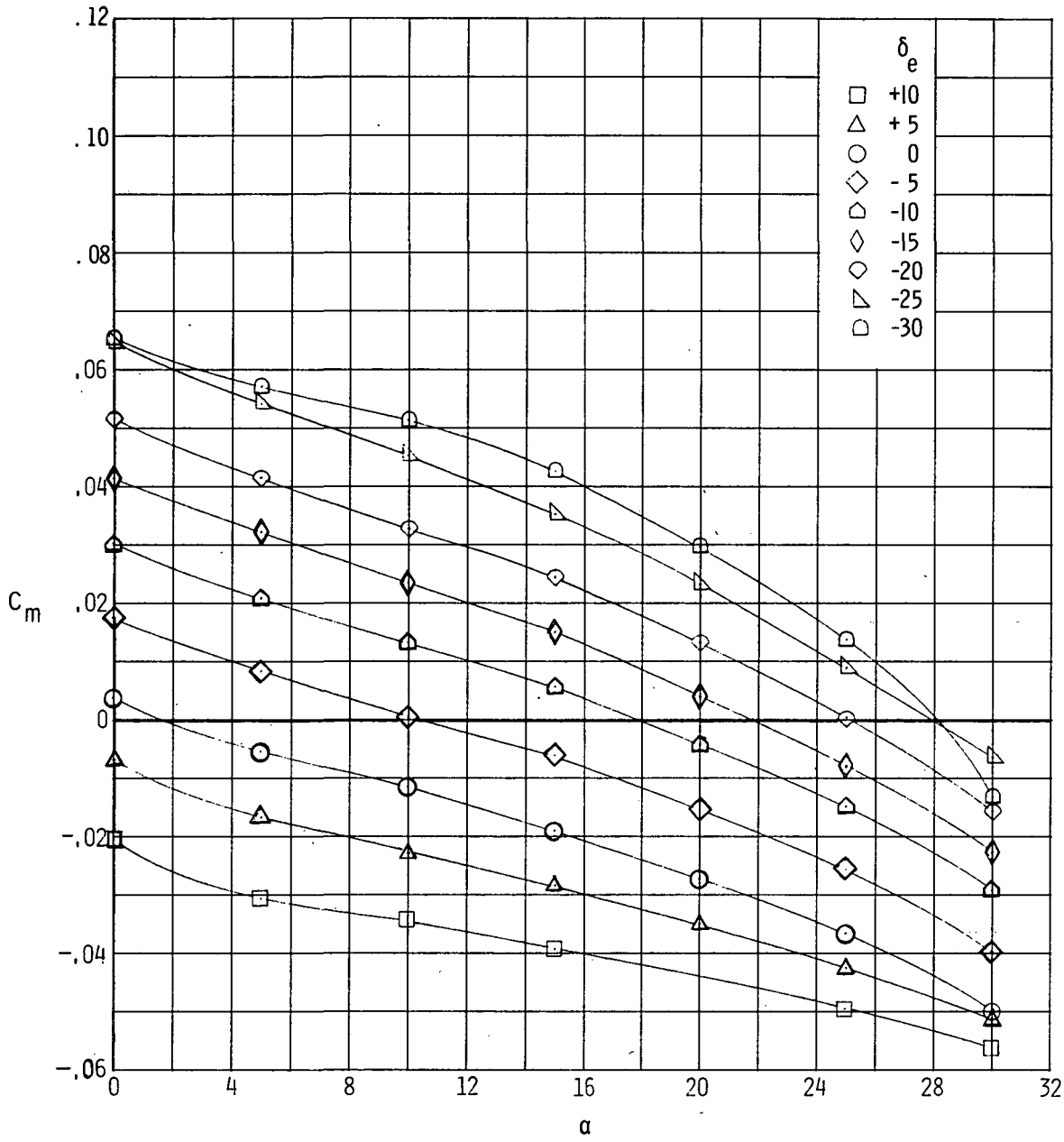

(c) Pitch.

Figure 6.- Continued.

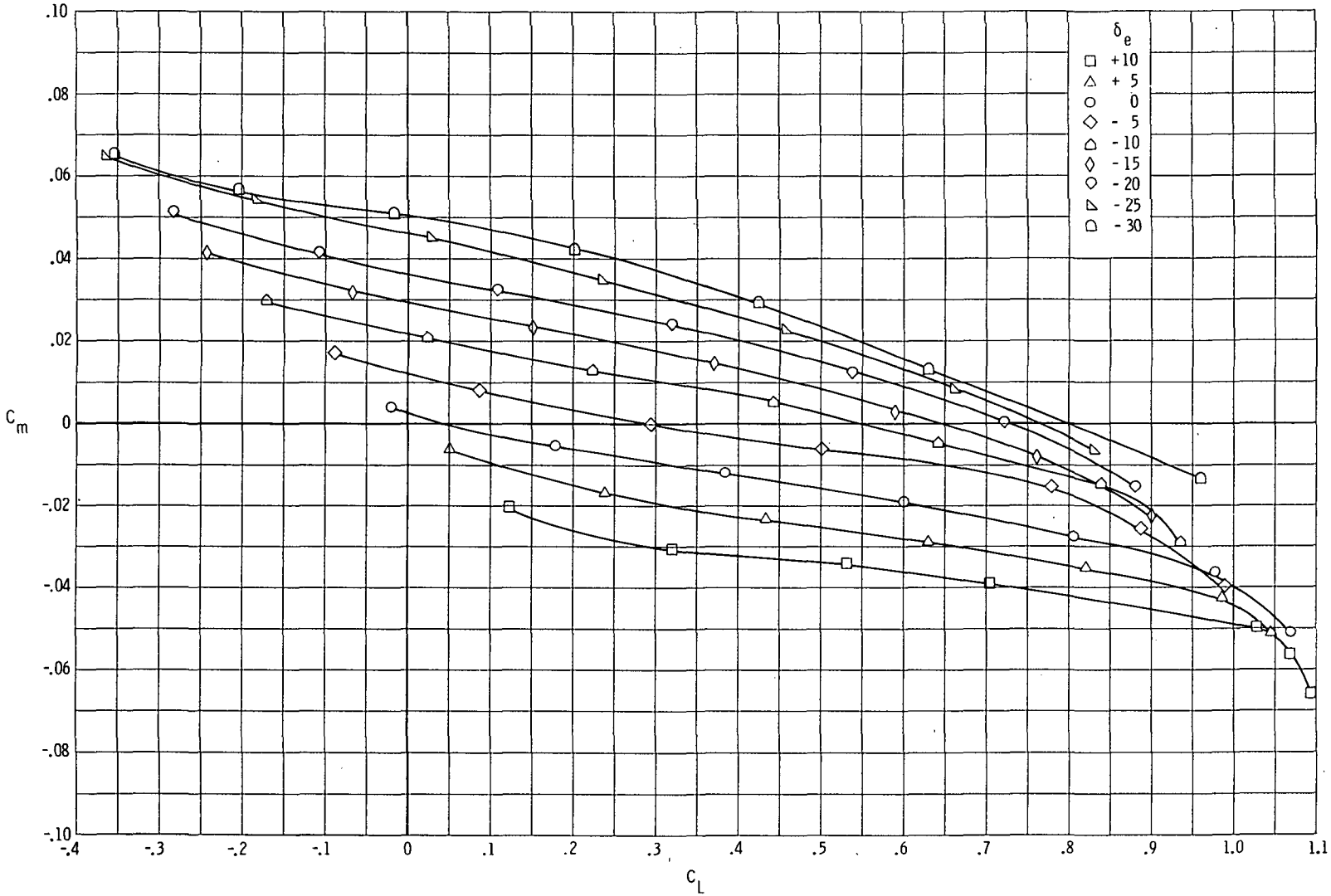

(d) Stability.

Figure 6.- Concluded.

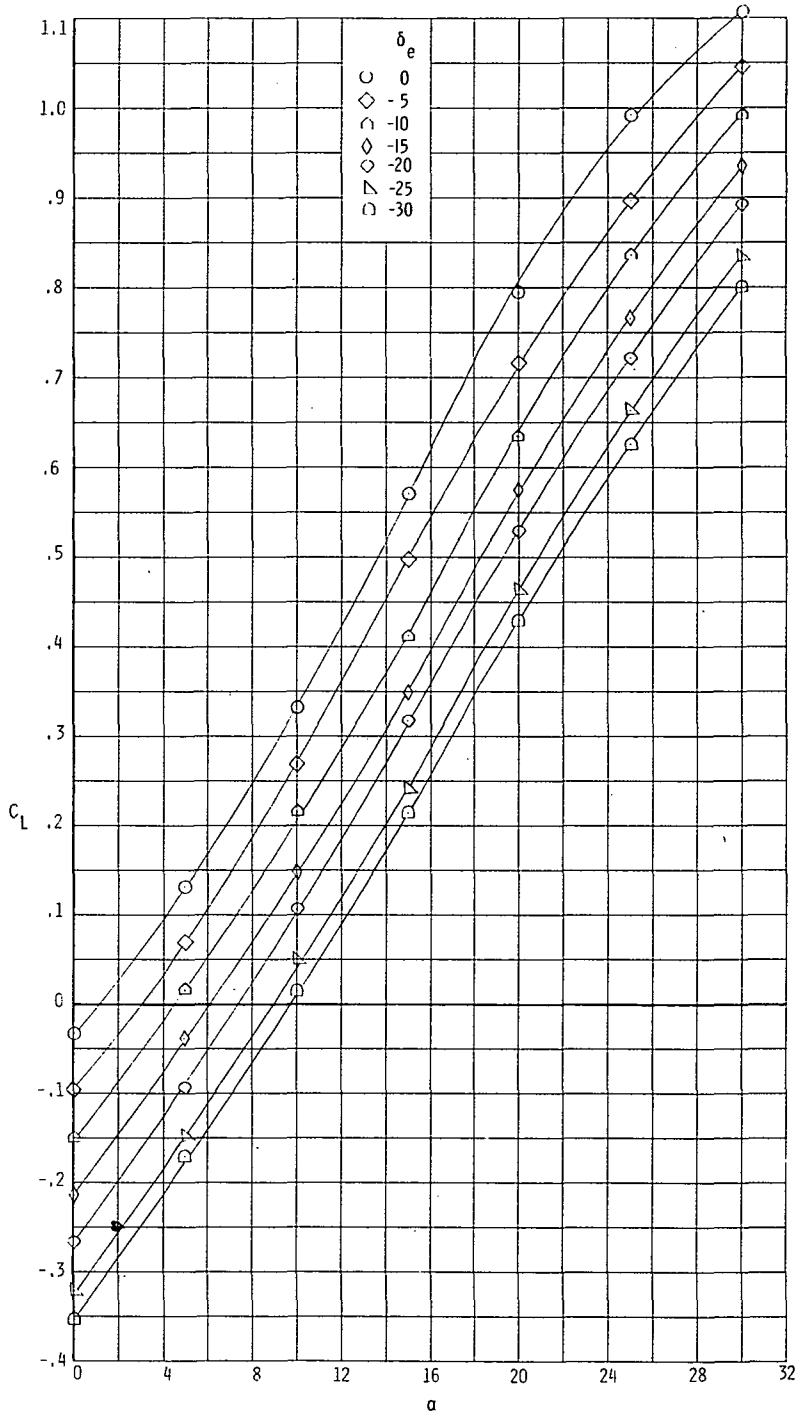

(a) Lift.

Figure 7.- Longitudinal characteristics of BWV_C configuration.

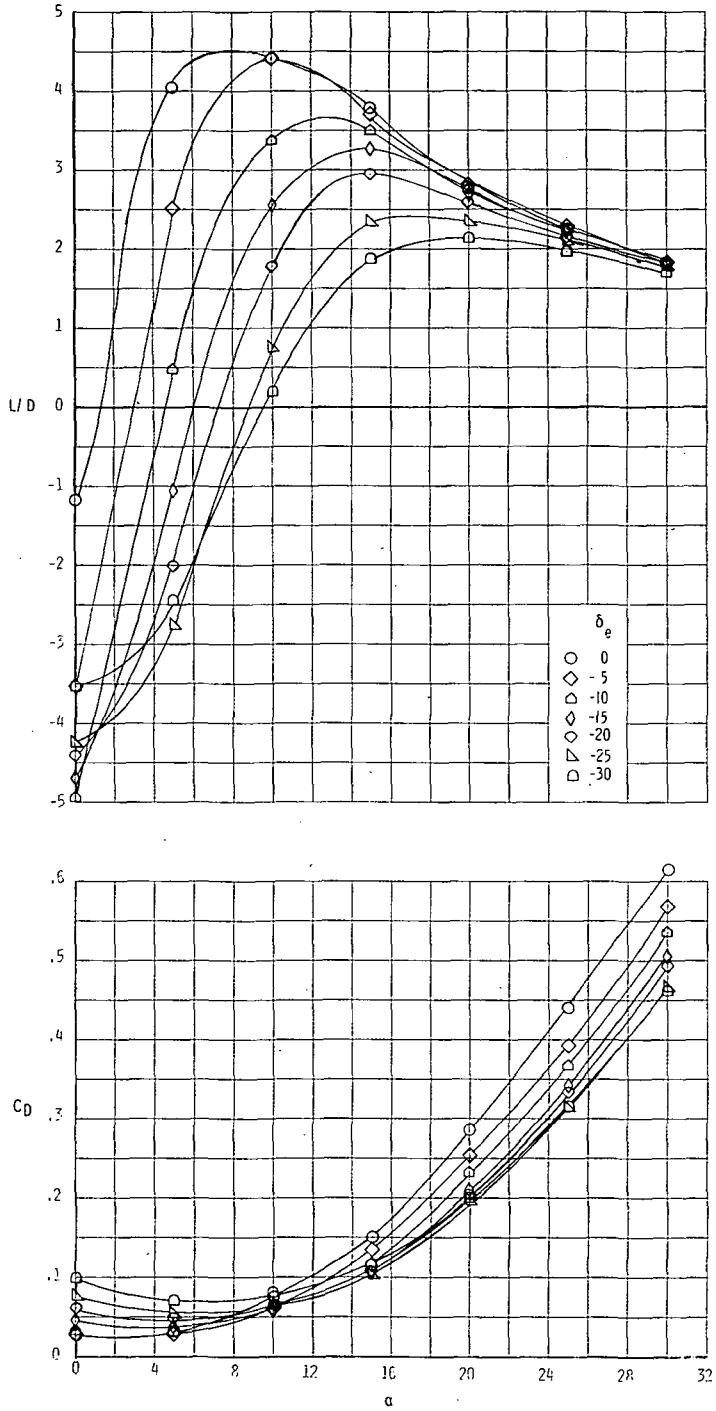

(b) Drag and lift-drag ratio.

Figure 7.- Continued.

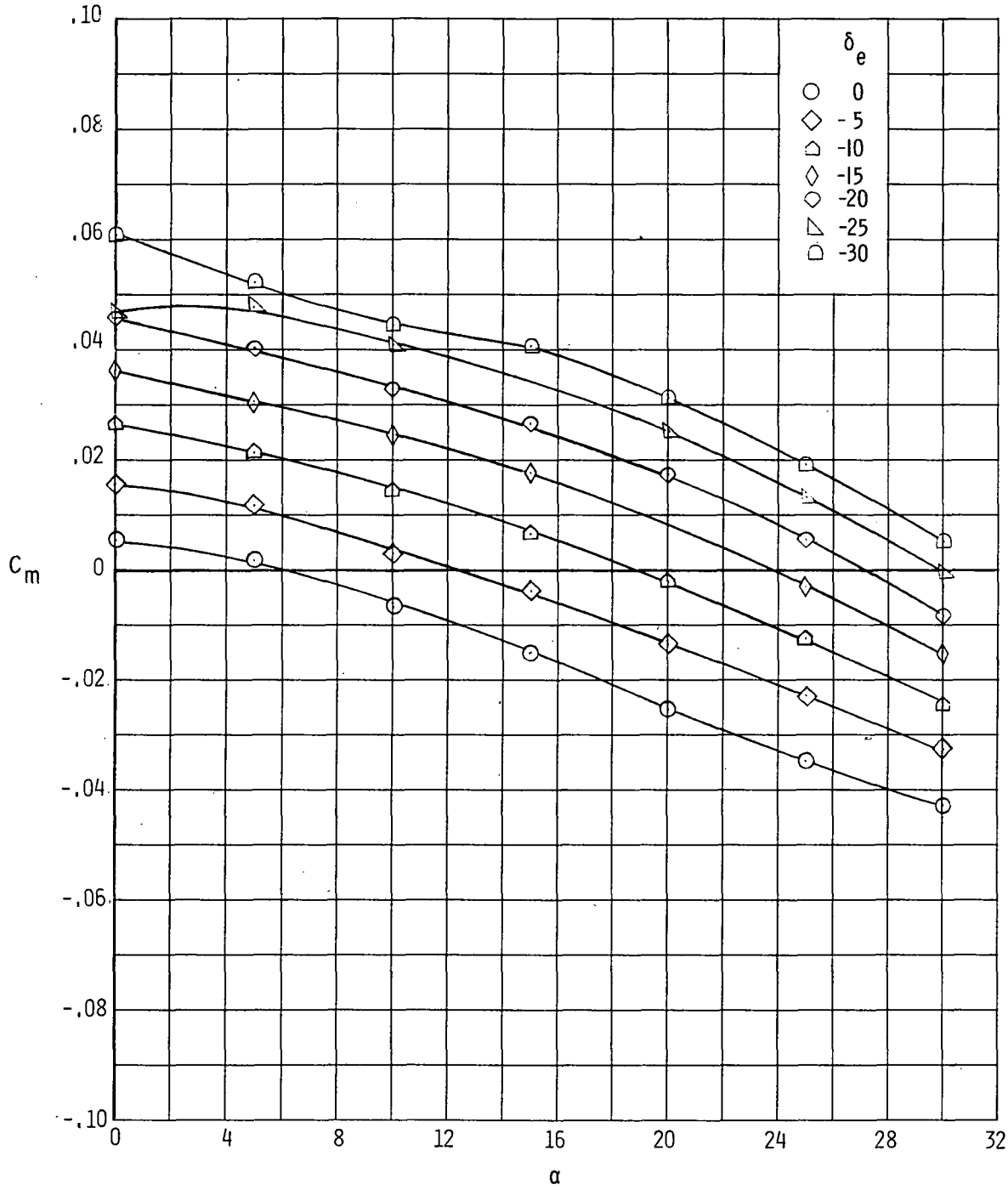

(c) Pitch.

Figure 7.- Continued.

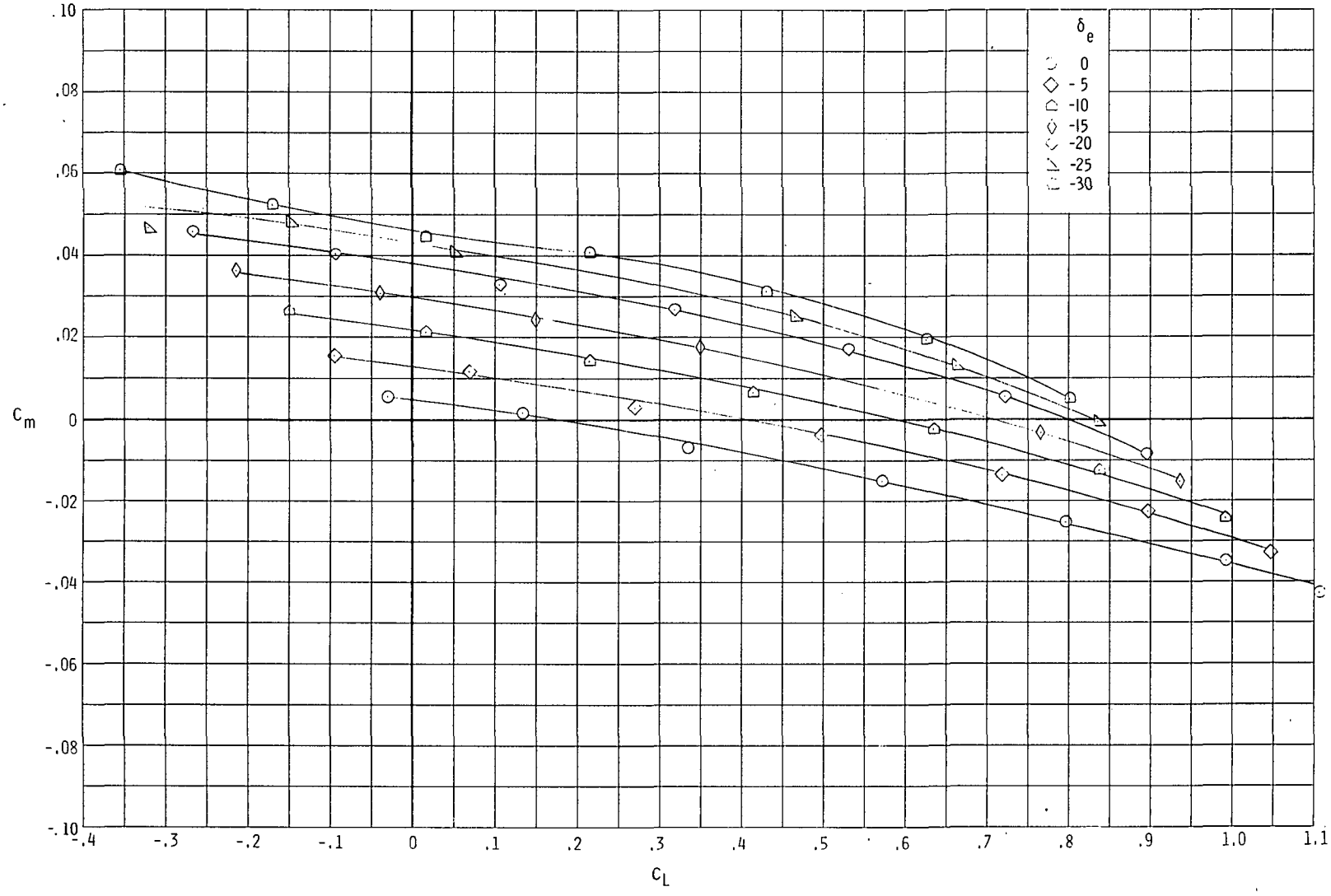

(d) Stability.

Figure 7.- Concluded.

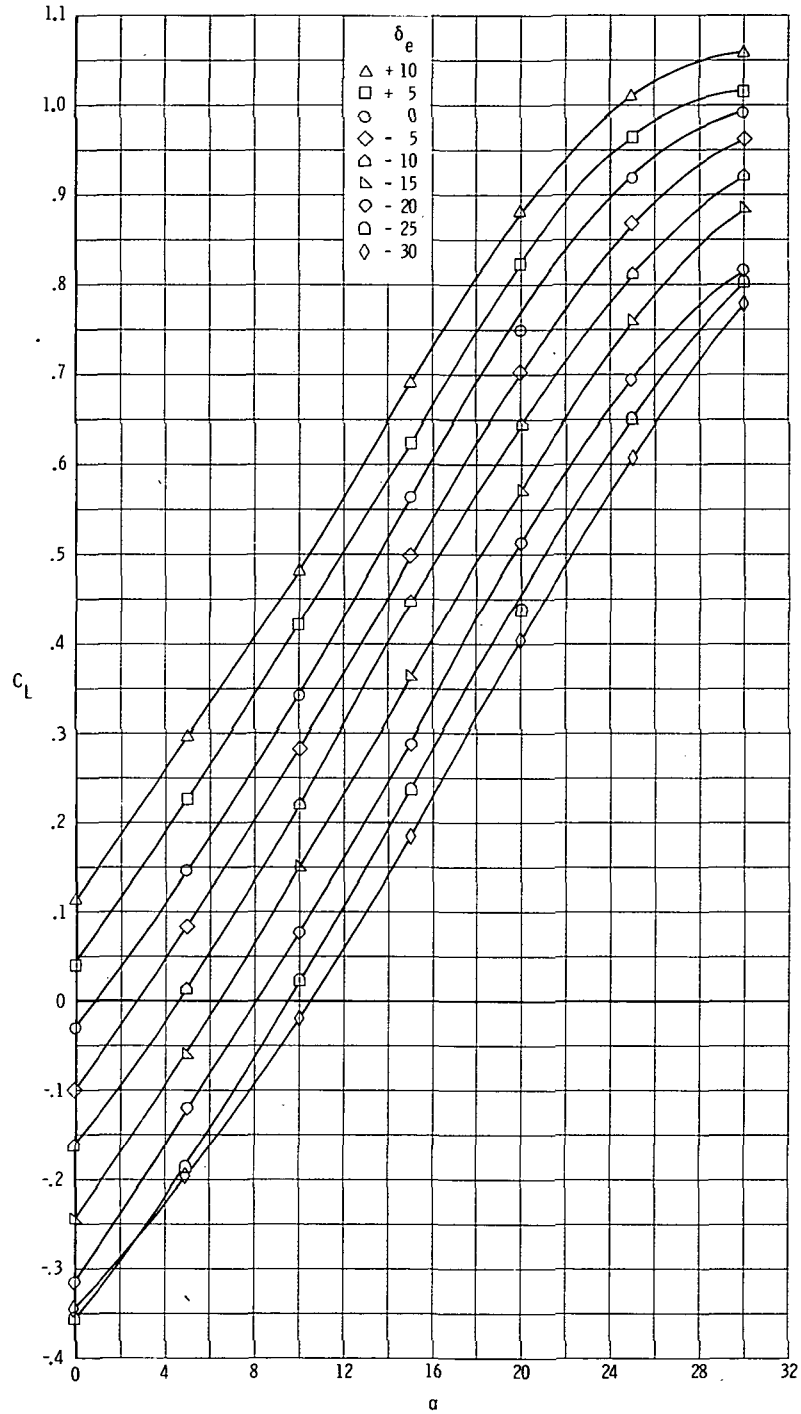

(a) Lift.

Figure 8.- Longitudinal characteristics of BWV_TE_O configuration.

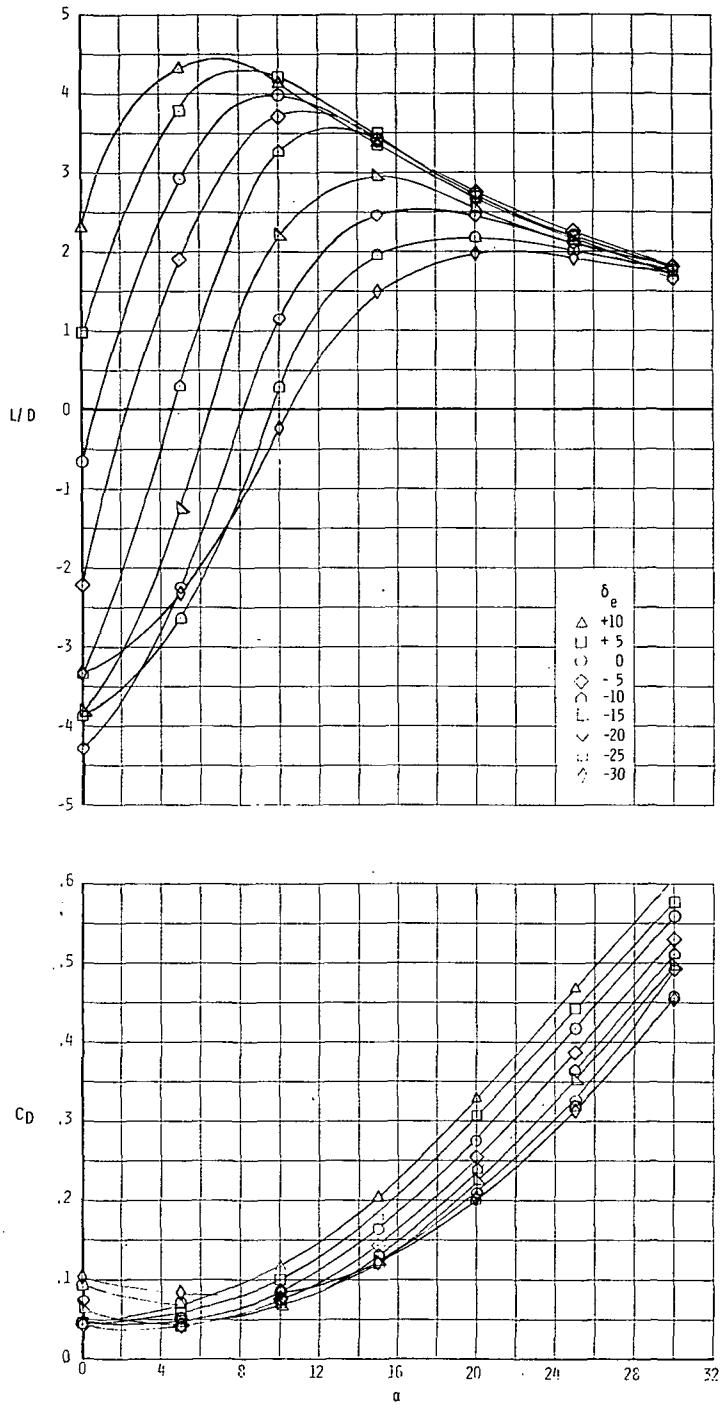

(b) Drag and lift-drag ratio.

Figure 8.- Continued.

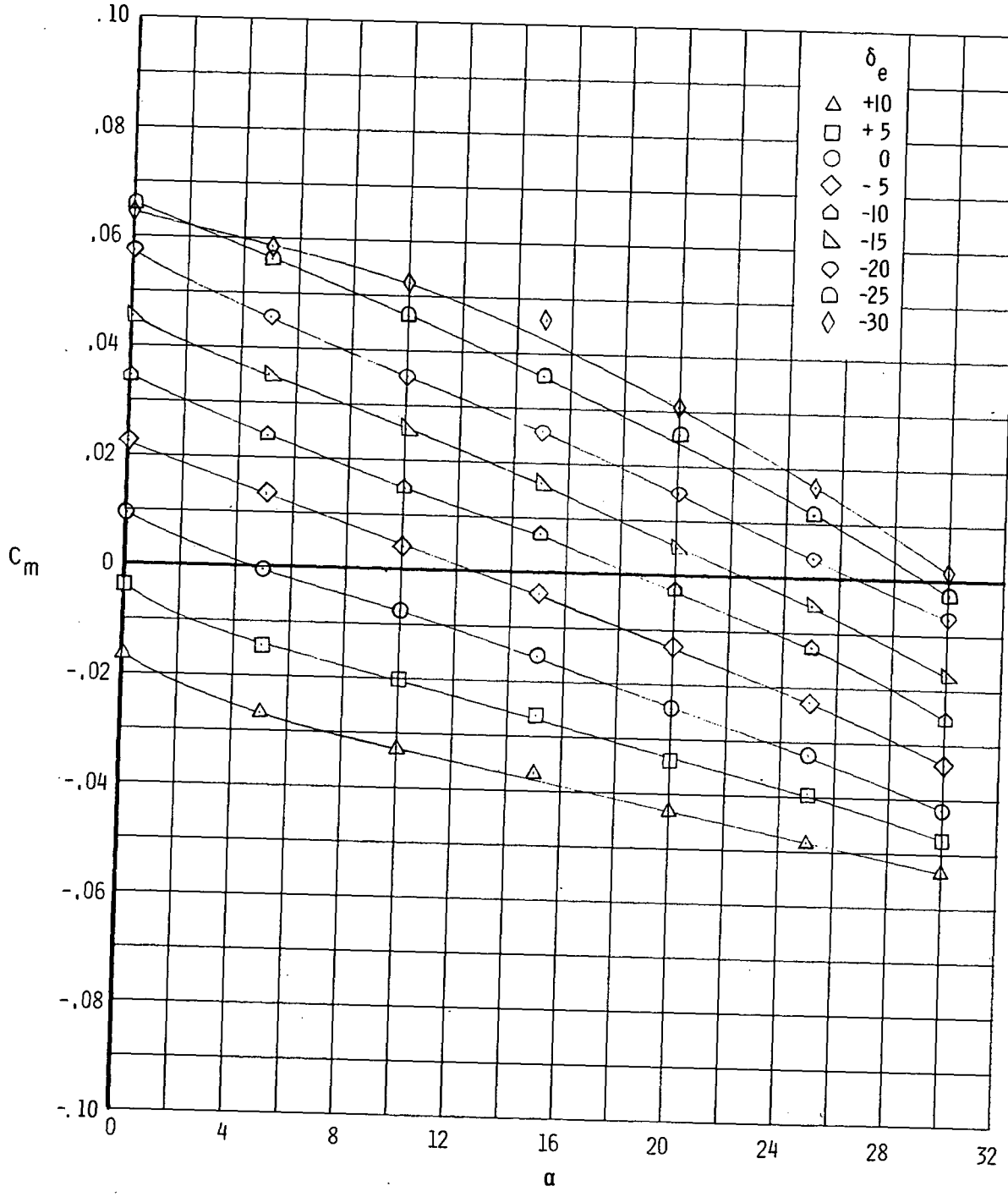

(c) Pitch.

Figure 8.- Continued.

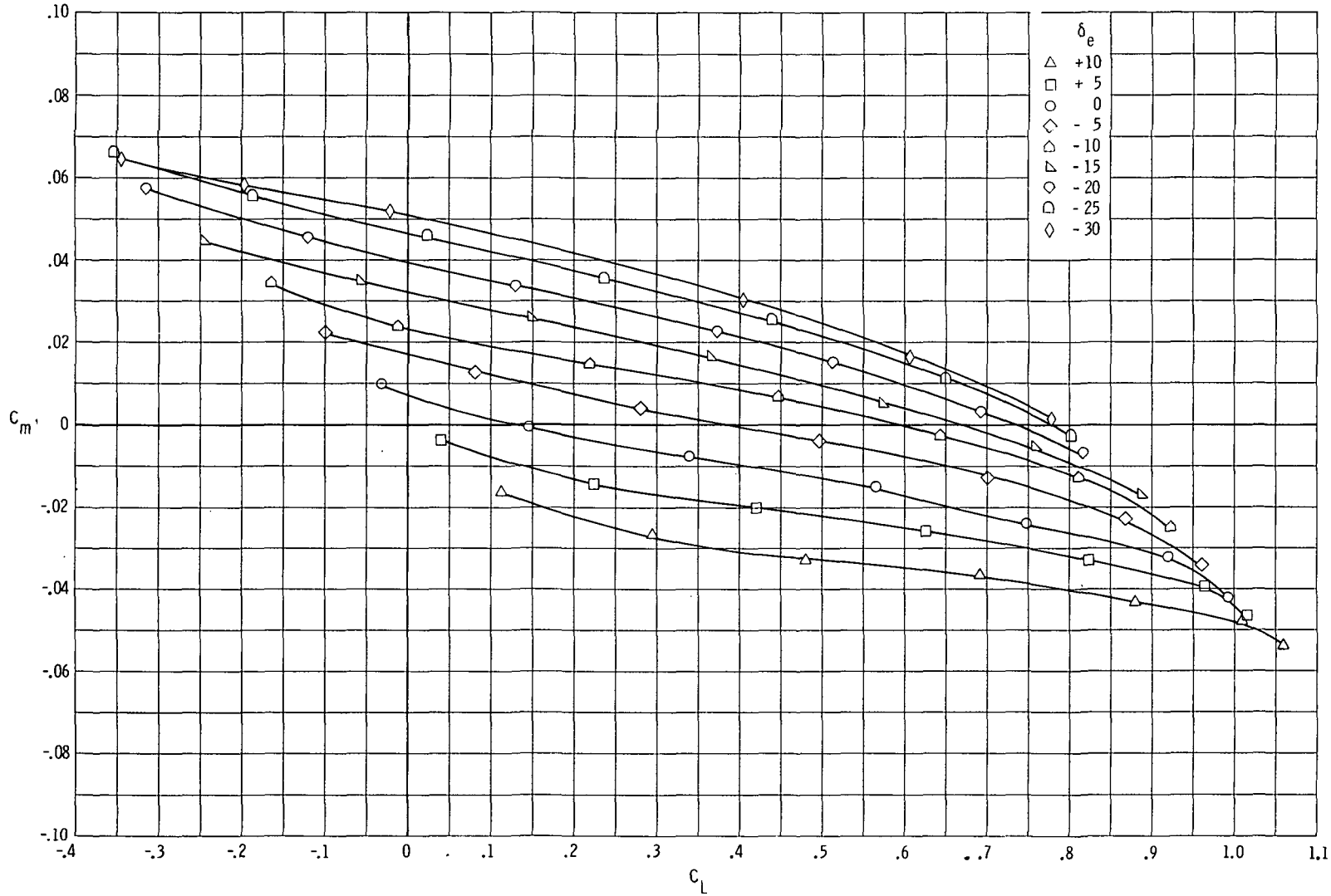

(d) Stability.

Figure 8.- Concluded.

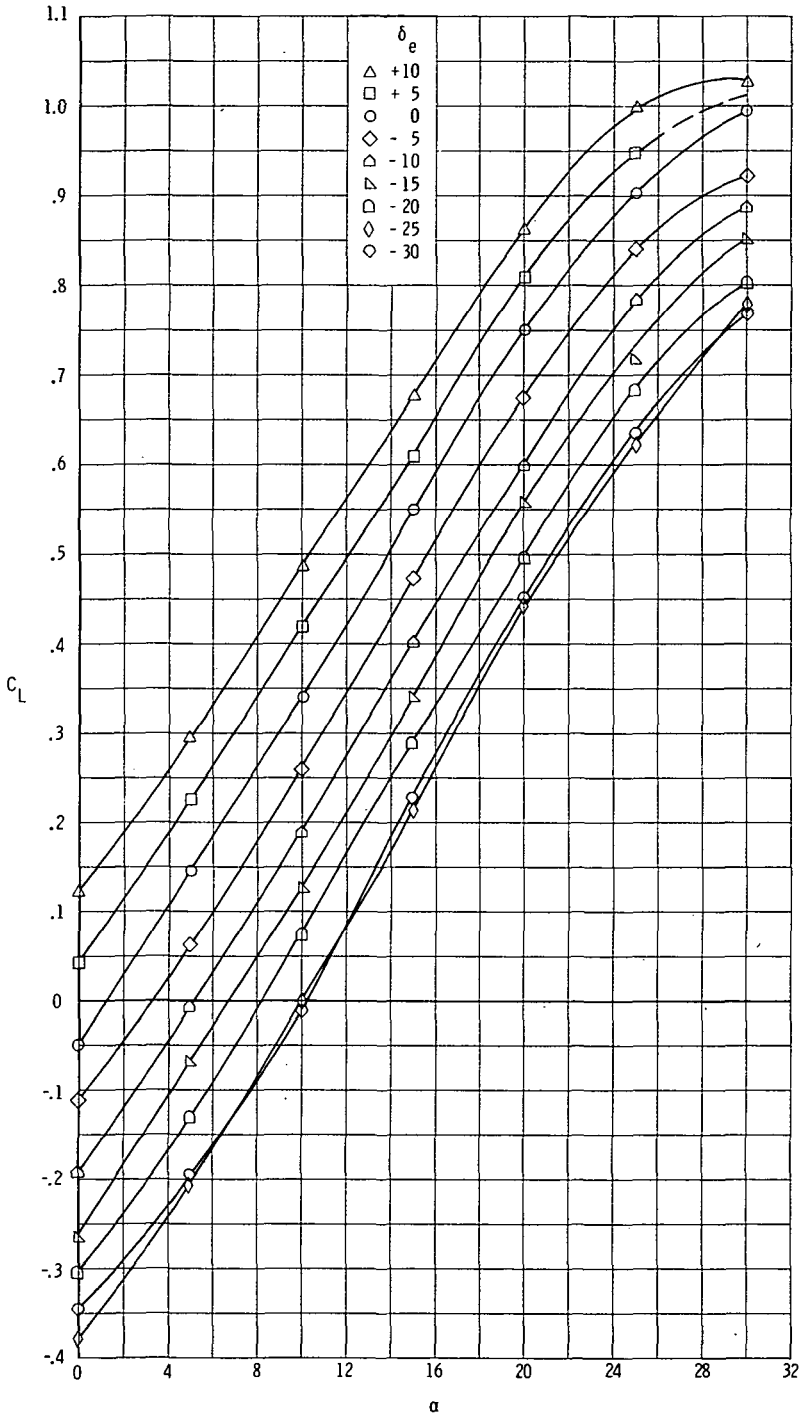

(a) Lift.

Figure 9.- Longitudinal characteristics of BWV_TE_R configuration.

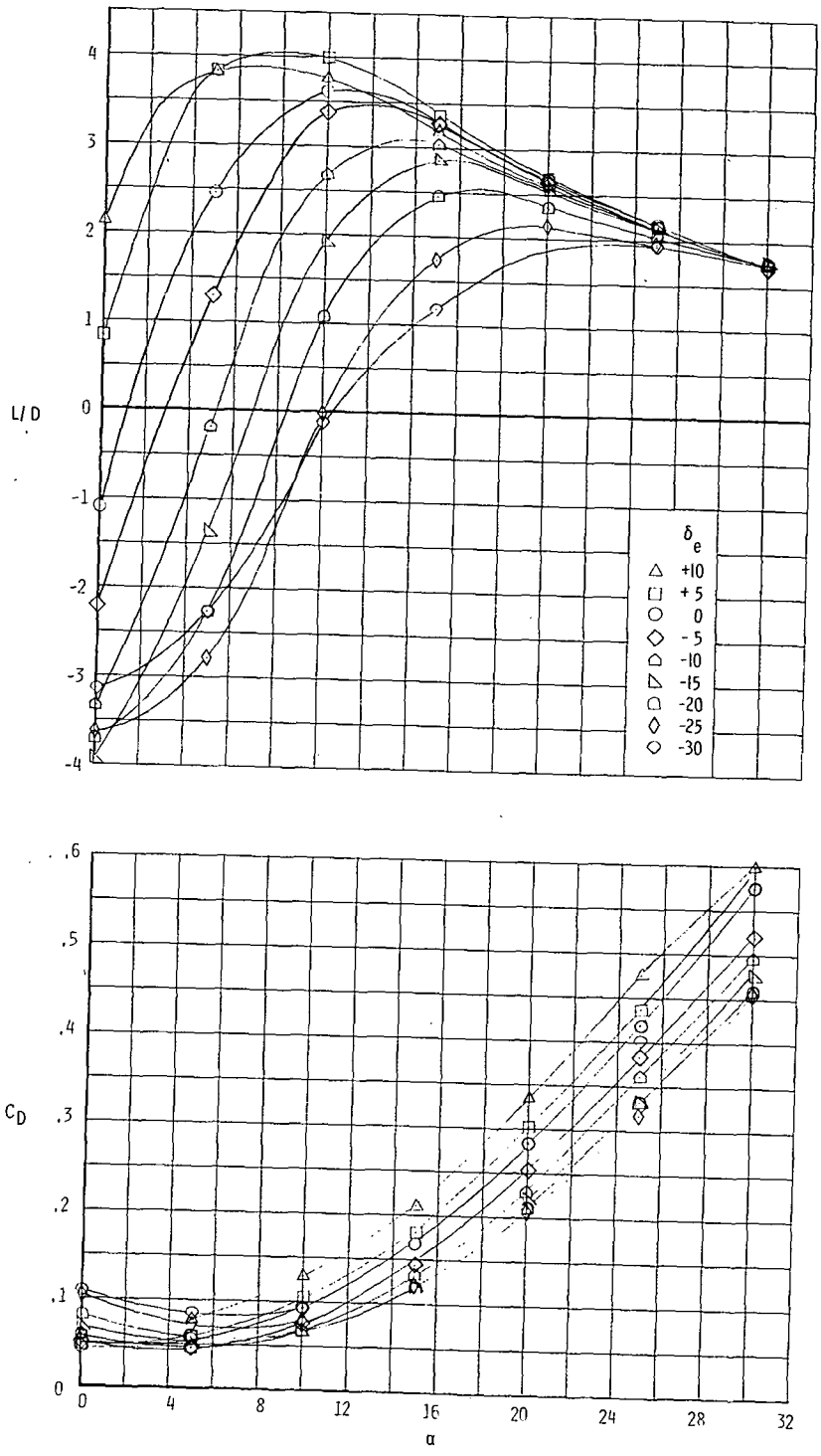

(b) Drag and lift-drag ratio.

Figure 9.- Continued.

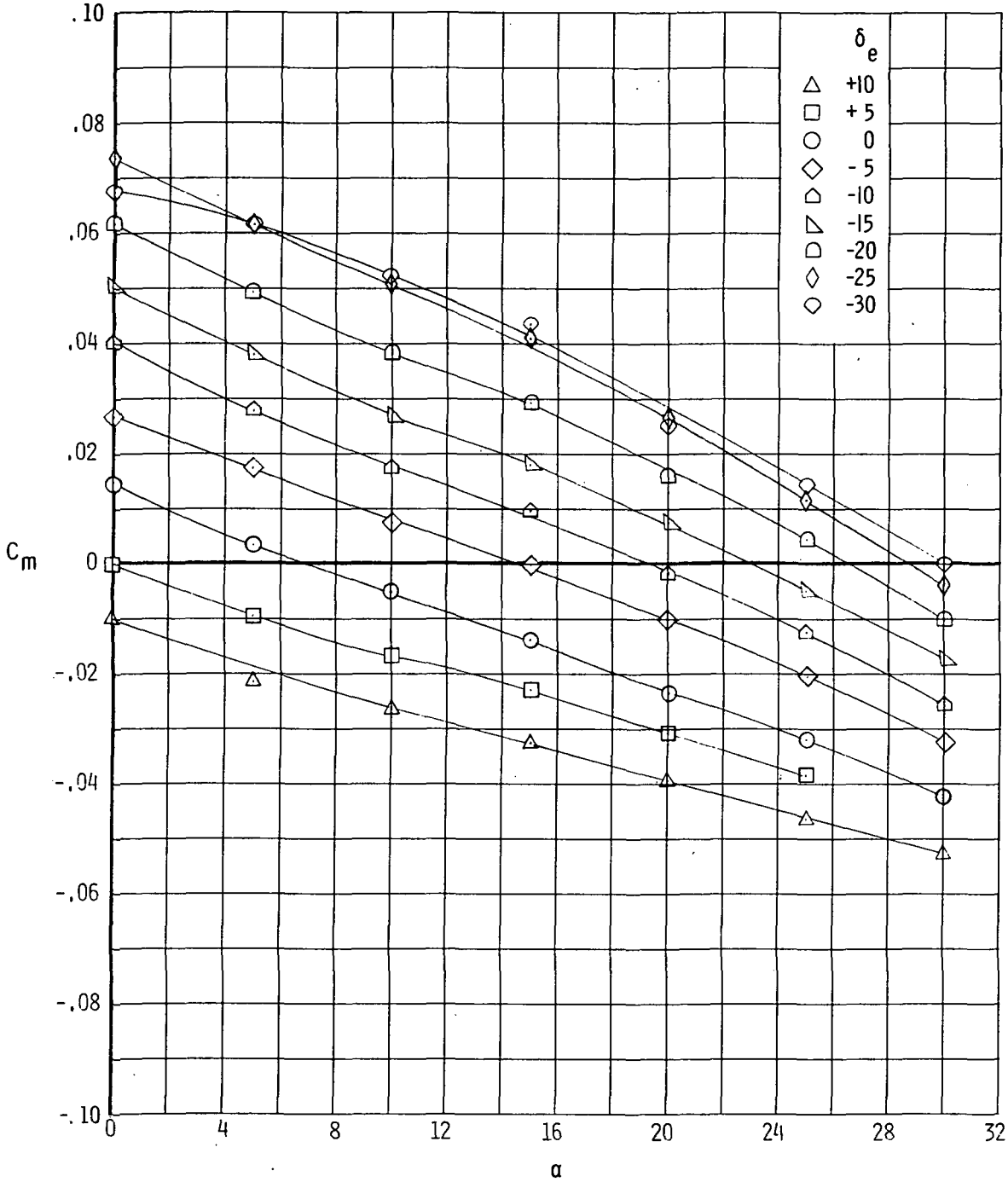

(c) Pitch.

Figure 9.- Continued.

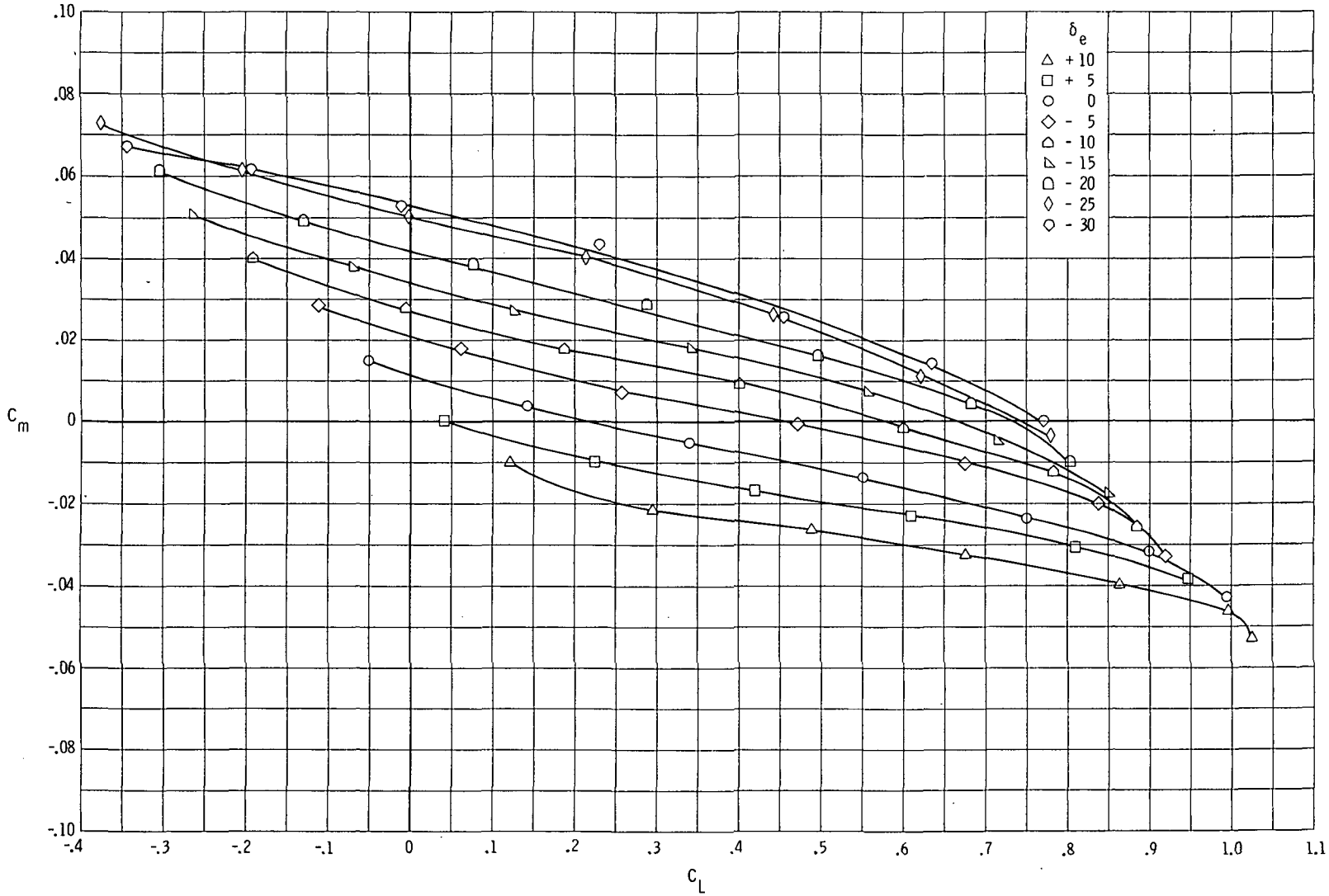

(d) Stability.

Figure 9.- Concluded.

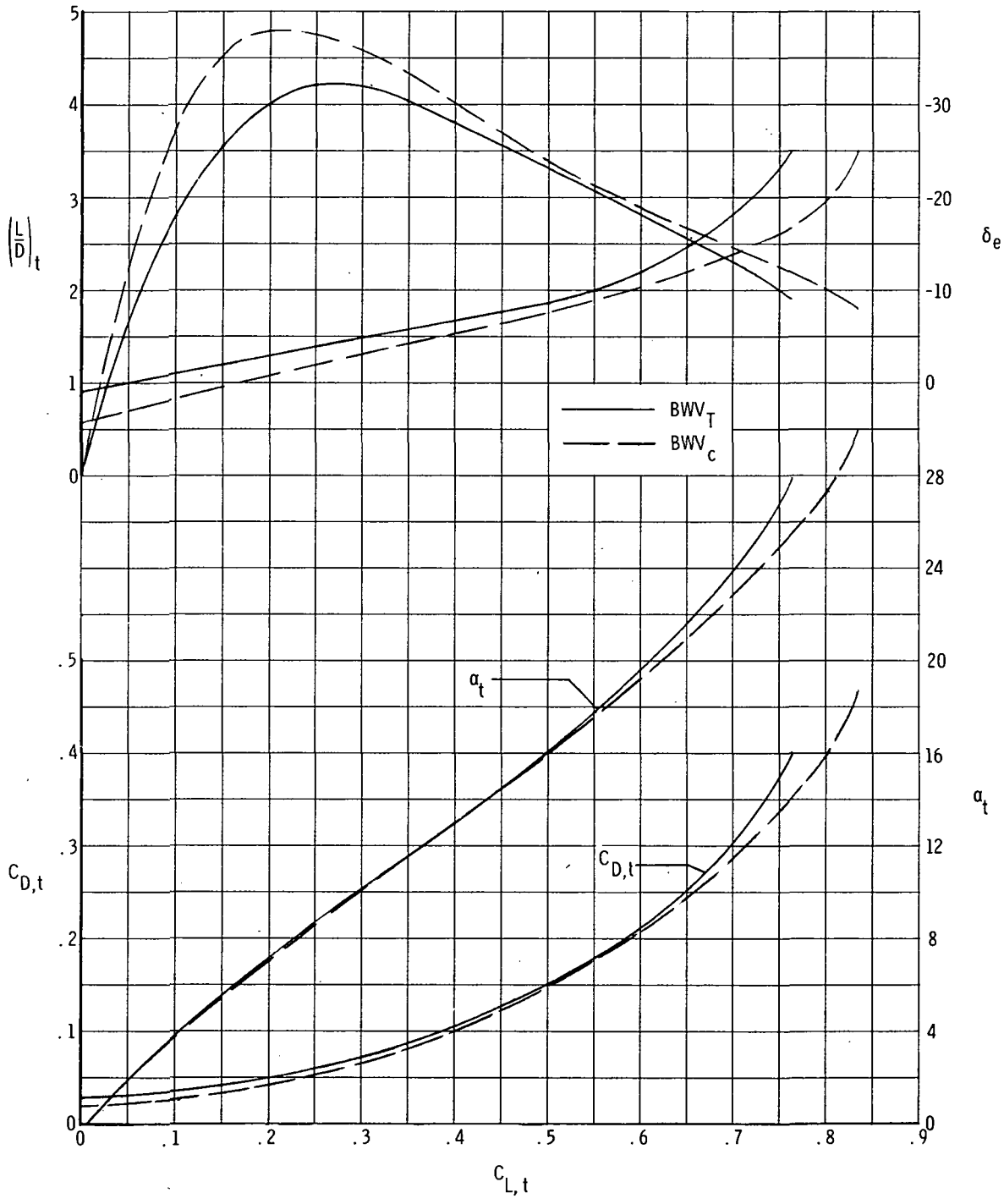

(a) Lift, drag, and lift-drag ratio.

Figure 10.- Longitudinal characteristics at trim of BWV$_T$ and BWV$_c$ configurations.

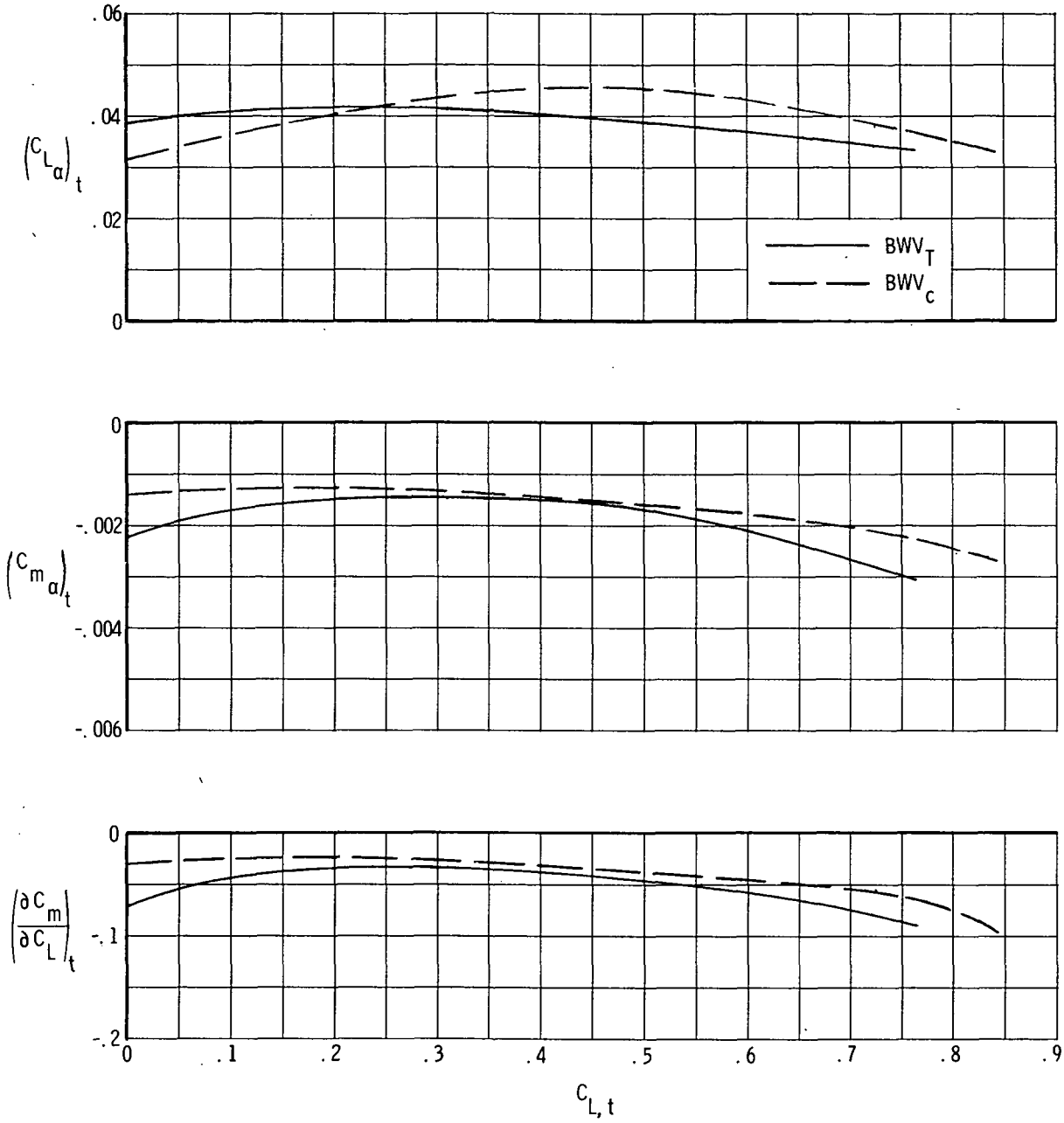

(b) Lift- and pitch-curve slopes and longitudinal stability.

Figure 10.- Concluded.

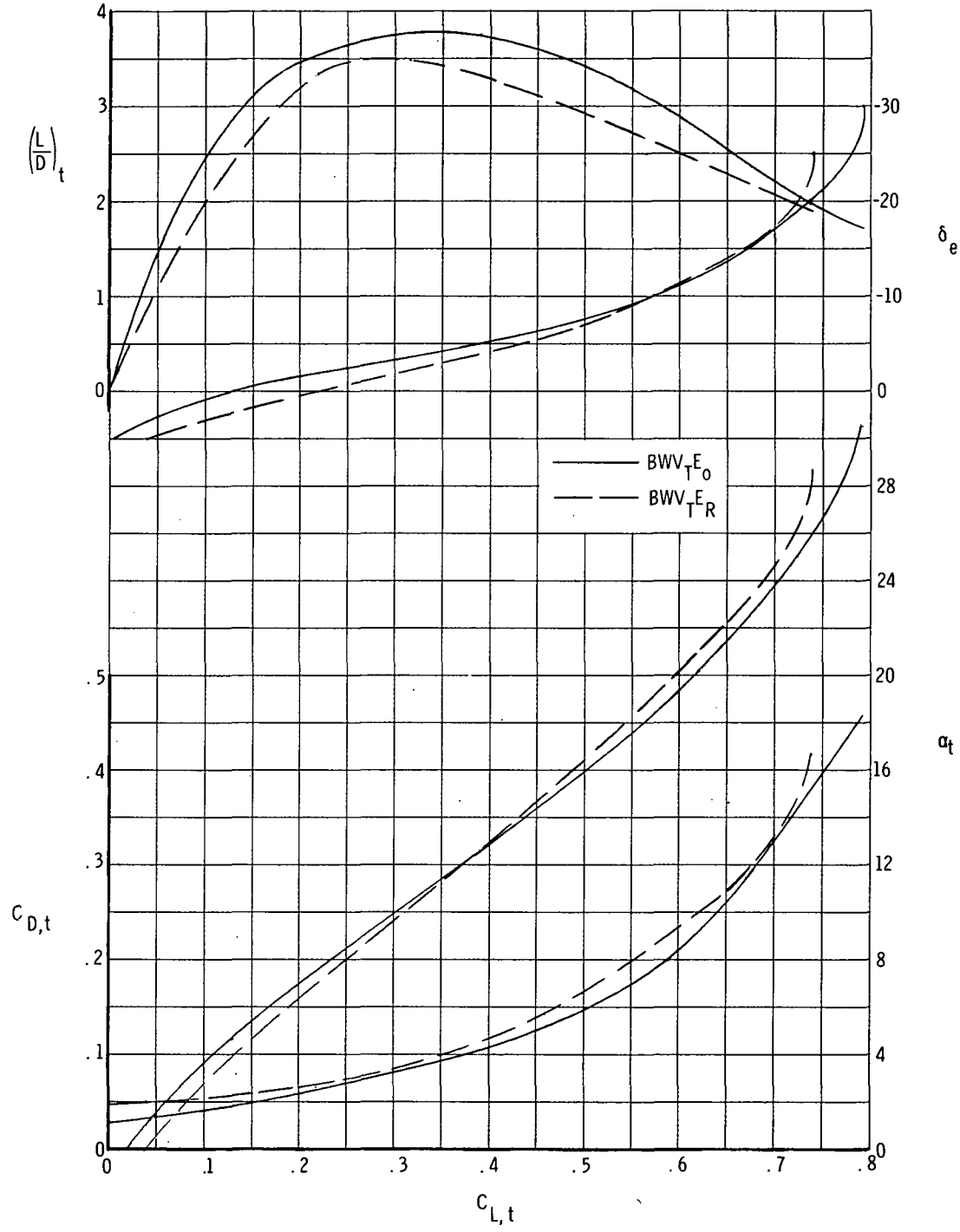

(a) Lift, drag, and lift-drag ratio.

Figure 11.- Longitudinal characteristics at trim of BWV_TE_O and BWV_TE_R configurations.

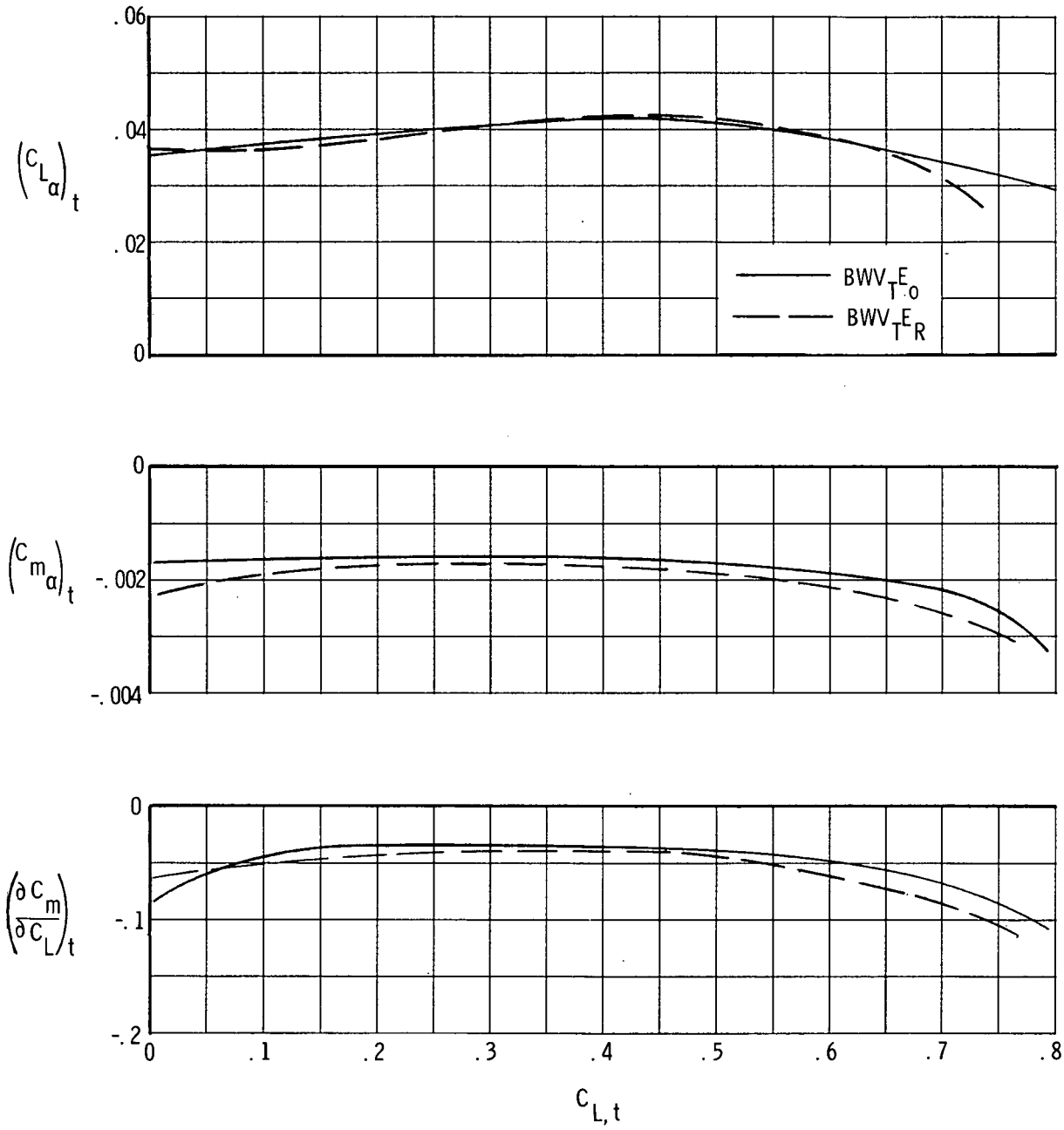

(b) Lift- and pitch-curve slopes and longitudinal stability.

Figure 11.- Concluded.

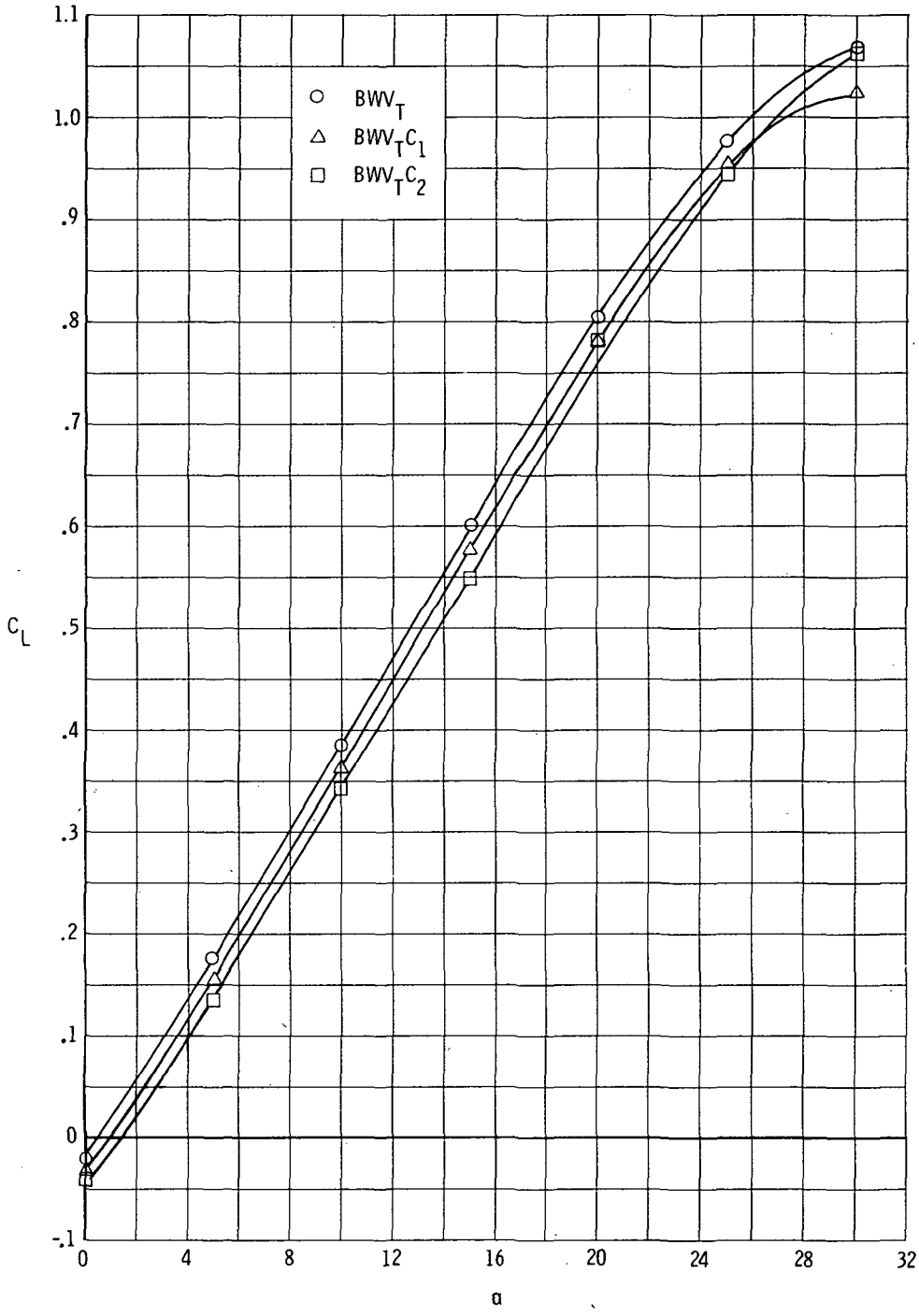

(a) Lift.

Figure 12.- Longitudinal characteristics of BWV_TC_1 and BWV_TC_2 configurations. Zero canard deflection.

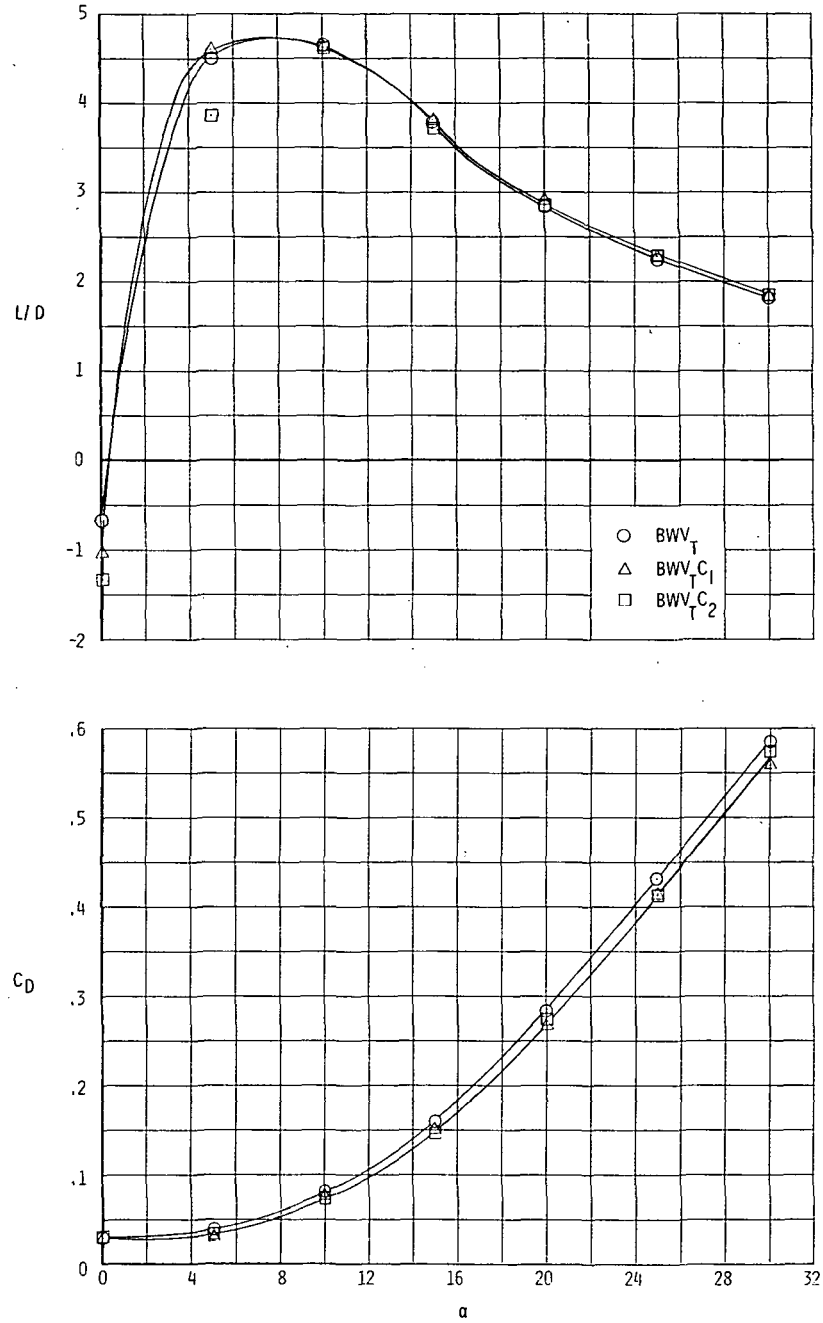

(b) Drag and lift-drag ratio.

Figure 12.- Continued.

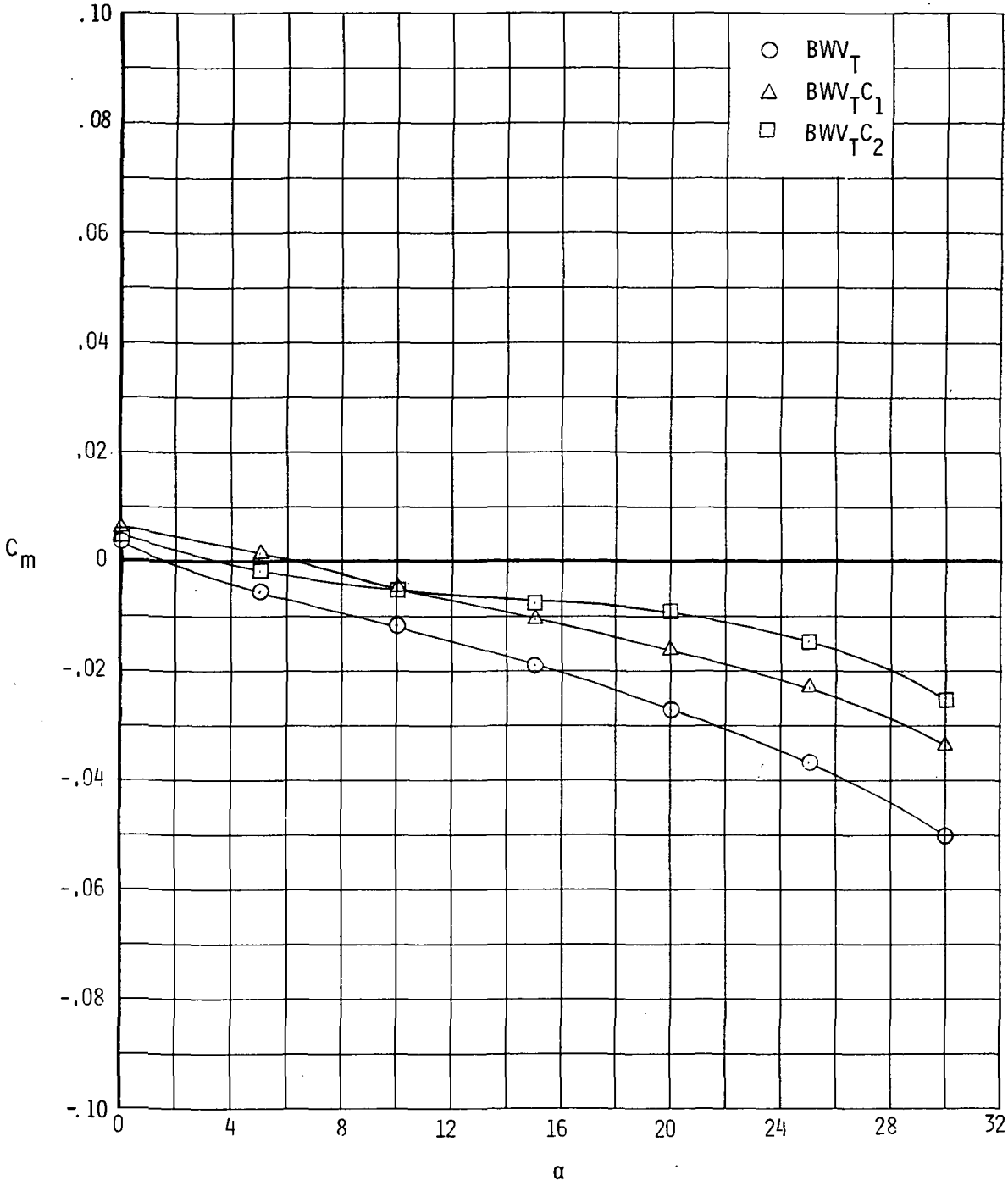

(c) Pitch.

Figure 12.- Continued.

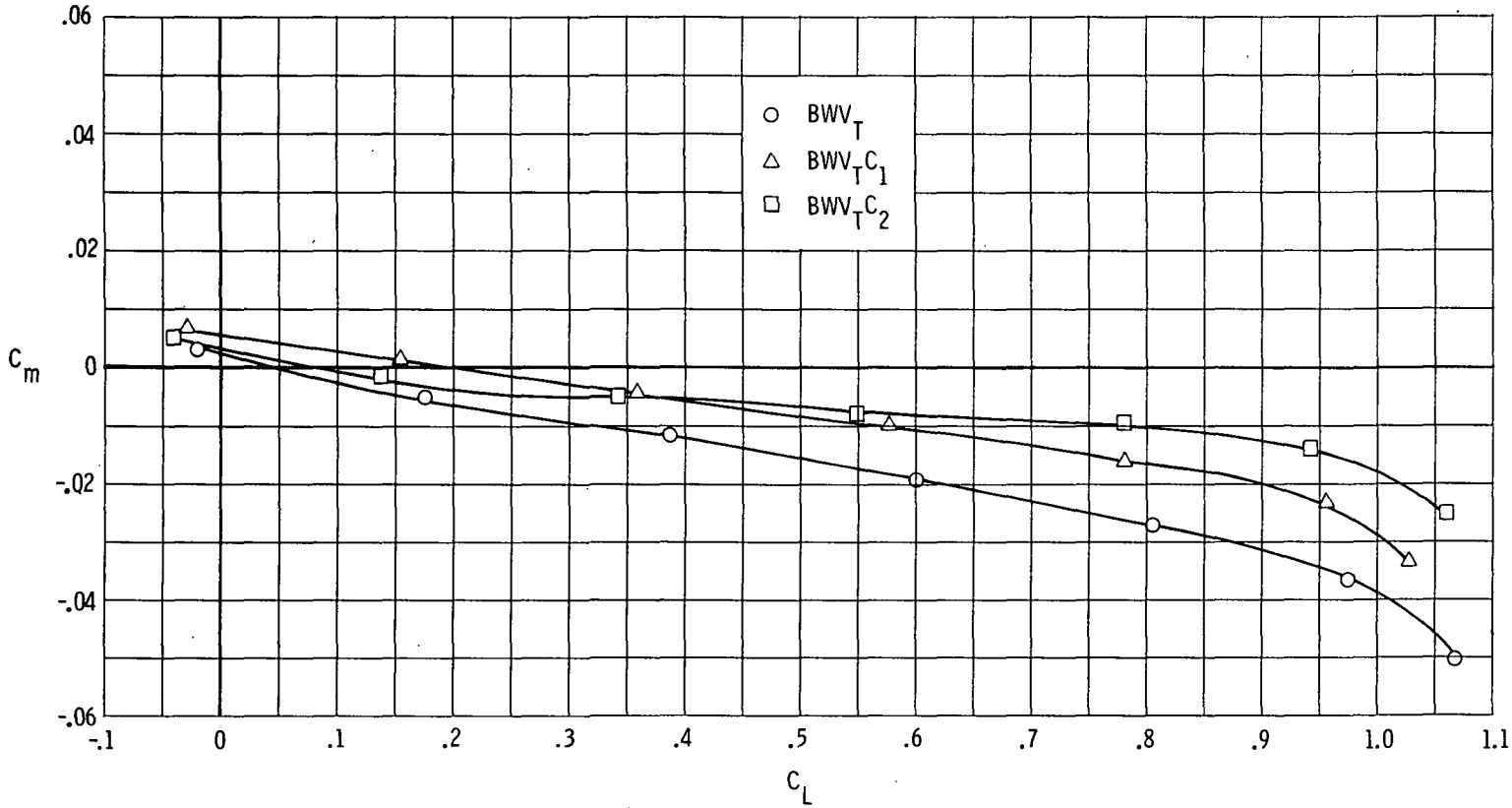

(d) Stability.

Figure 12.- Concluded.

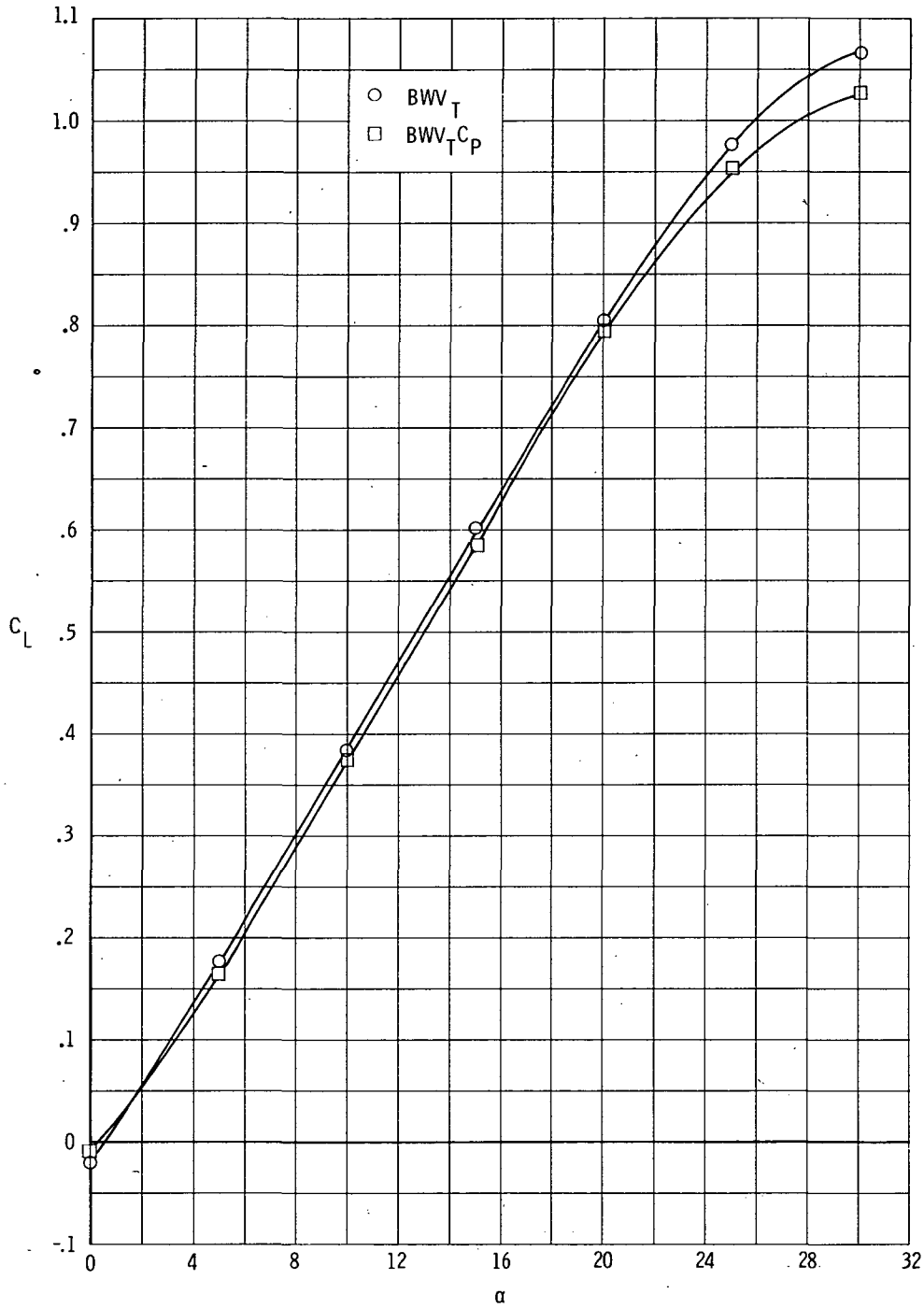

(a) Lift.

Figure 13.- Longitudinal characteristics of BWV_T and BWV_TC_P configurations.

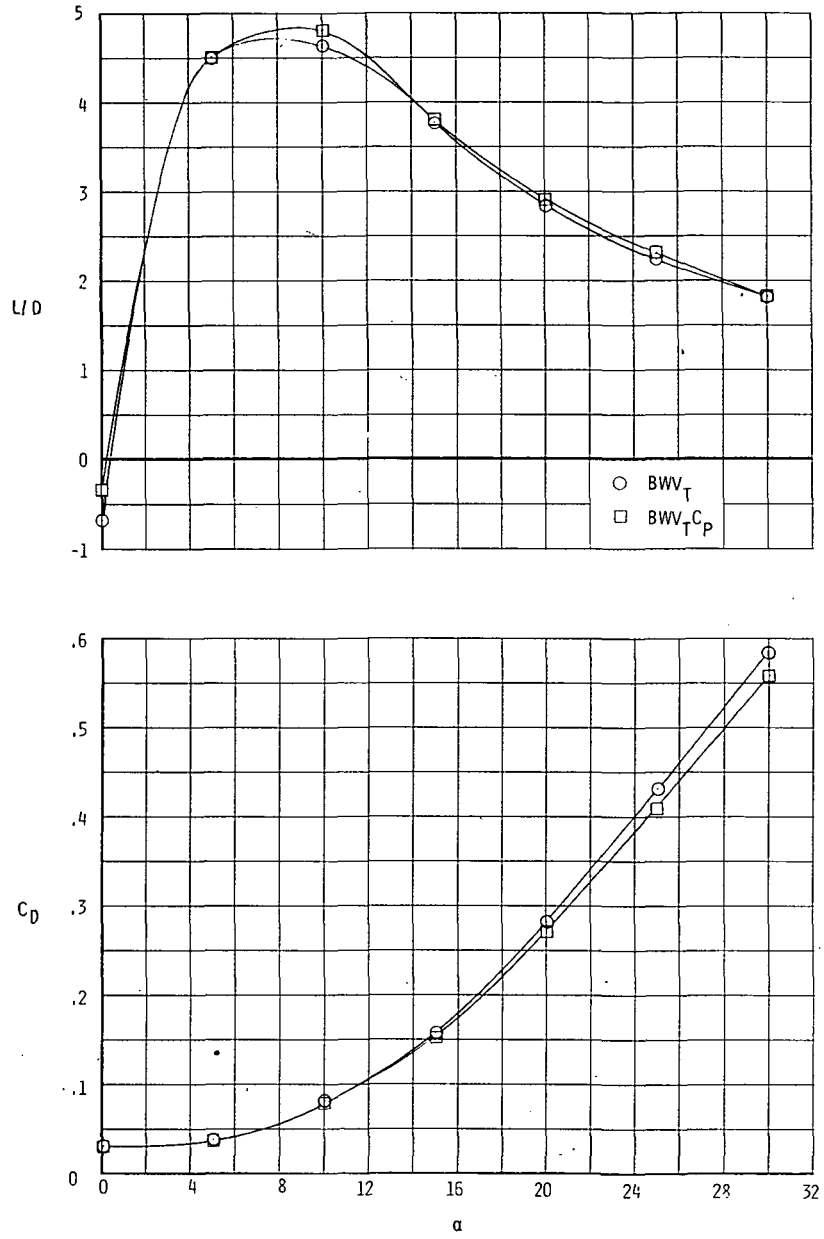

(b) Drag and lift-drag ratio.

Figure 13.- Continued.

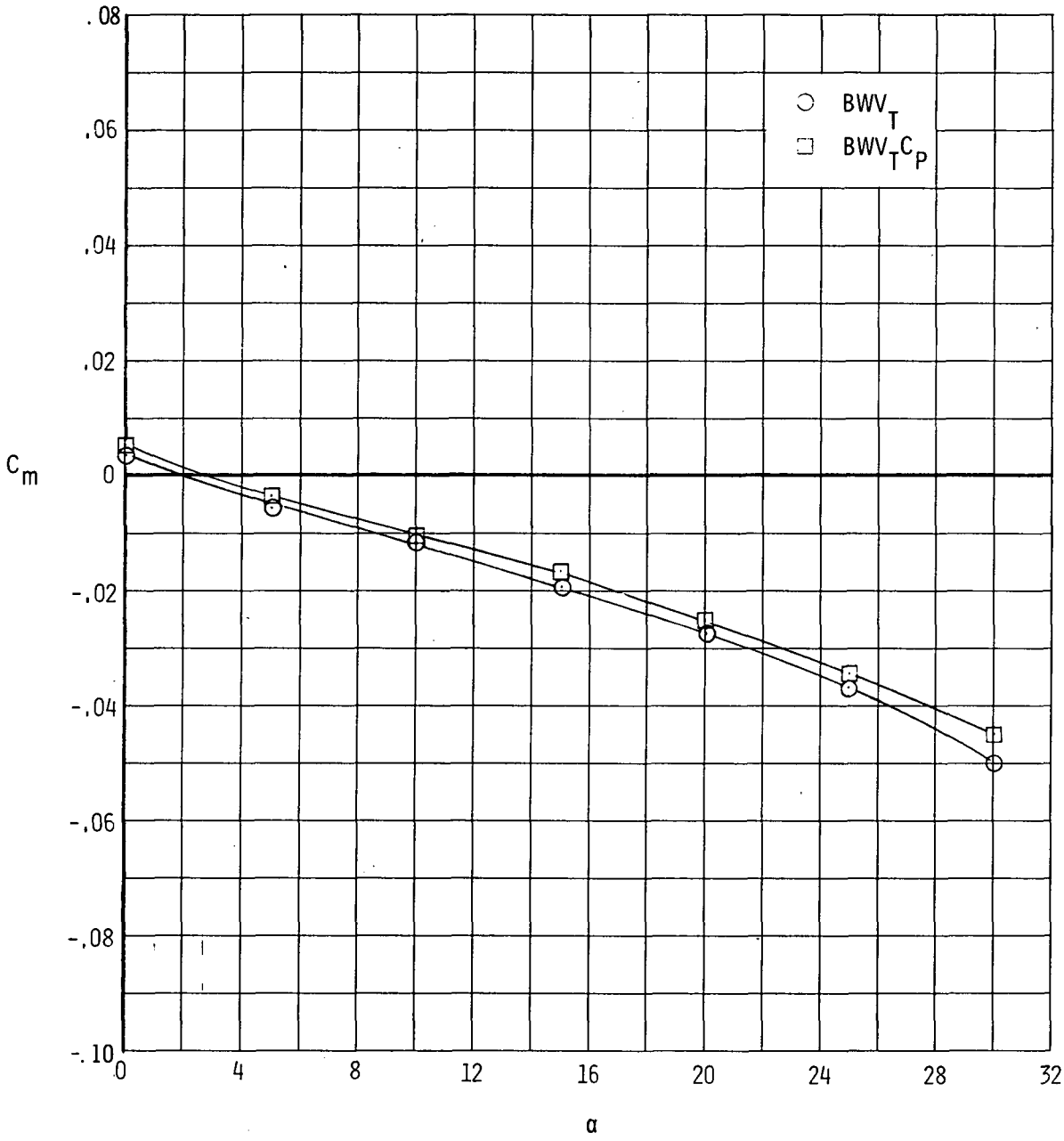

(c) Pitch.

Figure 13.- Continued.

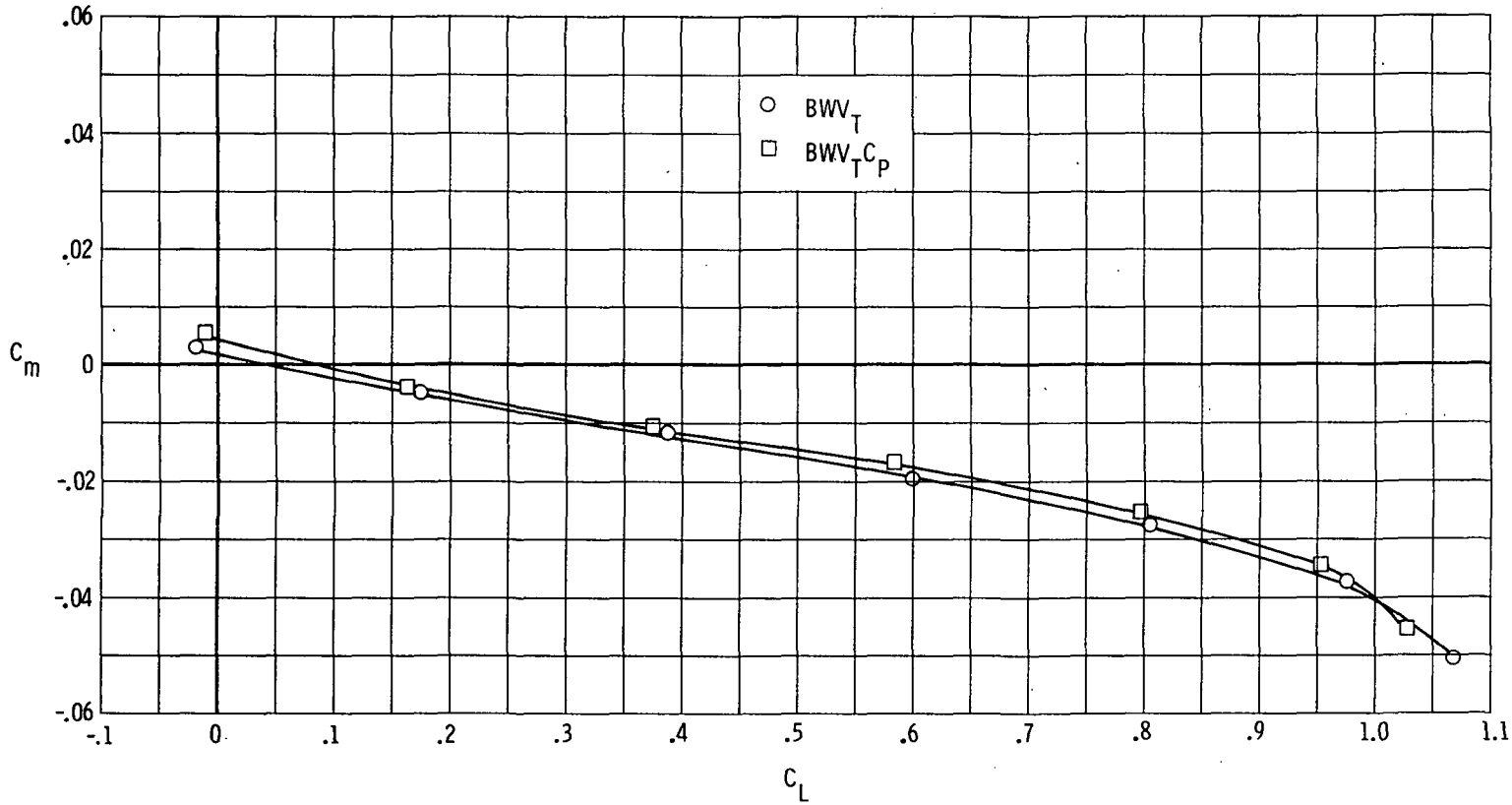

(d) Stability.

Figure 13.- Concluded.

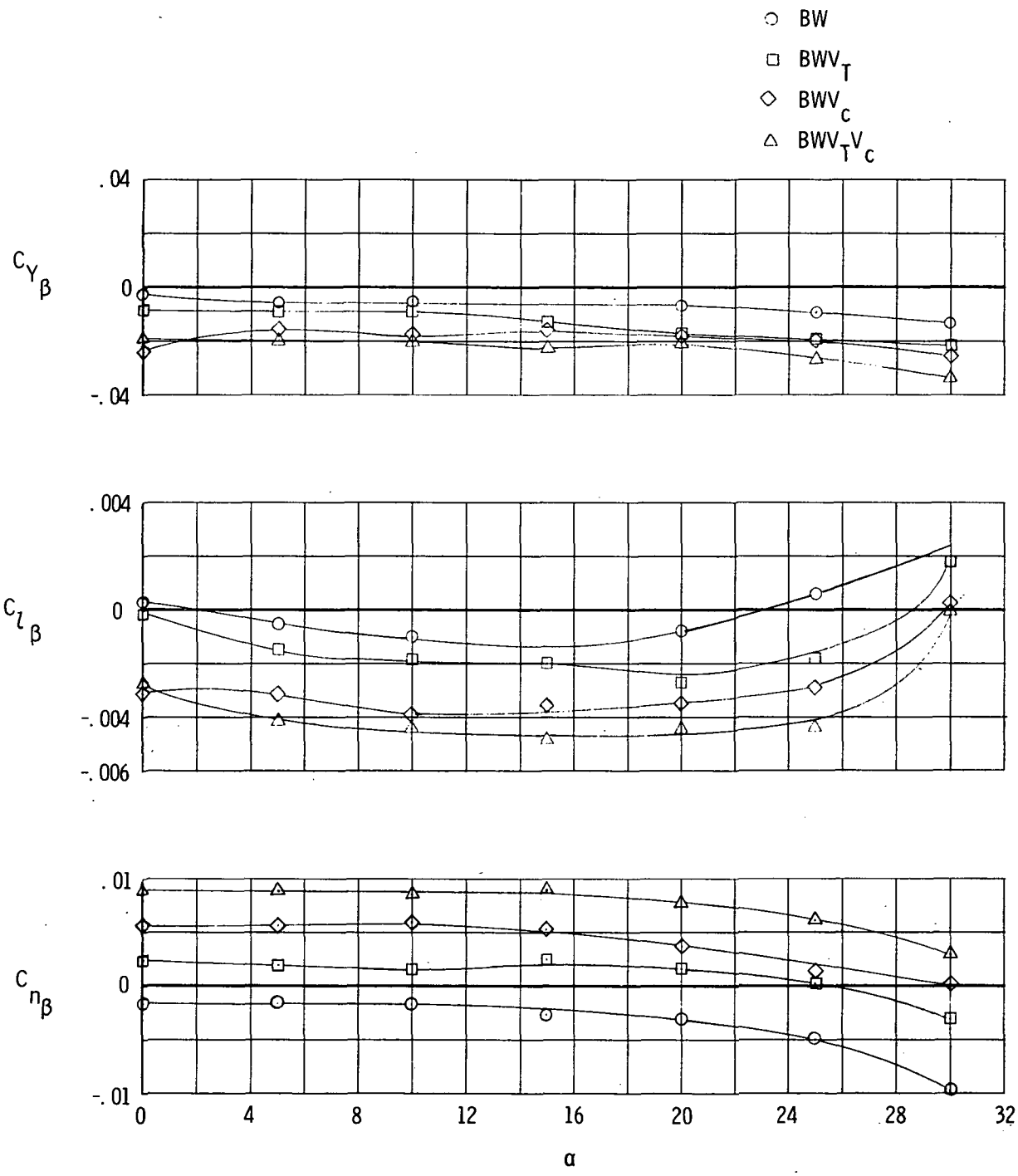

(a) Effect of vertical-tail location.

Figure 14.- Lateral and directional stability.

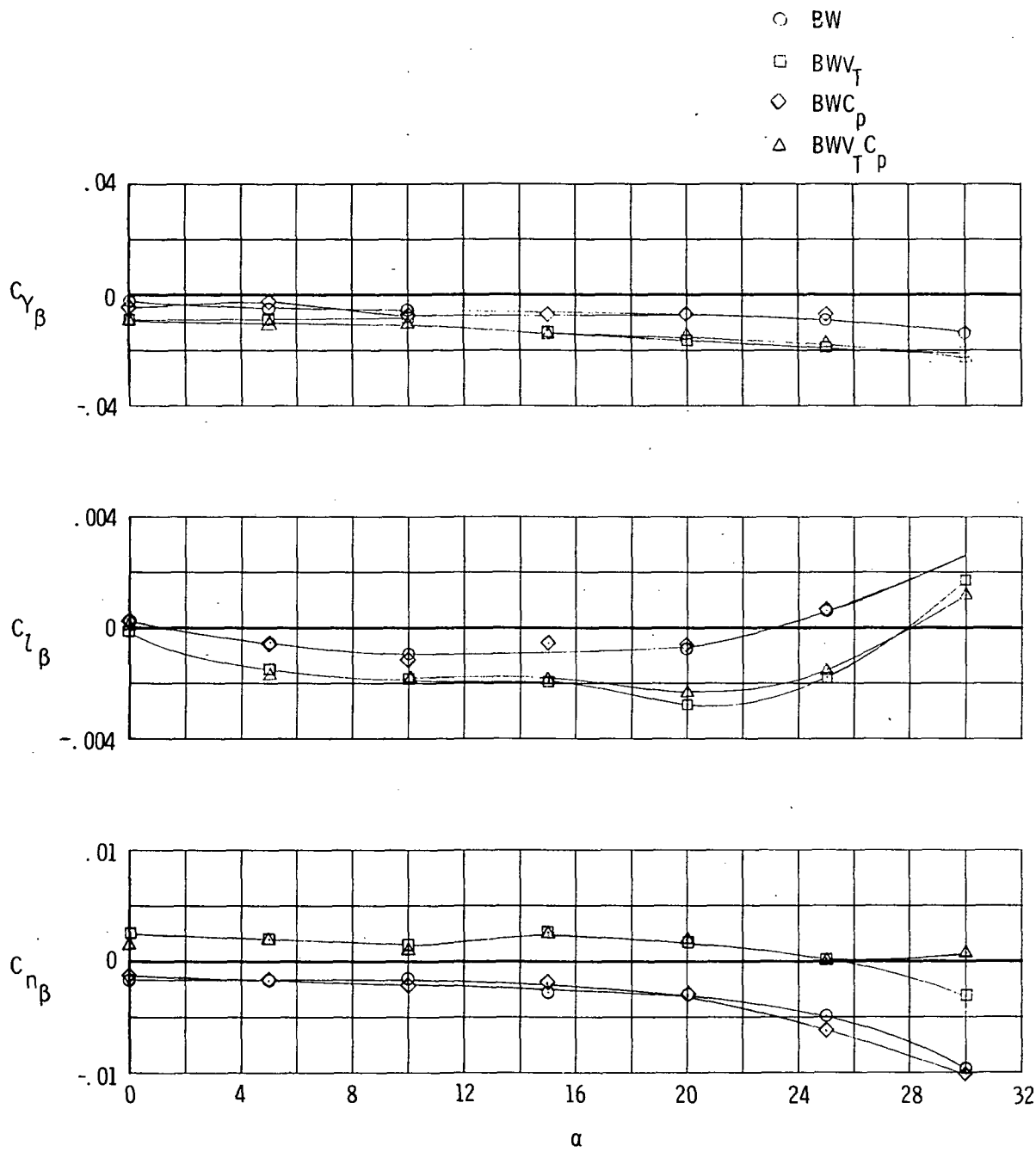

(b) Effect of canopy on BW and BWV$_T$ configurations.

Figure 14.- Continued.

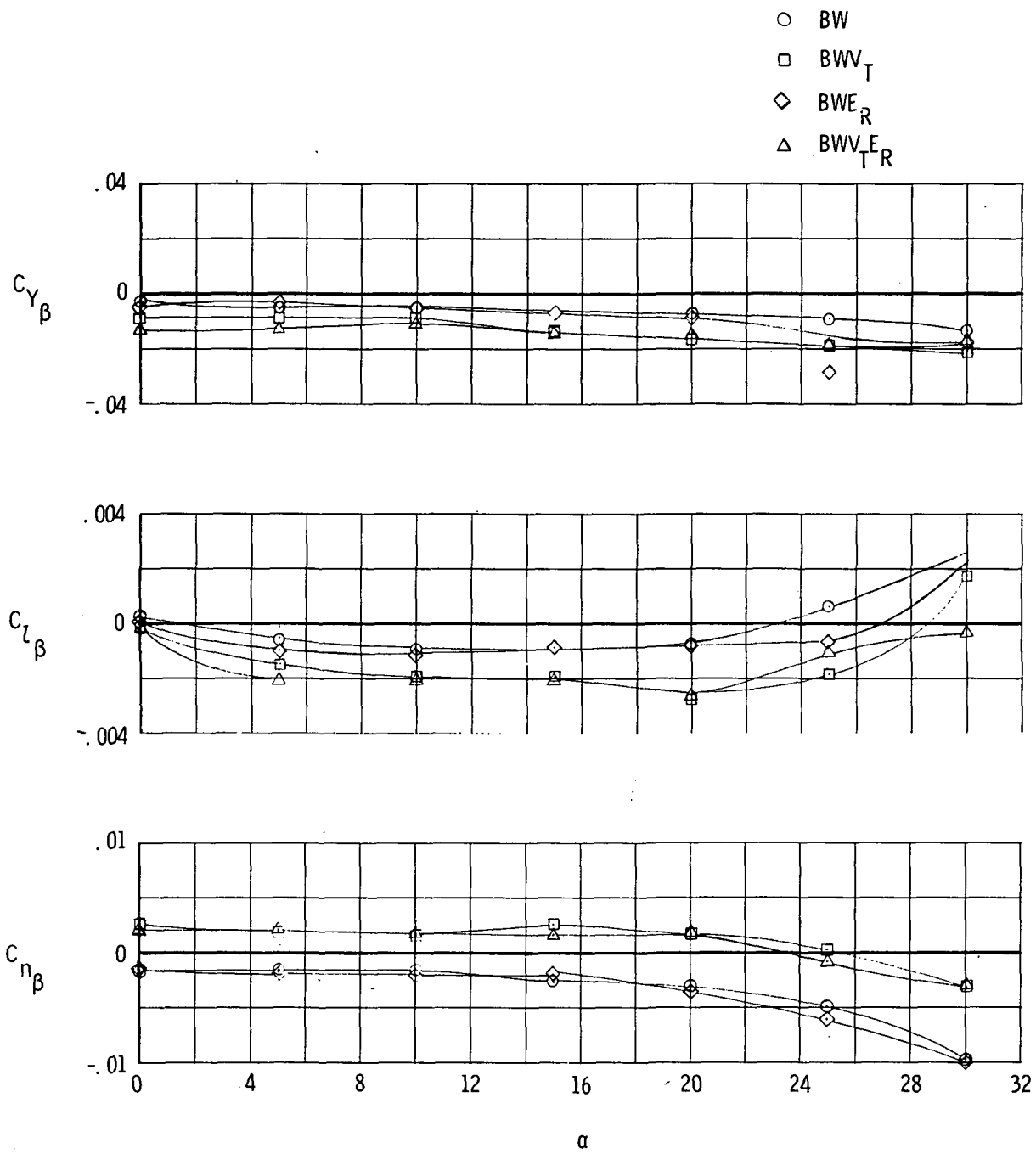

(c) Effect of retracted engine on BW and BWV$_T$ configurations.

Figure 14.- Continued.

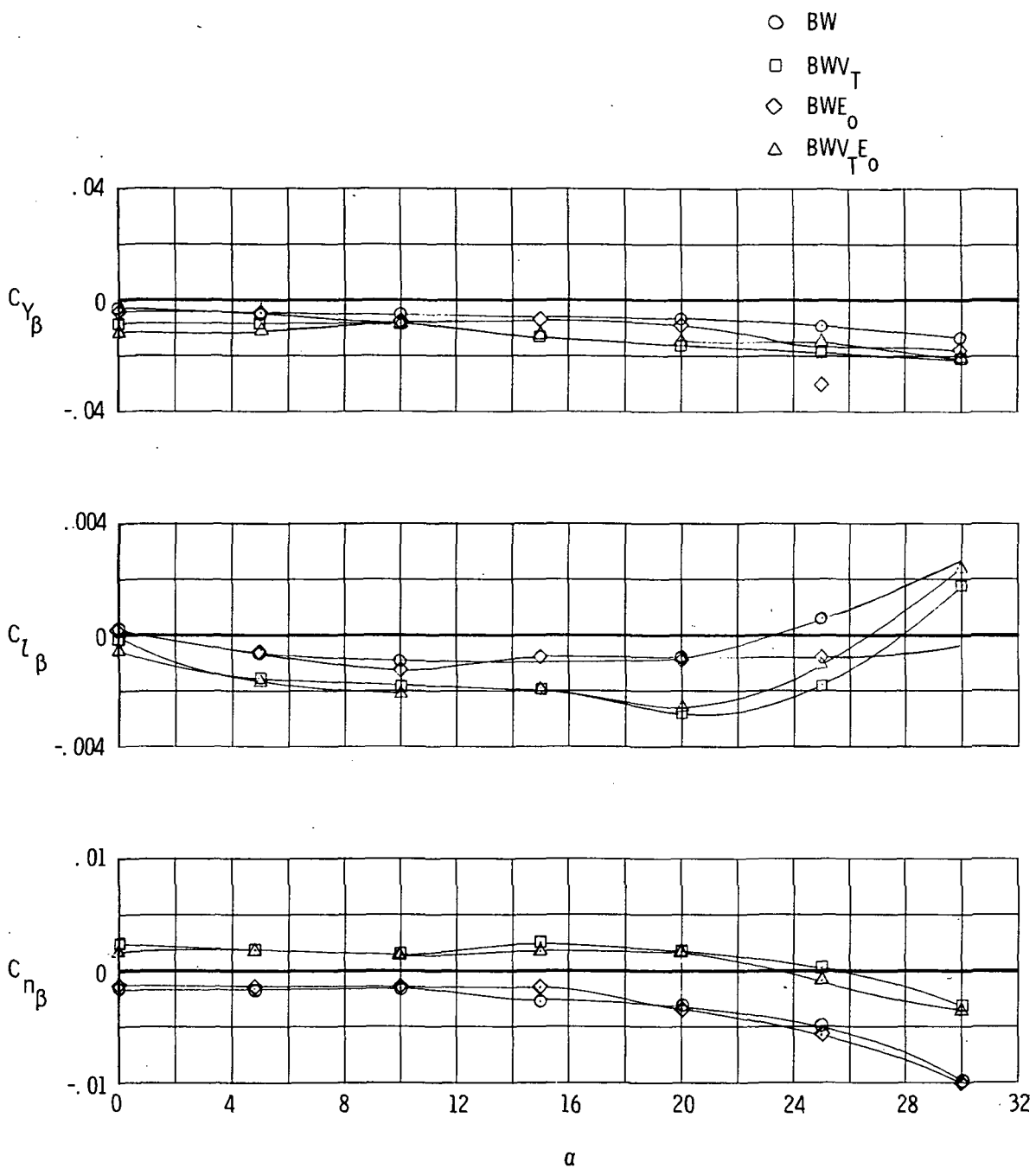

(d) Effect of open engine on BW and BWV$_T$ configurations.

Figure 14.- Continued.

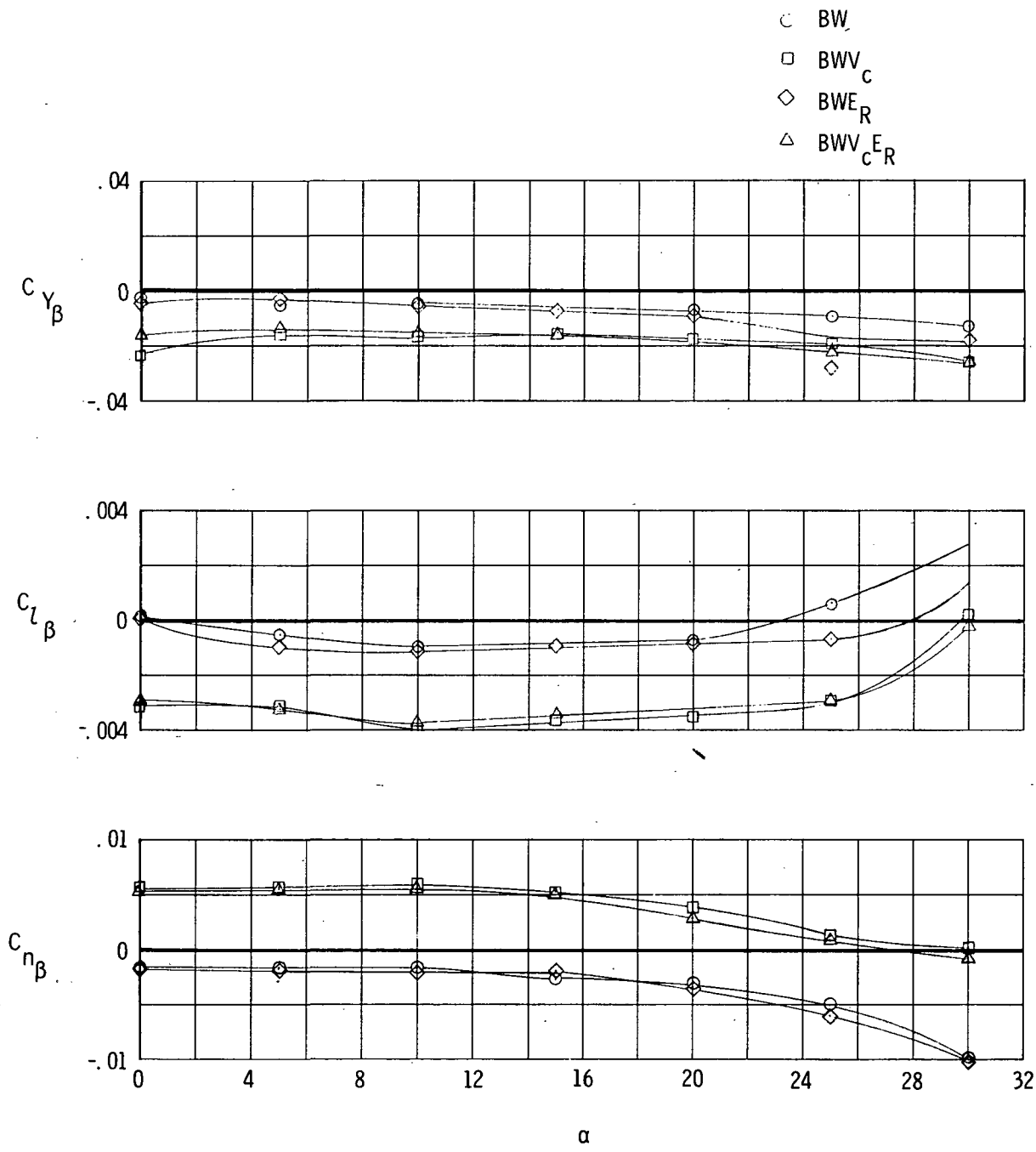

(e) Effect of retracted engine on BW and BWV$_C$ configurations.

Figure 14.- Continued.

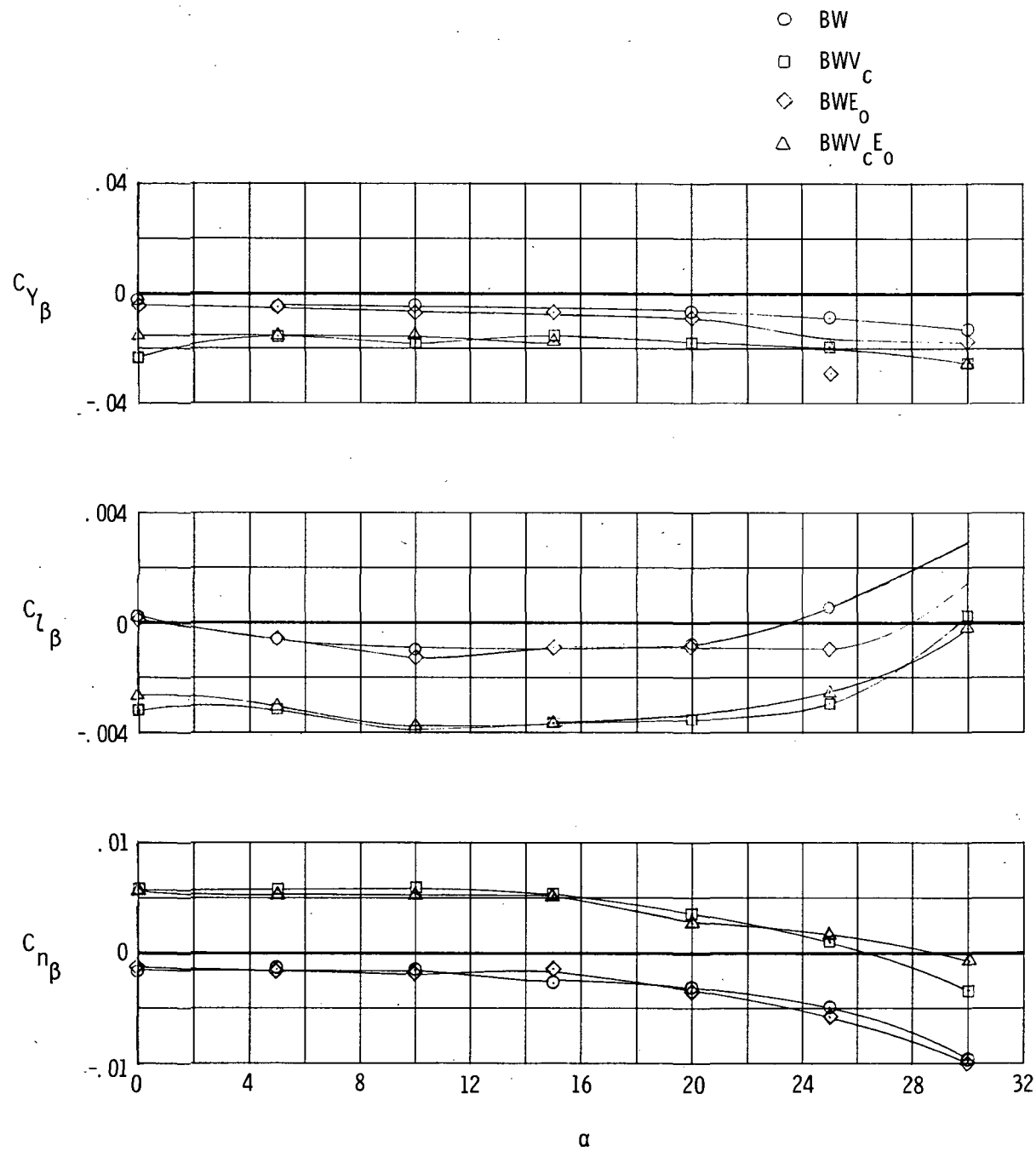

(f) Effect of open engine on BW and BWV$_C$ configurations.

Figure 14.- Continued.

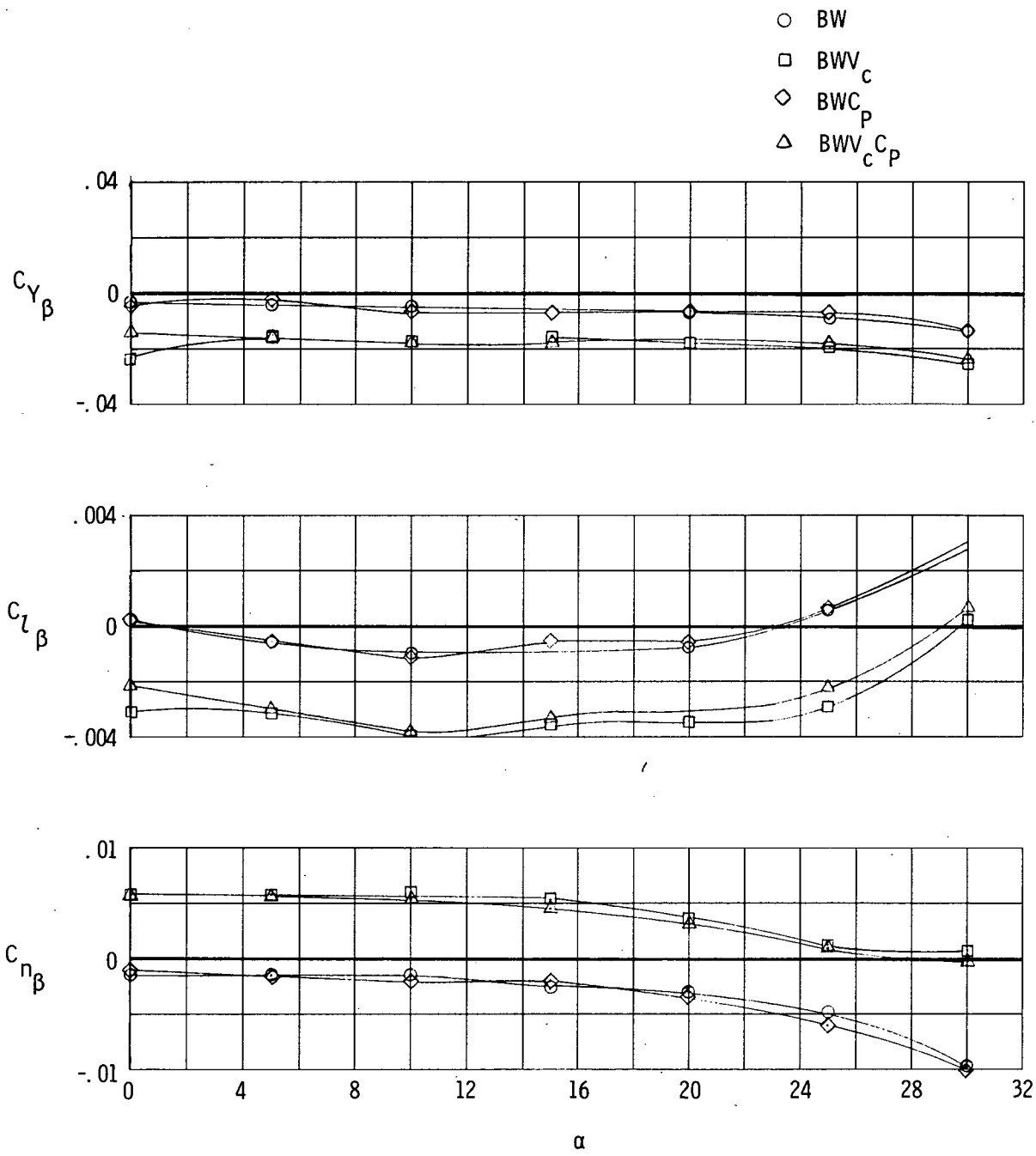

(g) Effect of canopy on BW and BWV$_c$ configurations.

Figure 14.- Concluded.

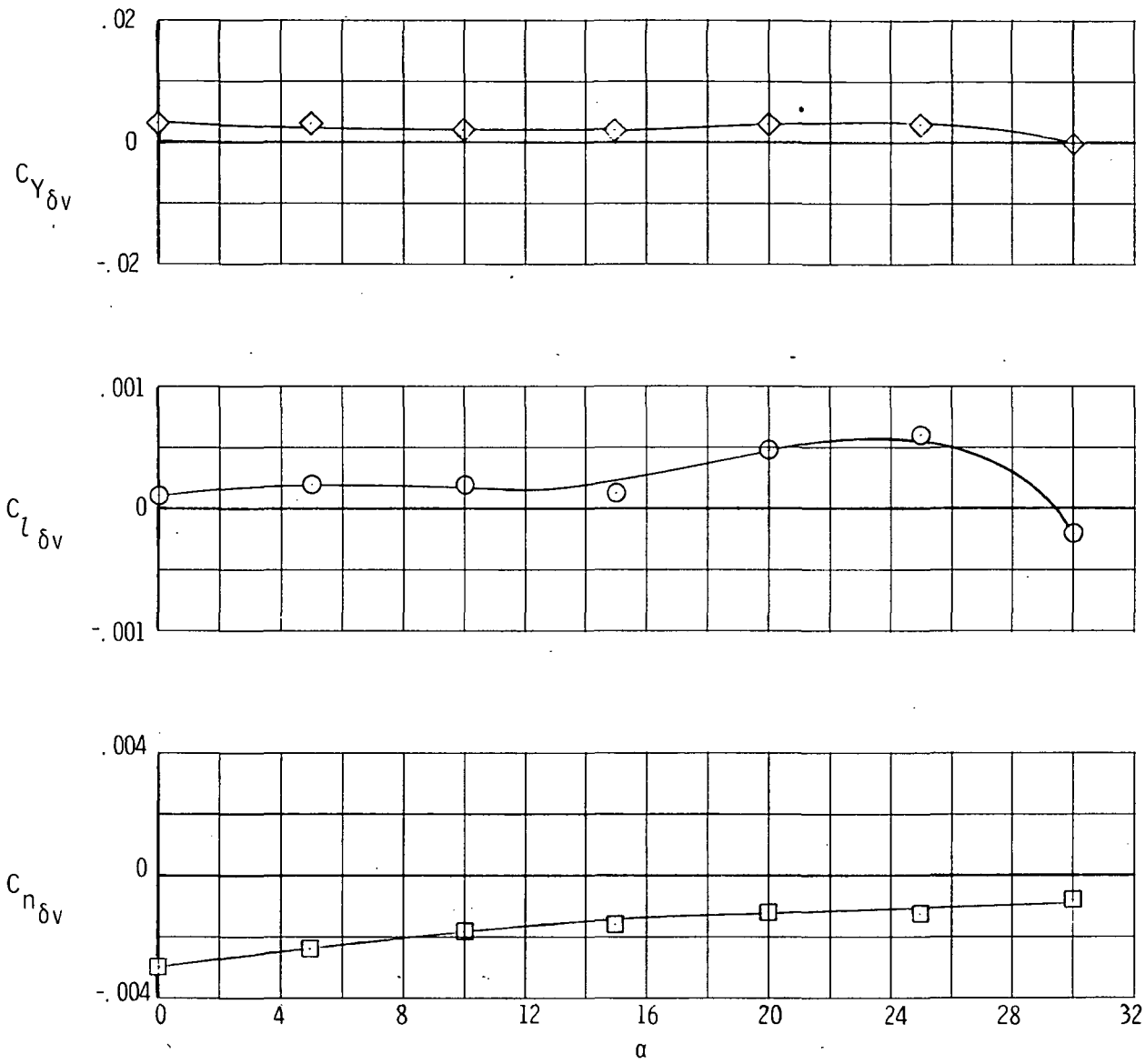

Figure 15.- Yaw control of BWV_T configuration.

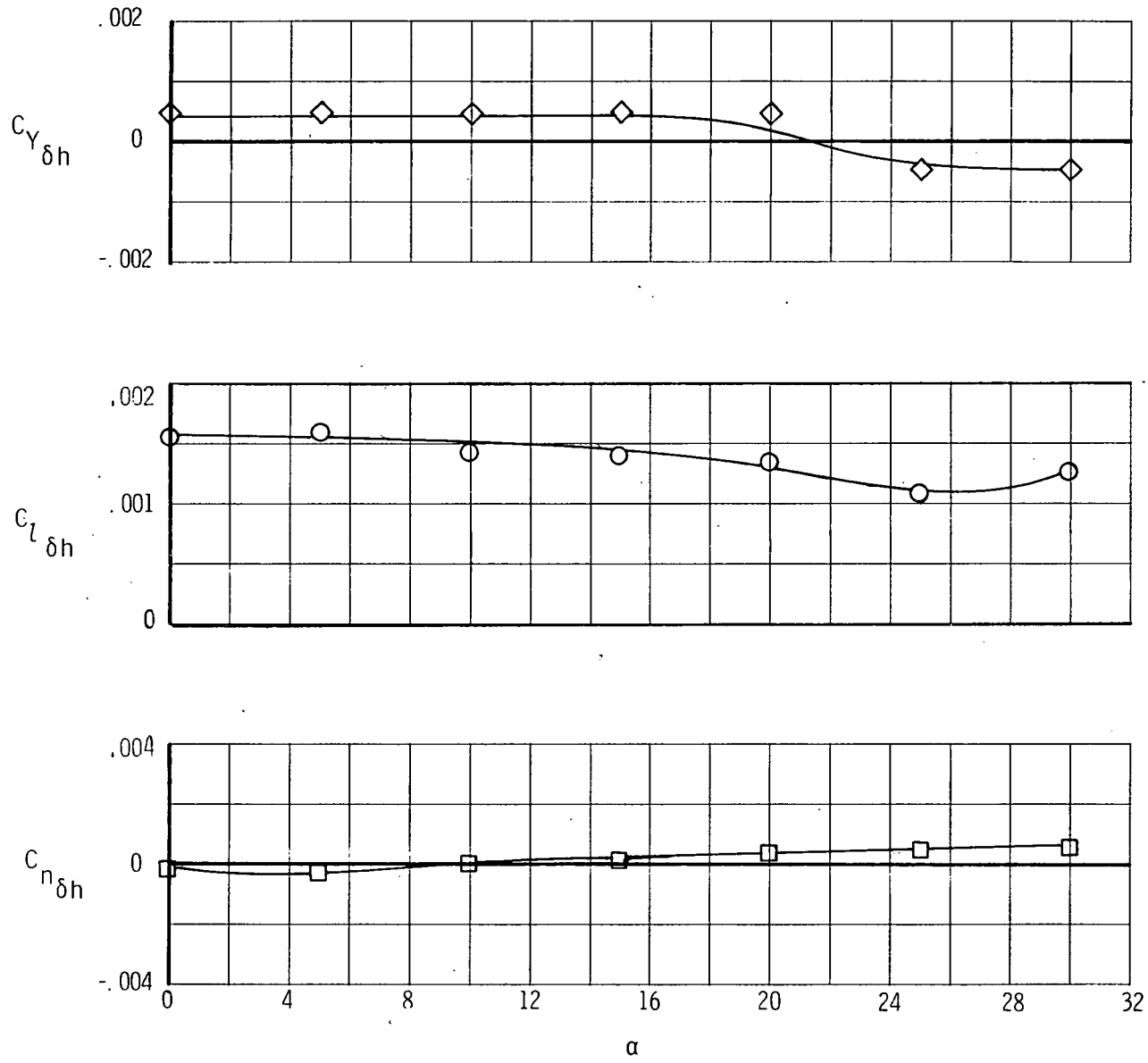

Figure 16.- Roll control of BWV_T configuration.

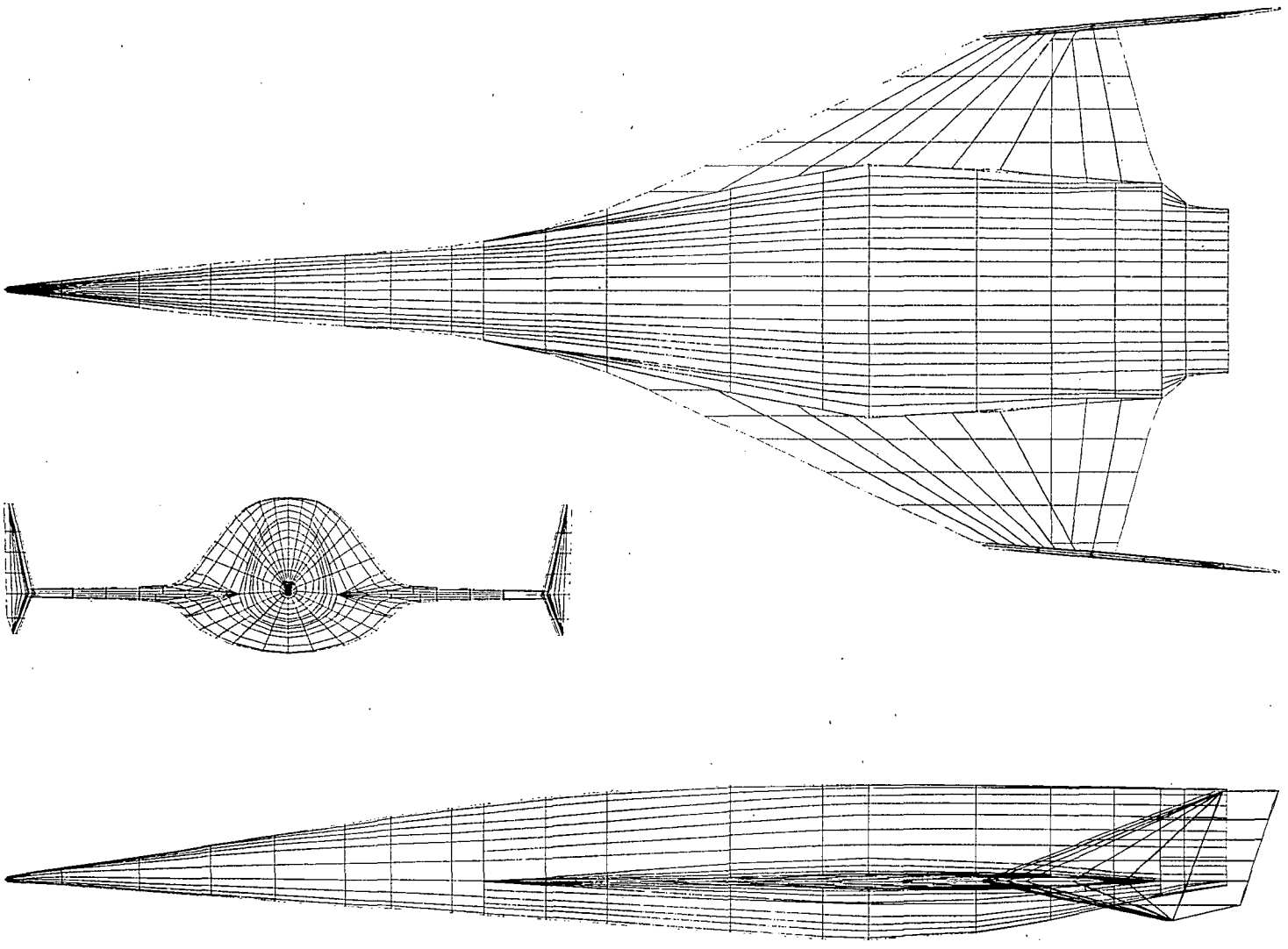

Figure 17.- Computer drawing of paneling scheme of BWV_T configuration as input for hypersonic aerodynamics calculations.

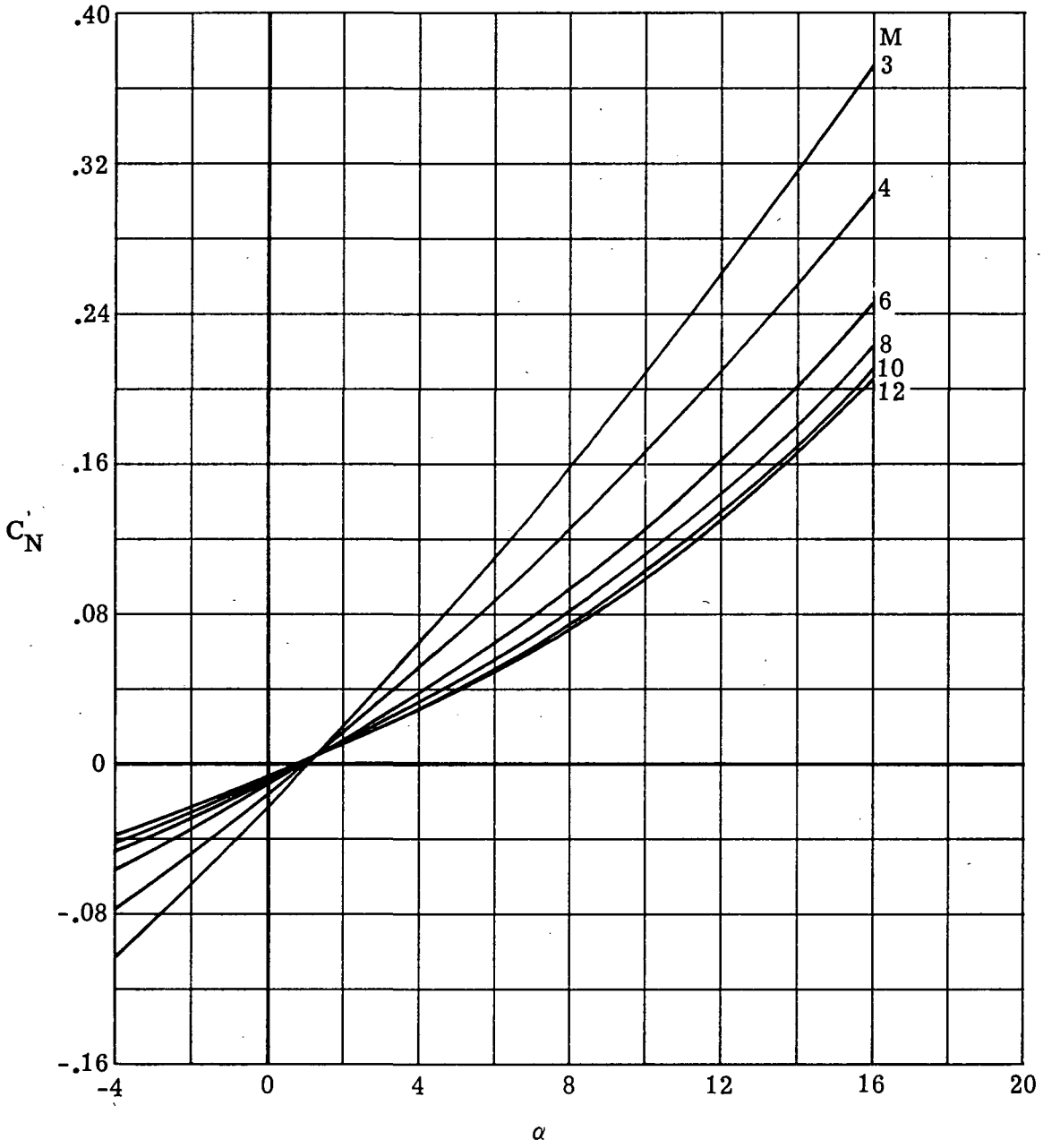

Figure 18.- Variation of calculated normal-force coefficient with angle of attack for various Mach numbers for q_∞ = 71.8 kPa (1500 psf).

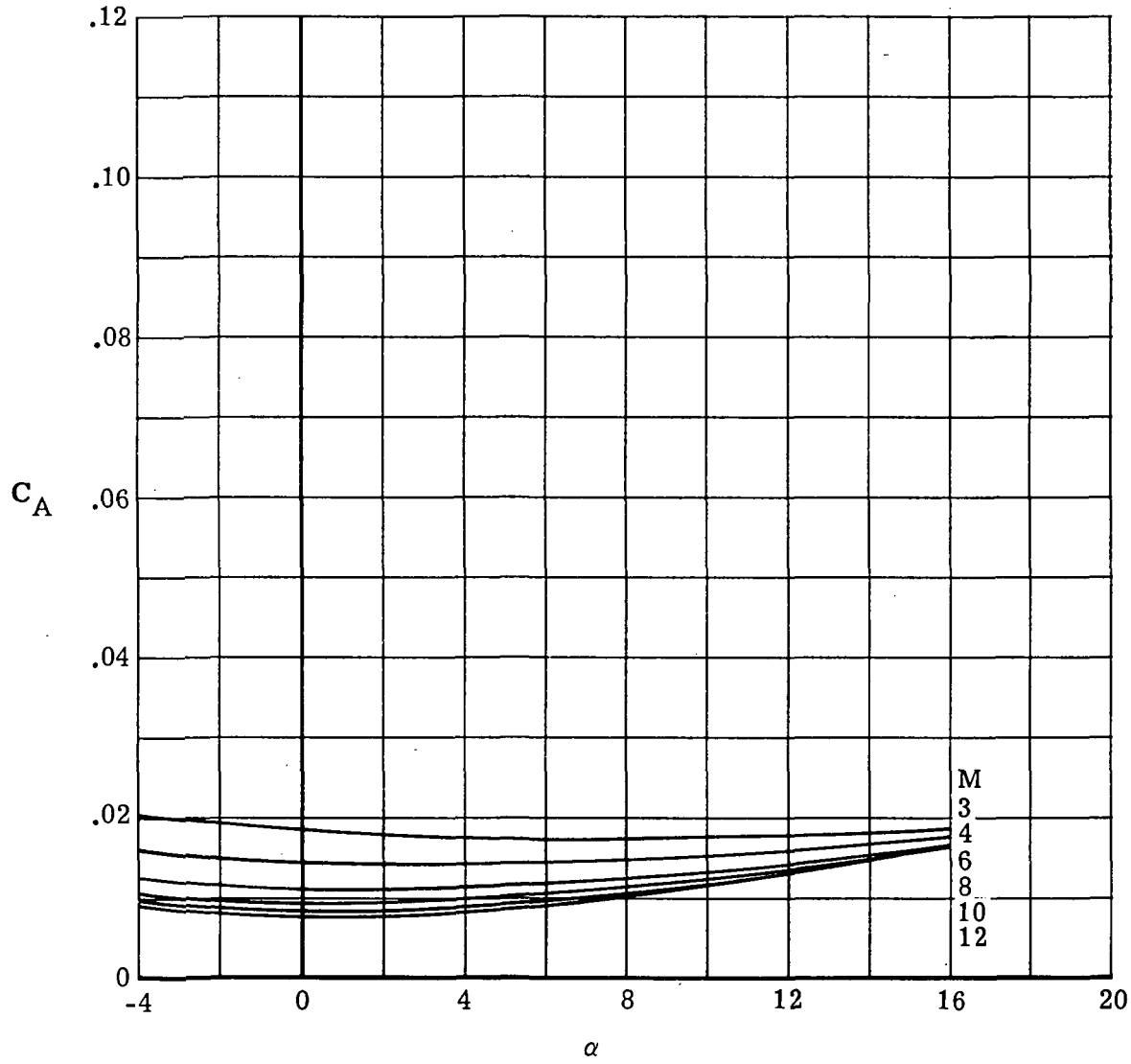

Figure 19.- Variation of calculated axial-force coefficient with angle of attack for various Mach numbers for q_∞ = 71.8 kPa (1500 psf).

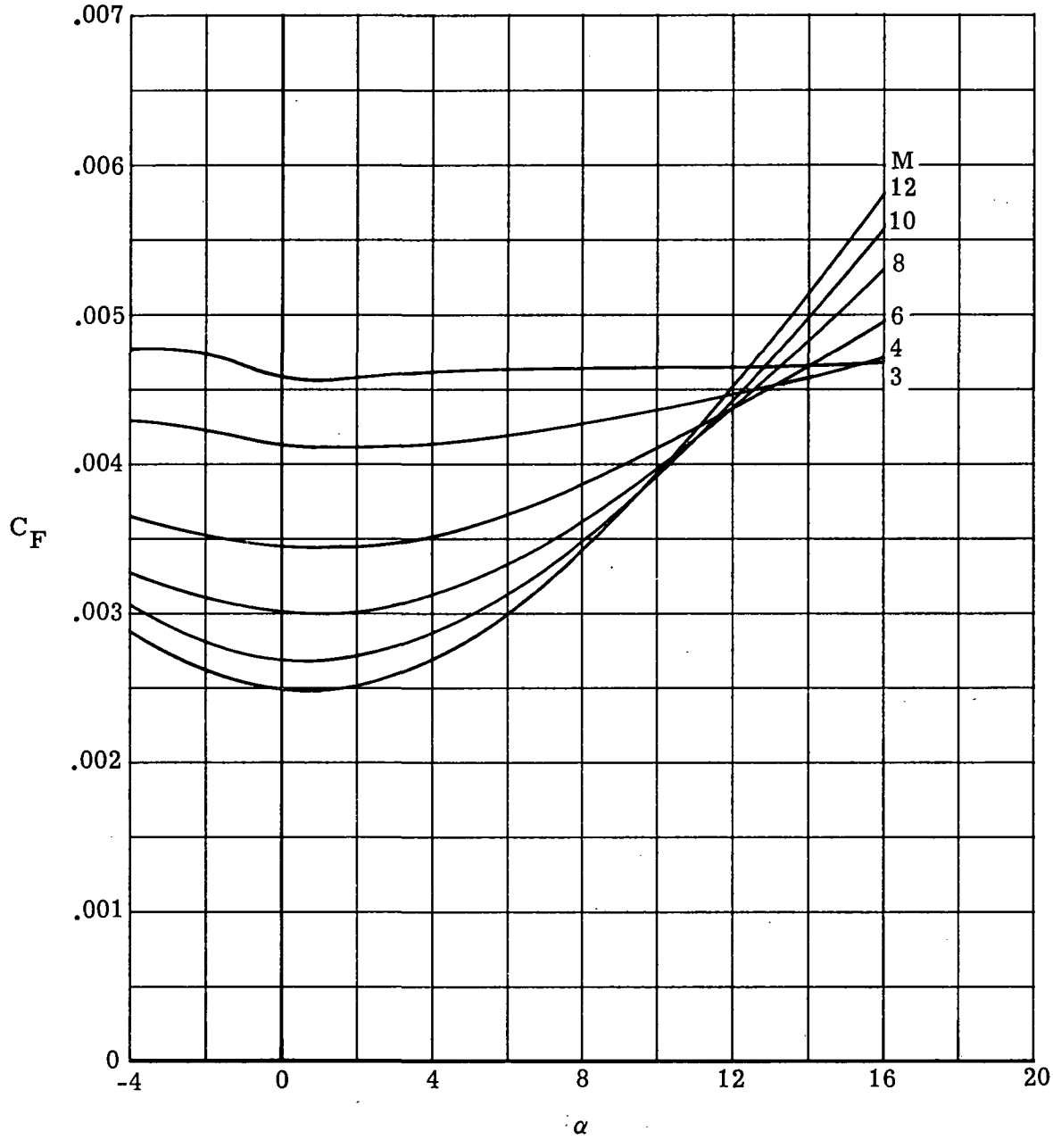

Figure 20.- Variation of calculated skin-friction coefficient with angle of attack for various Mach numbers for q_∞ = 71.8 kPa (1500 psf).

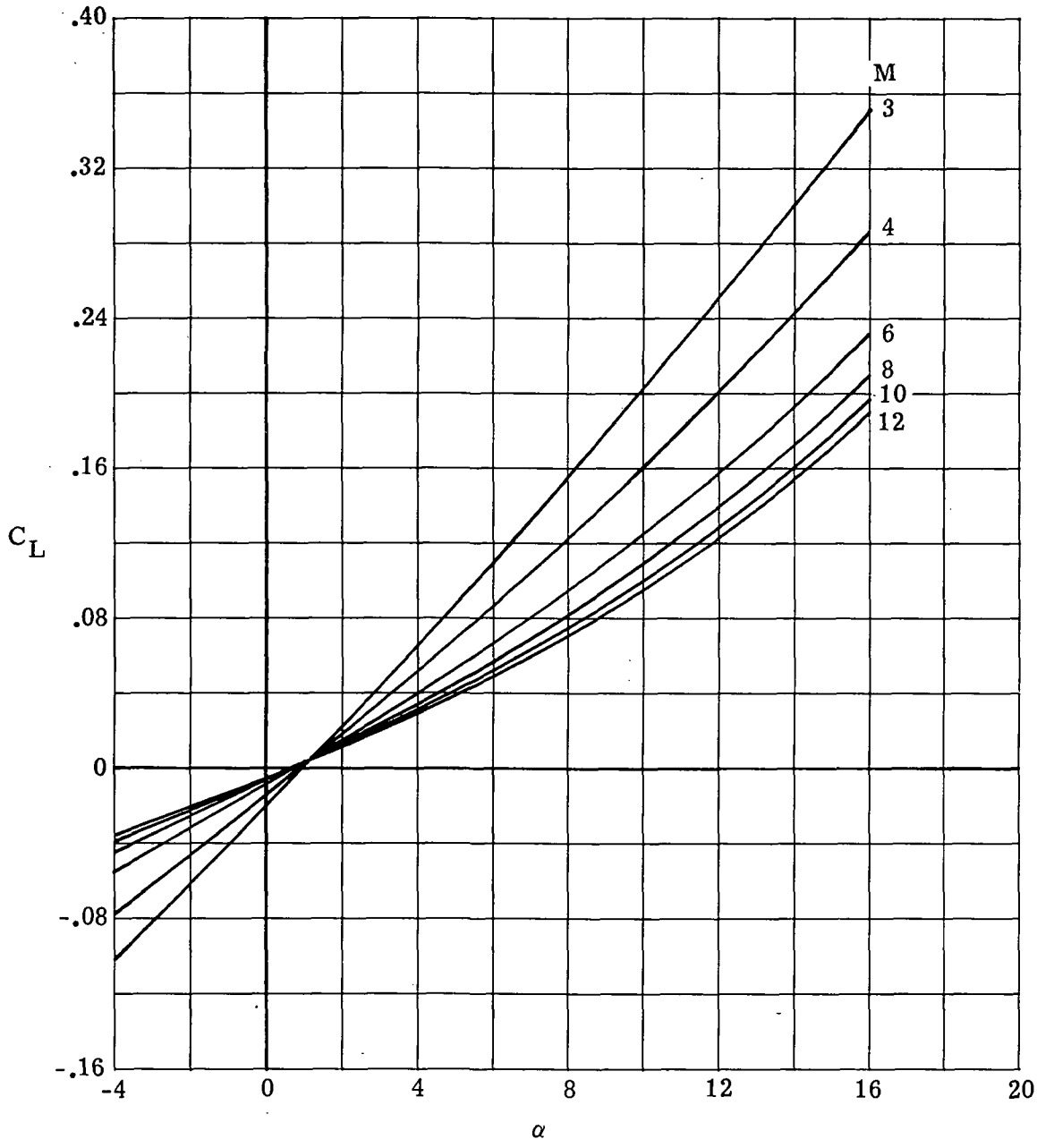

Figure 21.- Variation of calculated lift coefficient with angle of attack for various Mach numbers for q_∞ = 71.8 kPa (1500 psf).

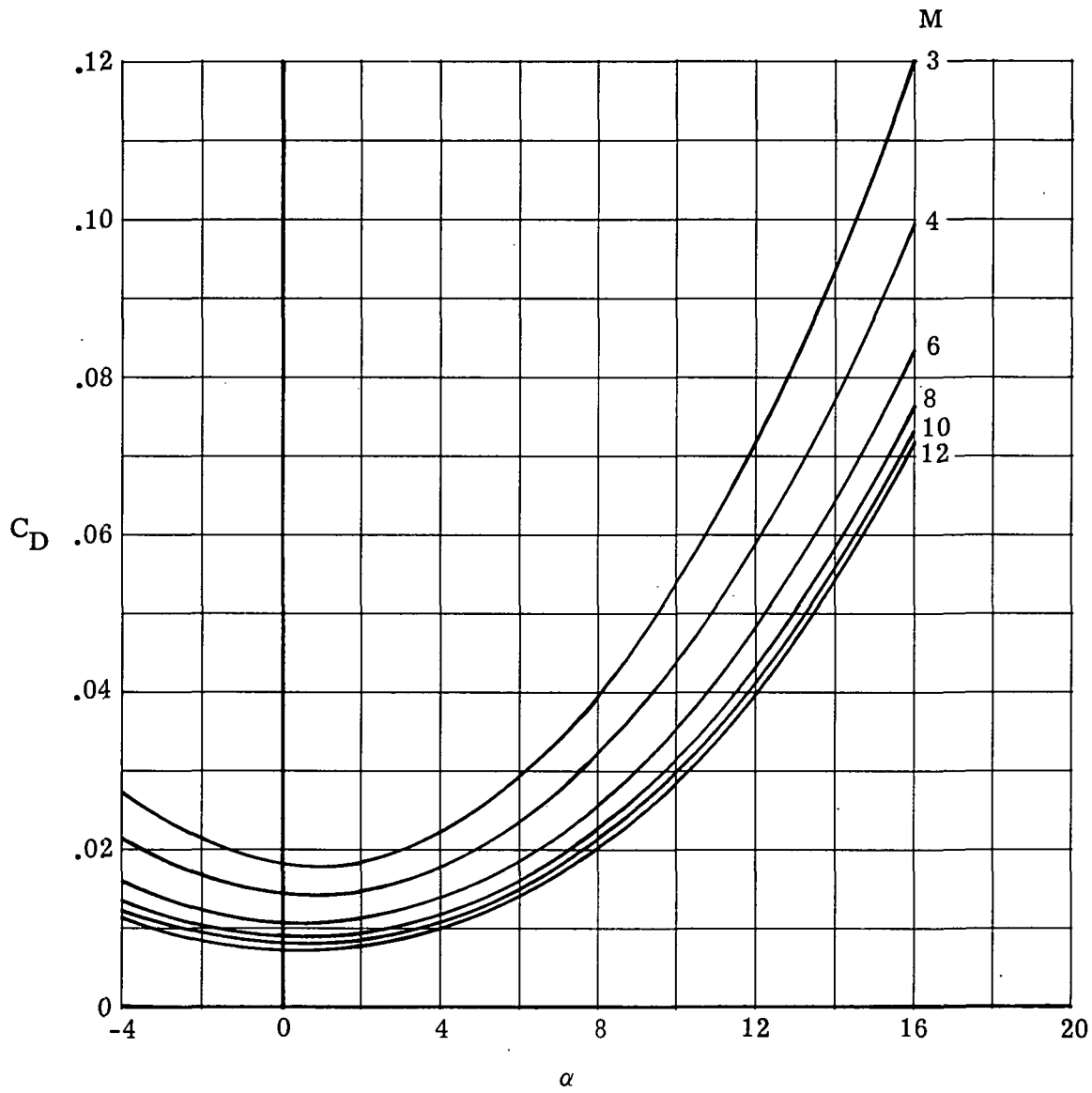

Figure 22.- Variation of calculated drag coefficient with angle of attack for various Mach numbers for q_∞ = 71.8 kPa (1500 psf).

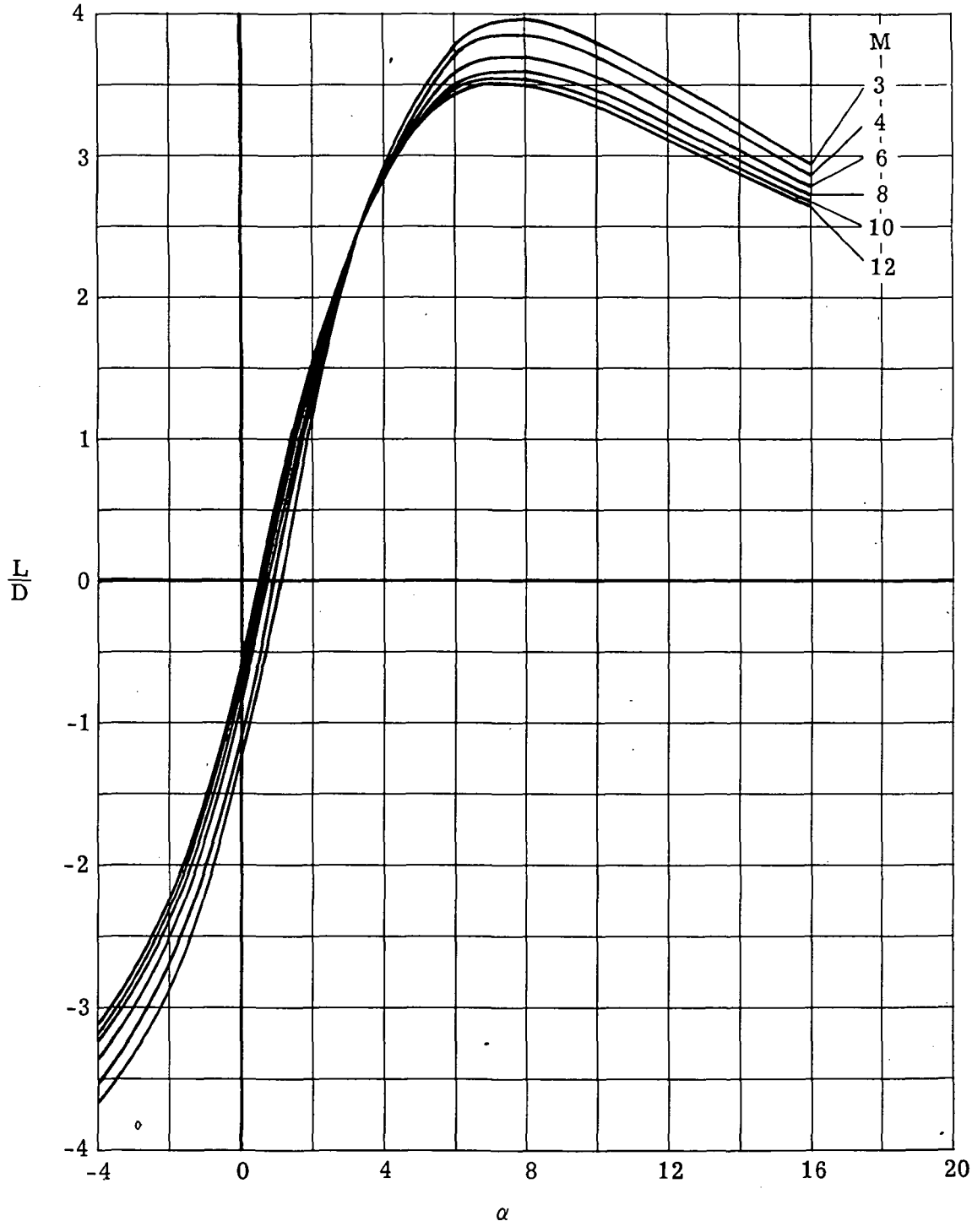

Figure 23.- Variation of calculated lift-drag ratio with angle of attack for various Mach numbers for q_∞ = 71.8 kPa (1500 psf).

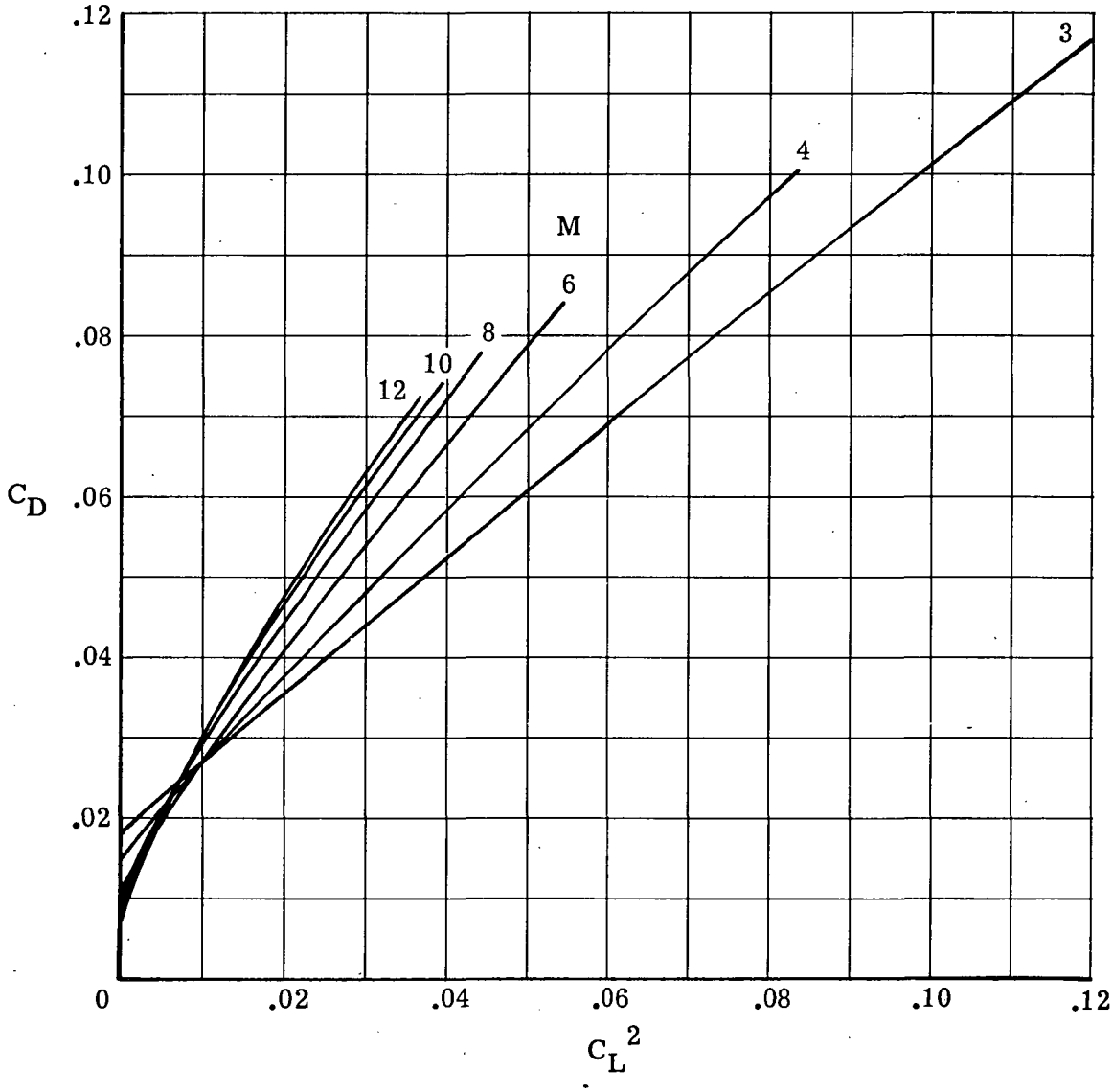

Figure 24.- Variation of calculated drag due to lift for various Mach numbers for q_∞ = 71.8 kPa (1500 psf).

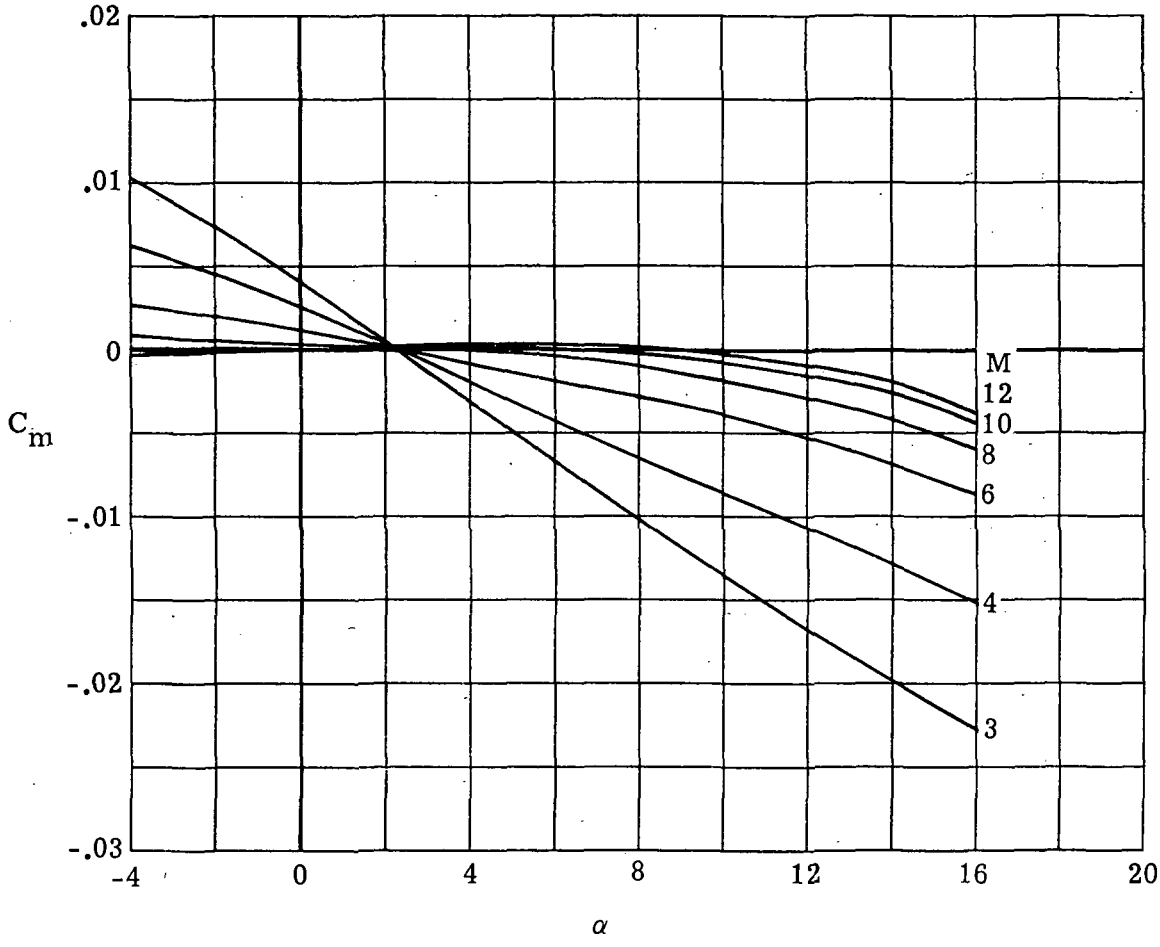

Figure 25.- Variation of calculated pitching-moment coefficient with angle of attack for various Mach numbers for q_∞ = 71.8 kPa (1500 psf).

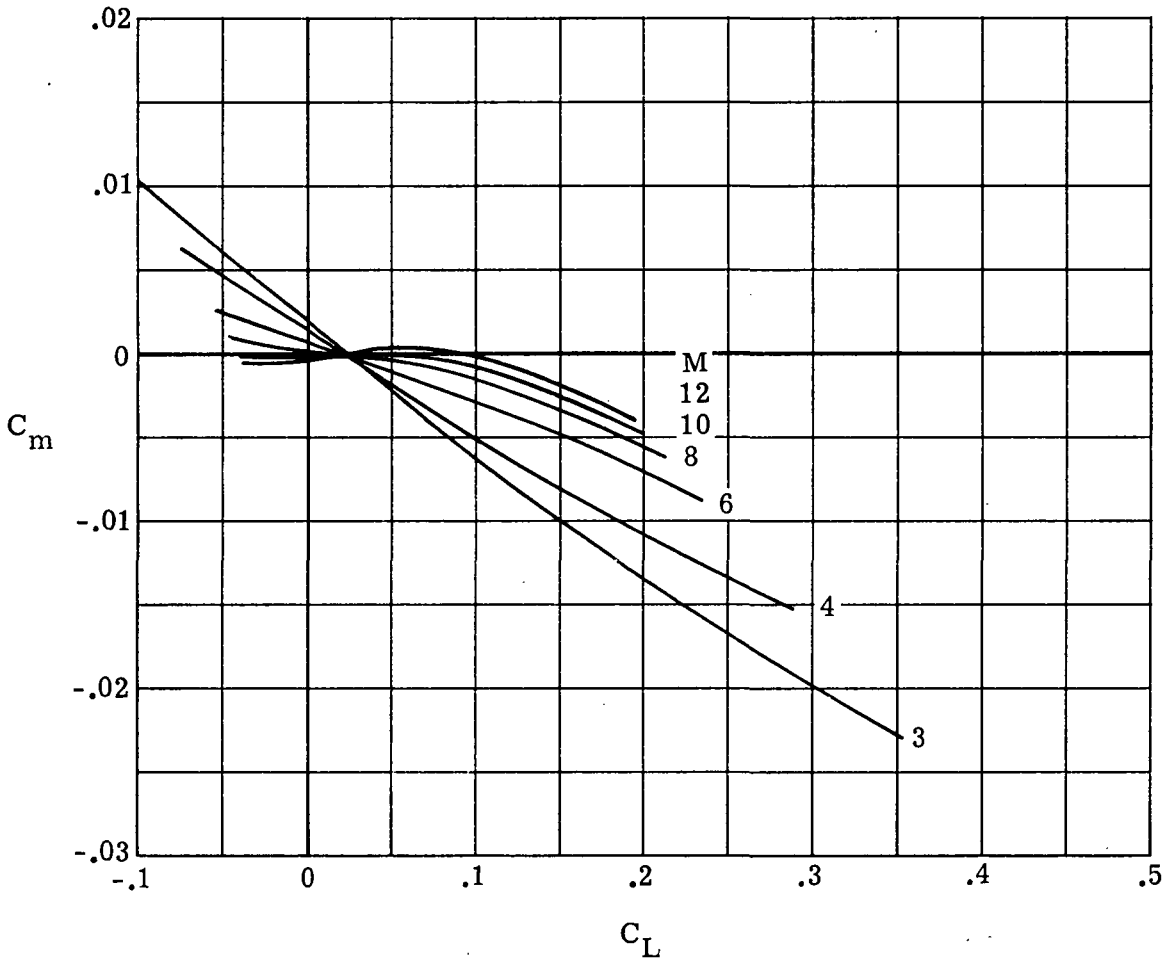

Figure 26.- Variation of calculated longitudinal stability for various Mach numbers for q_∞ = 71.8 kPa (1500 psf).

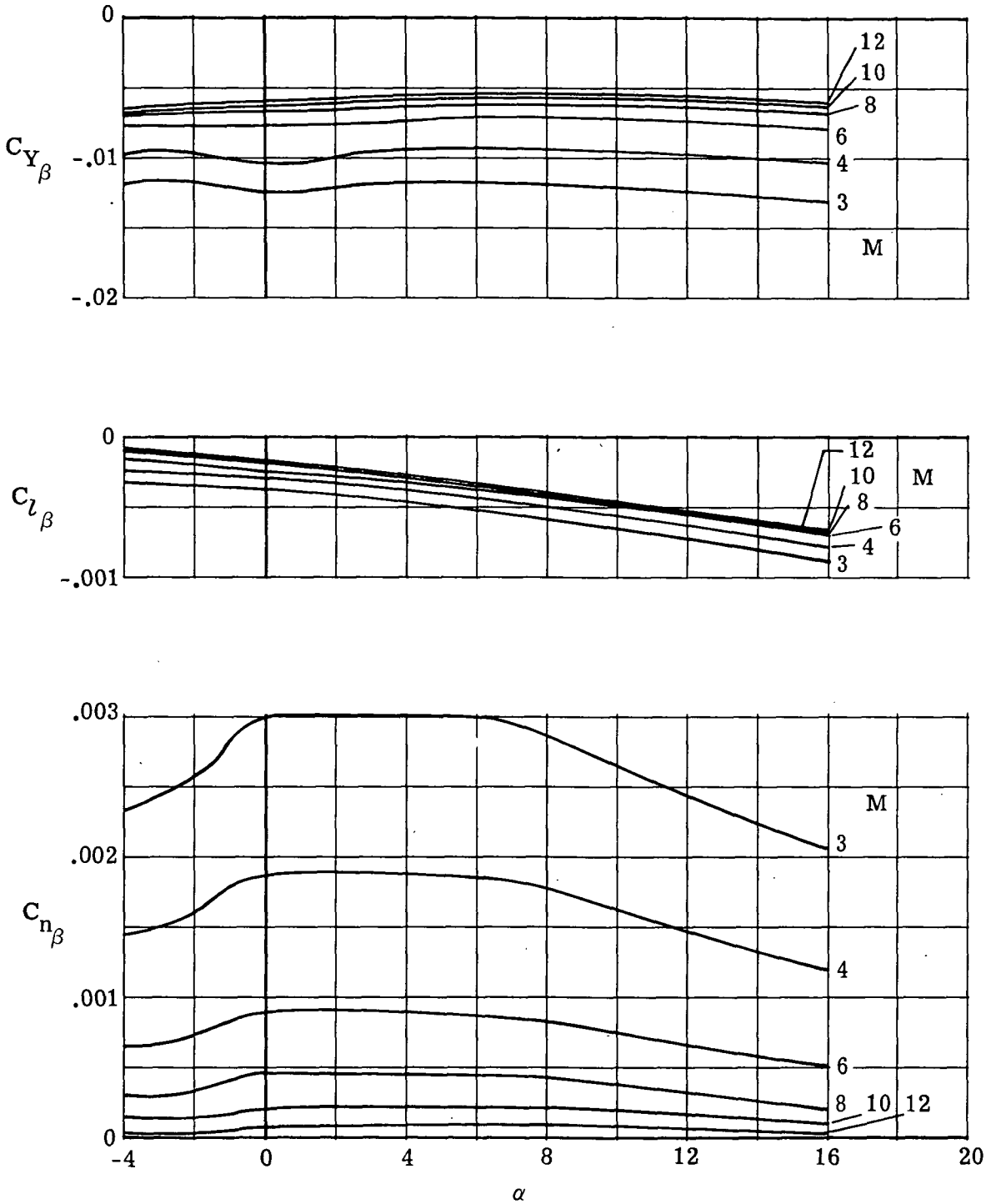

Figure 27.- Variation of calculated lateral and directional stability with angle of attack for various Mach numbers for q_∞ = 71.8 kPa (1500 psf).

"The aeronautical and space activities of the United States shall be conducted so as to contribute . . . to the expansion of human knowledge of phenomena in the atmosphere and space. The Administration shall provide for the widest practicable and appropriate dissemination of information concerning its activities and the results thereof."

—NATIONAL AERONAUTICS AND SPACE ACT OF 1958

NASA SCIENTIFIC AND TECHNICAL PUBLICATIONS

TECHNICAL REPORTS: Scientific and technical information considered important, complete, and a lasting contribution to existing knowledge.

TECHNICAL NOTES: Information less broad in scope but nevertheless of importance as a contribution to existing knowledge.

TECHNICAL MEMORANDUMS: Information receiving limited distribution because of preliminary data, security classification, or other reasons. Also includes conference proceedings with either limited or unlimited distribution.

CONTRACTOR REPORTS: Scientific and technical information generated under a NASA contract or grant and considered an important contribution to existing knowledge.

TECHNICAL TRANSLATIONS: Information published in a foreign language considered to merit NASA distribution in English.

SPECIAL PUBLICATIONS: Information derived from or of value to NASA activities. Publications include final reports of major projects, monographs, data compilations, handbooks, sourcebooks, and special bibliographies.

TECHNOLOGY UTILIZATION PUBLICATIONS: Information on technology used by NASA that may be of particular interest in commercial and other non-aerospace applications. Publications include Tech Briefs, Technology Utilization Reports and Technology Surveys.

Details on the availability of these publications may be obtained from:

SCIENTIFIC AND TECHNICAL INFORMATION OFFICE

NATIONAL AERONAUTICS AND SPACE ADMINISTRATION

Washington, D.C. 20546